UNIVERSITY OF OKLAHOMA

GRADUATE COLLEGE

END REGIONS REPAIR OF PRESTRESSED GIRDERS FOR RESTORING THE SHEAR CAPACITY USING UHPC, FR-SCC, AND MALP

A THESIS

SUBMITTED TO THE GRADUATE FACULTY

in partial fulfillment of the requirements for the

Degree of

MASTER OF SCIENCE

By

Mujtaba Ahmadi
Norman, Oklahoma
2021

END REGIONS REPAIR OF PRESTRESSED GIRDERS FOR RESTORING THE SHEAR CAPACITY USING UHPC, FR-SCC, AND MALP

A THESIS APPROVED FOR THE

SCHOOL OF CIVIL ENGINEERING AND ENVIRONMENTAL SCIENCE

BY THE COMMITTEE CONSISTING OF

Dr. Royce Floyd, Chair

Dr. Jeffery Volz

Dr. Jinsong Pei

ACKNOWLEDGEMENTS

I would like to extend my heartfelt thanks and appreciation to my advisor Dr. Floyd for his guidance throughout the research. It helped me learn the procedure for conducting experimental research and how to express the outcomes in this thesis. I also would like to thank the rest of my thesis committee members, Dr. Jeffery Volz and Dr. Jinsong Pei, for their comments to improve the thesis.

I want to thank my parents, who are the greatest source of strength and support in my life. Their encouragement propelled me to follow my academic goals with passion and interest.

During my research, I had the privilege of working with a team of dedicated and talented students, including Stephen Roswurm, Trevor Looney, Sereyvuth Chea, Jacob Starks, Richard Campos, Cole Walker, Phouc Huynh, Jacob G. Choate, and Michael D. Mesigh, who helped me build and test the specimens. Their contribution made it possible to complete the project on time, and I am grateful to all of them.

Last but not least, I thank my close friend Engr. Mohammad Sameer Attaee for his motivation and advice during my master's program at OU, which helped me adjust to the new educational environment.

Table of Contents

Table of Tables

Table of Figures

Abstract

One of the most important concepts in prestressed concrete is stress transfer from prestressing strands to the surrounding concrete. The efficiency of this process dictates the overall quality of the structural member, especially the performance of the end regions where the prestressing force provides a significant contribution to the concrete shear capacity. If this bond is affected due to any factor like vehicular load, collision force, impact, or corrosion due to water penetration from slab joints, the member may lose its shear capacity in that region. Bond loss is not the only factor causing a drop in shear strength. Sometimes the formation of shear cracks close to supports due to overloading also results in minor and moderate damages to the girder. Shear reinforcement may also corrode due to water intrusion from the bridge deck. For scenarios where shear capacity may be affected, the bridge girders can be repaired, or for severe damage, replaced.

In this research, the feasibility of restoring shear capacity by encapsulating the end regions with Ultra-High Performance Concrete (UHPC), Fiber Reinforced Self-Consolidating Concrete (FR-SCC), and Magnesium-Alumino-Liquid Phosphate (MALP) concrete is investigated. This operation does not bring back the lost prestressing force, but it increases the cross-sectional dimensions with higher quality material resulting in a structural retrofit. This repair also produces an impermeable barrier to resist further corrosion damage to the end regions. For this purpose, six approximately half-scale AASHTO Type-II girders were cast, tested, repaired, and tested again to highlight the repair's contribution to restoring the girder shear strength. All the repairs increased the ultimate load capacity of the girders and changed their failure mechanism from a bond-shear failure pre-repair to a bond-flexure post-repair failure. The repair maintained a good bond with the member, indicating an excellent integral behavior of composite material. The research outcome provides the Oklahoma Department of Transportation with a comparison between the performance of the three used repair materials, which can be a very cost-efficient substitute for girder replacement.

Chapter 1: Introduction

1.1 Background

The average age of the over 600,000 bridges in the United States is around 42 years (Sobeik, 2014), approaching the 50 years of design life for an ordinary concrete bridge which was based on the old codes in use at the time the bridges were constructed. More than 60% of the total bridges in the United States are concrete bridges (Ramseyer, 2012), and 23% of the 163,000 single-span concrete bridges in the country are classified as structurally deficient or functionally obsolete (Ghaffary, 2020). Structurally deficient means existence of cracks or corroded elements that need repair. Functionally obsolete means inconsistent with the current code requirements, such as narrow shoulders or inadequate width for oversize vehicles (Ghaffary, 2020). While bridge aging is natural and expected; using deicing salts, which have chloride ions, has accelerated the deterioration process, especially for the girders' end regions.

Most of the bridges encountered on a daily basis are simply supported multi-girder spans with girders as their primary element supporting the structural system. End regions of the bridge girders rest over the piers, which are typically below the expansion joints in the deck. A leaking joint allows the water with deicing agents used for the bridge surface to penetrate through the joint and flow over the girder. Penetration of water and chlorides to the level of the reinforcing steel results in corrosion that can lead to concrete spalling. As a result of continuous freeze-thaw cycles, the leaked water expands and can also cause spalling in the surrounding concrete. This deterioration can cause structural problems in bearing and shear as high shear force demand at the girder end regions requires a sound cross-section to resist the applied load.

The main causes of damage for the end regions of a concrete girder are:

- Insufficient reinforcement
- Low concrete strength
- Increased design load
- Corrosion of existing shear reinforcement

Based on the intensity of the damage, there are two options for improving the bridge condition when girder end region damage is present. The damaged member can be repaired or, in severe cases, replaced. Replacing the damaged girder disrupts traffic and overburdens the nearby infrastructure. Studies indicate that the average girder replacement costs about $8000 (USD) per ft of the girder and takes one to two months to complete, which is very expensive and time-consuming (Jones, 2015). On the other side, repair costs for prestressed I-girders range from 35% to 69% of the superstructure replacement cost and are expected to extend the structure's service life (Radlinska, 2014). According to Robert (2016), it would cost around $140 billion (USD) to repair all the deficient bridges in the United States. By observing the above two options, repair is the most cost-effective if the repair has sufficient longevity, but it is a considerable amount of money, and consideration should be made to ensure safety, repair time, and economy.

Two approaches are currently in practice for repairing concrete girders. The girder can be rehabilitated to restore the design capacity or retrofitted to enhance the strength beyond its initial design by increasing the member size or adding new structural elements to the existing girder like steel, external-post tensioning, or concrete encapsulation.

1.2 Purpose

In the research described in this thesis, the feasibility of restoring shear capacity by encapsulating the end regions of damaged prestressed concrete girders with UHPC, FR-SCC, and MALP concrete was investigated. This operation does not bring back the lost prestressing force, but it increases the cross-sectional dimensions by encapsulating the end region with higher quality material resulting in a structural retrofit. This repair also produces an impermeable barrier to resist further corrosion damage to the end regions.

For this purpose, six approximately half-scale AASHTO Type-II girders were cast, tested, repaired, and tested again to highlight the repair's contribution to restoring the girder shear strength. The research outcome provides a comparison between the three repair materials' performance, which can be a very cost-efficient substitute for complete girder replacement.

1.3 Objectives

The objectives of the research program are as follows.

- Identify a functional, cost-effective, and innovative repair technique for prestressed concrete girder end regions.
- Improve the shear capacity lost due to bond failure or cracks.
- Experimentally determine the mechanical properties and efficiency of the locally developed repair materials for girder repair.
- Compare the failure load of the original and repaired girder to provide design guidance.

Chapter 2: Literature review

2.1 Bridge Condition

Prestressed concrete bridges comprise 60% of newly constructed bridges in the United States, but the majority of those in service were built in the 1950s, 1960s, and 1970s and are approaching the end of their design life. The end region of a prestressed girder plays an important role in the overall performance of the member. High shear force concentration at these zones due to vehicular loads and water penetration from deck joints can cause localized damage to the girders, which may raise safety and durability concerns. Moisture intrusion leading to corrosion is the most common factor for damage and causes two significant defects. First, it decreases the cross-sectional area of steel, which can lead to reduced strength. Second, a rusted bar expands and exerts tensile stress to the surrounding concrete, causing cracking and spalling and making the beam more prone to deterioration. Figure 2.1 shows the end region damage of prestressed girders.

(a) (Shafei, 2020) (b) **(**Ramseyer, 2012)

Figure 2.1: End region damage of prestressed girders

According to recent research by Zmetra et al. (2015), at that time there were 66,749 structurally deficient bridges in the U.S, with an estimate of around $76 billion required to repair them. Finding novel, reliable, functional, and innovative repair techniques can improve the existing bridges' service life with the least cost and effort.

Before repair, a comprehensive survey is required to specify the root causes and level of damage to the member. Determining the level of damage for a particular concrete girder depends on the criteria the observer set for assessment, making the process somewhat subjective. There can be different levels of damage in a prestressed girder, which require different levels of repair. For this reason, it is important to highlight damage types and some relevant state-of-the-art repair guidelines. According to Shanafelt (1980), damage to a prestressed girder can be classified into three types; minor, moderate, and severe damage. Minor or light damage is the one in which there may be little or extensive concrete spalling, cracks, efflorescence, rust, or water stains, but no prestressed strand/reinforcement is exposed. The member maintains its full capacity, and repair is for preventive or aesthetic purposes. For lightly damaged beams, Cathodic Protection can reduce corrosion by giving a negative charge to the steel, which repels the chloride ions from attacking the reinforcement; however, a structural retrofit is not required. For moderate damage, the cracks may be wider with more spalling and exposure of strands/reinforcing steel. The member capacity is still not affected, but repair is needed to avoid further deterioration. For this purpose, unsound concrete should be removed, and the surface should be patched if required. The typical repair material for moderate damage is fiber-reinforced composites (FRC) (Shanafelt 1980).

Severe damage occurs when cracks are very large, and strands/reinforcement are exposed, or cross-section is lost to corrosion, which necessitates structural repair. For severe

damage, one objective is to restore the lost prestress, but the cross-sectional dimension can also be increased to produce design strength or higher (Shanafelt 1980).

Table 2.1: A Summary of Damage Levels and Need for Repair for Prestressed Concrete Girders (Ghaffary, 2020)

Damage classification				
Minor	Moderate	Severe		
		Severe I	Severe II	Severe III
Damage does not affect member capacity	Damage does not affect member capacity	Requires structural repair	Requires structural repair	Damage is too expensive
Repairs are for preventive or aesthetic purposes	Repair is done to prevent further deterioration	Repair is done to restore the ultimate limit state	Repair is done to restore both the ultimate limit state and the service limit state	The member must be replaced

Based on a survey by Shanafelt (1980) in the late twentieth century, 80.5% of prestressed girder damage was due to overloading, and 72% of overall deterioration was counted as minor damage. Minor and moderate damage can typically be easily repaired, which is both safe and cost-efficient. However, if cracks extend from flange to the web or more than 25% of prestressing strands are lost (Harries, 2009), a replacement or post-tensioning technique should be used. In any case, the best repair technique is the one giving the highest load capacity. The following section includes a description of the most common material used for repair and how they are applied for prestressed concrete bridges.

2.2 Repair Materials and Their Application

2.2.1 Fiber-Reinforced Composites

Fiber-reinforced composites are a combination of two different materials (i.e., the reinforcing fibers and the polymer resin matrix), as shown in Figure 2.2.

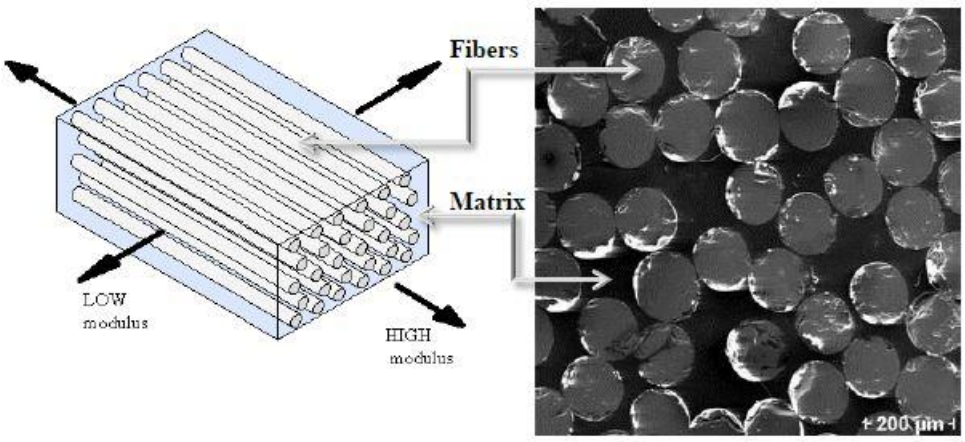

Figure 2.2: Fiber-reinforced composites (Sobieck, 2014)

The mechanical properties of the composite are affected by the type of the matrix and fiber, the orientation of the fibers, and the ratio of the matrix to the fiber content (Sobieck, 2017). Fiber-reinforced composites were first used for aerospace applications in the mid-1980s (Ghaffary, 2020). Characteristics like high strength-to-weight ratio, anti-corrosive properties, high tensile strength, ease of installation, insect and fungal resistance, low thermal conductivity, and flexibility in application make it an optimal material for bridge repair (Jones, 2015). Fiber-reinforced composites are about 73-85% lighter than steel (Ghaffary, 2020), making them easier to handle with a smaller workforce.

Based on the type of matrix used, fiber-reinforced composites are divided into three groups: polymeric composites, cement-based composites, and hybrid composites.

2.2.1.1 Fiber-Reinforced Polymer (FRP)

Fiber-reinforced polymer (FRP) is a composite material made of high-strength continuous fibers such as carbon, basalt, steel, or glass wires as the main load-bearing elements that make CFRP, BFRP, SFRP, or GFRP, respectively. The fibers are responsible for the strength and stiffness and are backed by a polymer such as epoxy resin, unsaturated polyester, vinyl ester, phenolic, and polyurethane resins for binding FRP to the member and distributing the load between the fibers.

FRP is an anisotropic material, which means its properties are different in different directions. If it is loaded in uniaxial tension, the relationship between stress and strain remains linear up to failure without yielding or plastic deformation, indicating a brittle failure. This material is used for improving the flexural, shear, and ductility by even 40%; however, some certain limits should be considered before using it for repair purposes (Alkhardiji, 2015):

- FRP's strength is affected by environmental factors; therefore, it is multiplied with an adjustment factor of 0.85 if used for exposed conditions.
- For a member to qualify for FRP repair, its ultimate strength without FRP should be greater than the stress due to service load in typical conditions. This means that in case of FRP failure, the member should be able to resist the applied load by itself.
- If the strength improvement requirement is higher than 40%, FRP repair is not applicable.
- The compressive strength of existing concrete should be more than 2500 psi to transfer the stress from concrete to FRP safely.

- FRP may need fireproofing, which can increase the cost.

To mitigate shear damage in a girder, FRP is applied to the outer damaged surface using three possible configurations. Externally bonded (EB) technique, near-surface mounted (NSM) technique, and embedded reinforcement (ER).

2.2.1.1.1 Externally Bonded Technique (EB)

The externally bonded (EB) method is when the repair material is attached to the member's external surface using an adhesive material or a fastener. The advantage of the EB technique is that it does not require removing surface concrete or drilling holes into the member, which makes it easy to apply without risking reinforcement exposure. The EB technique can be used in three common forms: complete wrapping, three-sided U-wraps, and two-sided face plies (Andrawes, 2018), as illustrated in Figure 2.3. According to Ghaffary (2020), ACI and AASHTO prefer a complete wrapping method, but since most beams are cast monolithically with the deck at the top, it is impossible to apply complete wrapping.

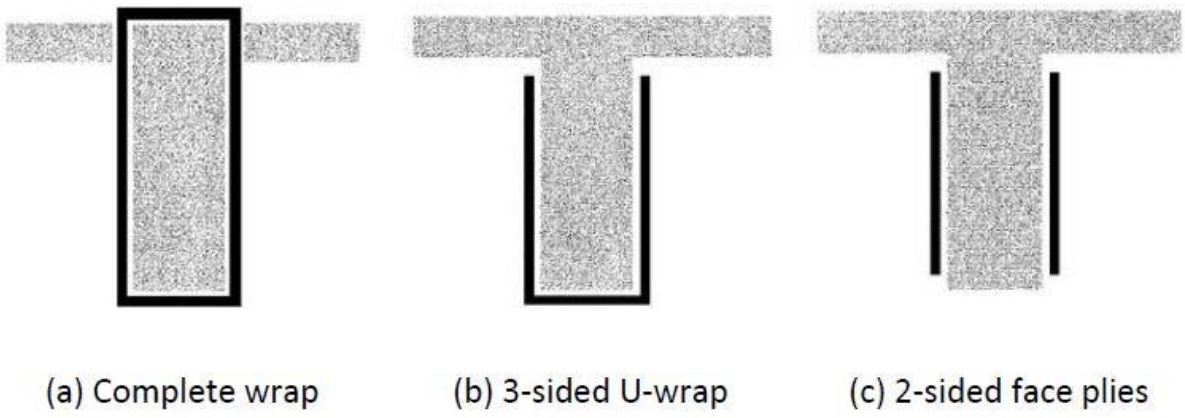

Figure 2.3: Three configurations for FRP application to repair shear damage (Andrawes, 2018)

The FRP repair technique can be passive repair in which the attached sheets do not carry any load up to a certain level of loading, or it can be prestressed before applying to the member. Prestressing changes the behavior from passive to active, increasing the chances of abrupt collapse without warning; therefore, a partial prestress can be a good option without compromising the failure mechanism (Shafei, 2020). Increasing the length of FRP enhances the beam's stiffness with no effect on flexural capacity. For increasing the flexural capacity, the number of FRP layers should be increased (Shafei, 2020). As mentioned previously, FRP failure is mainly brittle, which is due to the formation of flexural cracks that cause debonding. To avoid debonding and to utilize the full capacity, FRP stirrups (or U-wraps) are used to increase the bond between the sheet and the concrete girder. These stirrups are applied perpendicular to the length of FRP in specified intervals. Figure 2.4 shows the U-wrap application for a prestressed concrete girder.

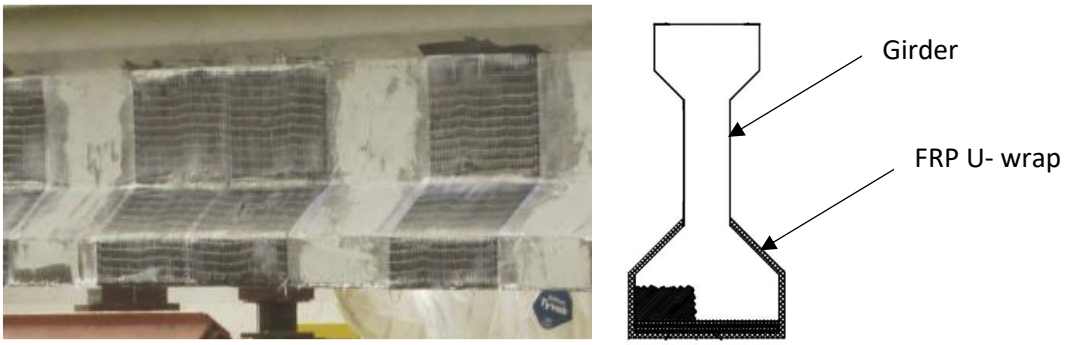

Figure 2.4: U-wraps on a prestressed beam (Shafei, 2020)

2.2.1.1.2 Near-Surface Mounted (NSM) Technique

In the NSM method, FRP bars are embedded in the concrete surface to enhance the member's capacity. This is done by cutting grooves at the concrete surface and attaching the bars in the grooves using filler materials like epoxy or cement grout (Ghaffary, 2020). The bars used have rectangular or circular cross-sections and are typically deformed or sandblasted to increase their bond with the repair surface. There are two advantages of NSM compared to EB. First, a higher bond can be achieved using the NSM method since the material is fully embedded in the repair surface, which transfers more stress to the surrounding concrete. Second, the NSM requires lesser material due to enhanced bond behavior (Harries, 2012). Figure 2.5 shows the steps for the application of NSM bars to a girder's end regions.

Figure 2.5: Application of NSM bars (Andrawes, 2018)

2.2.1.1.3 Embedded Reinforcement (ER)

In the embedded reinforcement method, vertical or inclined holes are drilled upward from the soffit to the top of the beam. After removing the dust from the holes, epoxy is injected to fill them. Then the FRP bars are inserted in the holes, which bond to the concrete through the epoxy resin. Figure 2.6 illustrates the strengthening technique using the embedded reinforcement method.

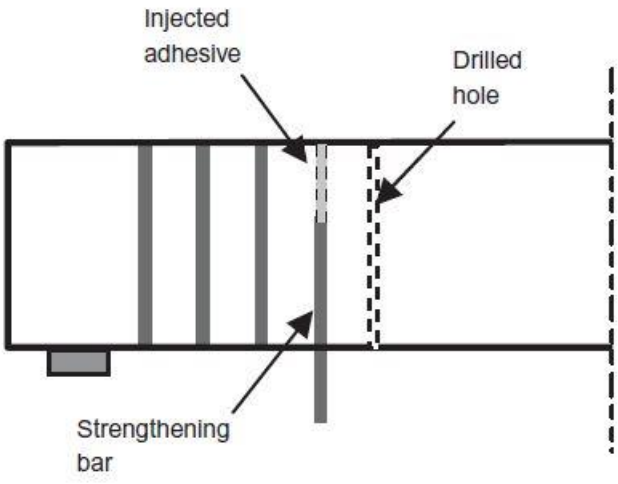

Figure 2.6: Shear repair using the embedded reinforcement method (Valerio, 2009)

2.2.1.2 Cement-Based Composites

Cement-based composites utilize cementitious material instead of epoxy resin and were proposed in the early 1980s. However, this repair material did not gain popularity until the late 1990s. Cementitious materials have several advantages over epoxy resins in providing better fire resistance, possibility for application to wet surfaces, and a good performance against UV radiation (Ghaffary, 2020). The different types of cement-based composites are sprayed concrete, textile-reinforced mortar (TRM), textile-reinforced concrete (TRC), fiber-reinforced

cementitious mortar (FRCM), and mineral-based composites (MBC) (Gangi, 2018; Ghaffary, 2020).

2.2.1.3 Hybrid Composites

As mentioned in Section 2.2.1.1, traditional fiber-reinforced polymer materials exhibit elastic behavior to failure without yielding, giving a brittle failure mode to the member. To avoid abrupt failure, different fiber-based composites can be combined to produce a hybrid material. The hybrid material can have a higher ductility and yield like steel. Examples of such materials are CFRP, CFRP-honeycomb, and GRFP-honeycomb (Mosallam, 2015).

2.2.2 Steel

Steel has been used for the repair of concrete elements for decades. It is used in different forms such as rods, bars, tendons, plates, strand splice systems, and steel jackets. Figure 2.7 shows an example of steel rods used for improving the shear behavior of a girder. Repair began by removing the loose concrete and filling the missing parts using rapid setting cement. Subsequently, the cracks were filled by injecting epoxy to supply a level of stability and stiffness. Once the epoxy had cured, the surface was smoothened, and FRP sheets were applied. During the curing of FRP, five sets of steel rods (stirrups) were mounted in conjunction with steel angle sections on each end of the girder as shown in Figure 2.7 (Ramseyer, 2012). Rods act similar to the internal shear stirrups. It is reported that the surface-mounted rods helped for strength recovery.

(a) Beam after steel repair (b) Steel repair and support

Figure 2.7: Shear damage repair using surface-mounted rods (Ramseyer, 2012)

2.2.3 Ultra-High Performance Concrete (UHPC)

Most repair failures are due to incompatibility between the repair material and substrate, resulting in debonding and cracking at the interface (Angel, 2012). Besides a better bond, a good repair material should have higher strength, ductility, and durability. Considering the mentioned criteria, UHPC is one of the best available materials for this purpose.

UHPC is a cementitious material composed of cement, supplementary cementitious materials (e.g. silica fume, silica flour, fly ash), fine sand, steel fibers, superplasticizer, and water. The water-cementitious materials ratio for UHPC is typically below 0.25, which, based on Abram's rule, is one reason for its high compressive strength (Rao, 2001). According to the U.S. Department of Transportation/Federal Highway Administration (2011), the main characteristics of UHPC are its high compressive strength that reaches 21.7 ksi (150 MPa), high pre-and post-cracking tensile strength greater than 0.72 ksi (5 MPa), and enhanced durability due to its high density and discontinuous pore structure which prevents liquid ingress. However, the above threshold numbers, especially for the compressive strength, can be found differently in other

resources. The superior mechanical and durability characteristics make UHPC an optimal material for a thin layer repair to prestressed girders providing additional strength, ductility, and durability.

So far, most UHPC utilized in construction has been in the form of proprietary mixtures produced by a limited number of manufacturers. Multiple mix designs have been developed for UHPC mainly because the proportion of ingredients changes significantly for different sizes of the particles based on their availability, which makes mix development by trial batches a common approach for mixture development.

UHPC can fill complex formwork due to its self-consolidating property, which is essential for ornamental and aesthetic purposes. Also, it is a common material for precast bridge connections due to its shorter development length requirement (Yuan, 2016). In some parts of the world, construction of whole bridges using UHPC is getting more common (Gunes, 2012) as it provides more strength which allows for adopting smaller sections while decreasing the self-weight of the structure. However, it should be noted that it is only cost-efficient to use this material where it is necessary since UHPC is significantly more expensive than conventional concrete.

UHPC can gain strengths of up to 9.4 ksi within around 48 hours. The high curing rate makes it possible to reopen a bridge shortly after repair (Angel, 2012). The post-cracking tensile strength of UHPC is its unique feature that provides equal or greater tensile strength compared to the cementitious matrix even after the formation of cracks (FHWA, 2011).

Lab experiments have been conducted on UHPC for the repair of steel girder end regions. In a research project by Zmetra (2017) to examine the suitability of UHPC to repair the end region of steel bridge girders, shear studs were used on the web and bottom flange of a damaged

girder's end region to connect a UHPC repair to the steel girder (Figure 2.8). This repair method was reported to provide shear capacity equal to or greater than the original member while protecting the end region from further corrosion, keeping the ductile failure mode unchanged, and resulting in a negligible increase in dead load as the weight of the repair is directly carried by the bearing without changing flexure or shear stresses. Figure 2.9 shows the post-repair failure for the different sections of the steel girder.

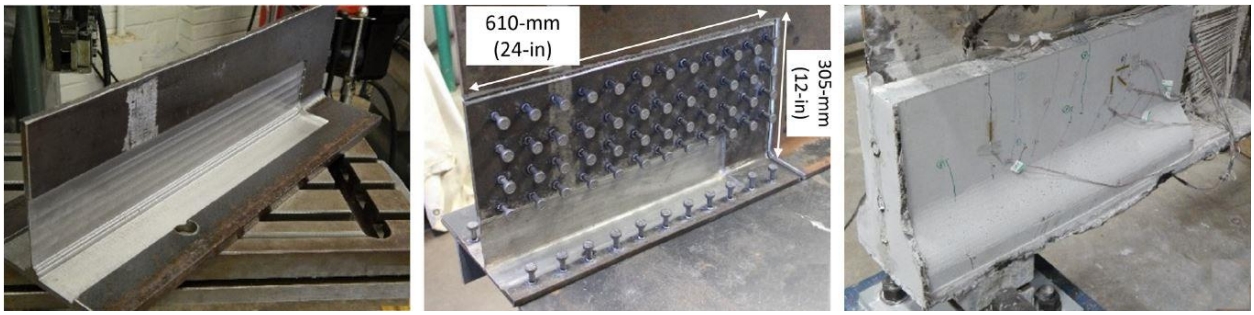

(a) (b) (c)

Figure 2.8: Uniform section loss applied to the girder, (b) welded stud arrangement on the repaired girder, and (c) UHPC repair panel (Zmetra, 2017)

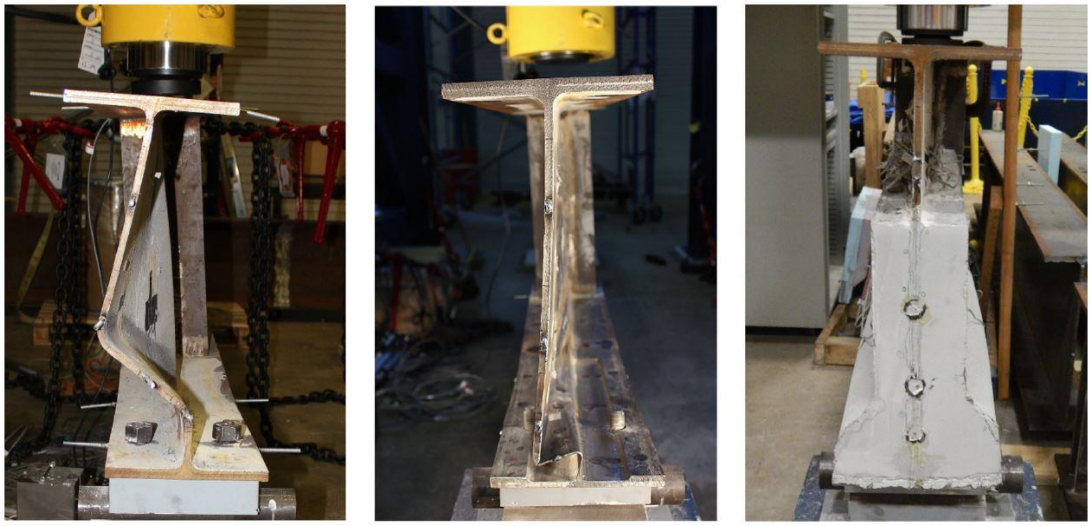

(a) (b) (c)

Figure 2.9: The final condition of the end cross-section after testing for the: (a) undamaged girder, (b) damaged girder, and (c) repaired girder (Zmetra, 2017)

In a research project by Shafei (2020), a long bulb-tee-C- shaped beam with 115 ft length was used to evaluate the performance of a UHPC patch to rehabilitate end region damage. After removing the highly-dense shear reinforcement region at the ends, the beam was cut to eight mirror-image pieces of each 11 ft (shown in Figure 2.10) to ensure the shear failure of the beam.

(a) (b)

Figure 2.10: (a) Cut beam segment marked for controlled damage and (b) loading setup for testing repaired beam segment (Shafei, 2020)

The web of the girder was thinned by approximately 30% to represent shear damage at the location marked in Figure 2.10. Forms were put along the girder's sides with weep holes at the top to avoid entrapped air and were wetted before casting to reduce water absorption. After the UHPC was poured and hardened, the beams were tested with the loading arrangement shown in Figure 2.10 (b). It was reported that the patch demonstrated a good bond with the girder, with substrate concrete failure occurring before the UHPC patch failed.

In research regarding fatigue behavior of UHPC in the tensile flexure region, a number of rectangular reinforced concrete beams were cast and repaired with a 10 mm thin strip of UHPC. The beams were loaded to 70%, 80%, and 90% of the maximum load of the control beams and then tested under fatigue loading. The fatigue behavior of the UHPC repaired beams, including both the number of cycles and the stiffness, was better than control beams, which indicates UHPC is an excellent repair material for rehabilitating flexural damage as well shear damage (Murthy, 2018).

2.2.4 Fiber Reinforced Self-Consolidating Concrete (FR-SCC)

Self-consolidating concrete (SCC) can be defined as a "highly flowable, non-segregating concrete that can spread into place, fill the formwork, and encapsulate the reinforcement without any mechanical consolidation" (Kassimi, 2014). SCC was first developed in Japan in the 1980s as structures were heavily reinforced to resist seismic loads, and there was a peak demand for a flowable concrete to fill complex formwork with congested reinforcement without or with least mechanical vibration, decreasing construction time, and giving a smooth surface finish. Workability changes were only useful if there was no negative impact on concrete strength. Therefore, self-consolidating concrete was developed with increased workability but without

changing the water-cementitious materials ratio. This is mainly accomplished by introducing high range water reducing admixture (HRWRA) (Kassemi, 2013), properly proportioning the cementitious materials and aggregate, or adding viscosity modifying admixtures (VMA) to the concrete.

Fiber-reinforced SCC (FR-SCC) is made of cement, sand, coarse aggregate, water, admixtures, and fibers. The addition of fibers can improve the different properties of the concrete, like post cracking response, energy absorption capacity, and reducing the possibility of cracking due to shrinkage.

Using fibers can impact both the workability and mechanical properties of the concrete, depending on fiber's physical, mechanical, and geometrical characteristics (Kassemi, 2013). For example, steel fibers enhance the mechanical properties, whereas polypropylene fibers are used primarily to control cracks due to plastic shrinkage (Kassimi, 2014). Despite improving flexural and shear behavior due to fiber addition, they can have a negative effect on the workability of the concrete mainly because of friction between fibers and coarse aggregate. This necessitates some adjustments like reducing the length of fibers, changing nominal aggregate size, and decreasing the overall volume of coarse aggregate compared to the previous mixture with lesser flowability. Experiments have shown that good workability can be achieved with up to 0.5% V_f (fiber volume) (Kassimi, 2014); however, greater V_f hinders self-consolidating properties (Khayat, 2014).

One of SCC's major challenges is segregation, which is uneven distribution or settling of aggregate particles in the mix. According to Junwon Seo (2017), three main factors influence the segregation resistance of SCC: 1) the viscosity of cement, 2) the difference between specific densities of cement and aggregate, 3) the particle size of the aggregates. Mixture segregation can

increase the chances of blockage during its flow and decrease the bond between the repair material and both reinforcement and substrate due to bleeding (Kassemi, 2013).

A combination of advantages of both SCC (high strength and workability, economy) and fibers (high ductility, crack control, and higher tensile strength) can provide an optimal repair material that outperforms conventional concrete. However, remarkable mechanical properties cannot guarantee that it will be a successful repair material unless experimentally proven (Abdulhameed, 2018).

The initial case study of SCC as a repair was performed in 1996 for parking garage girders in Quebec. SCC was used to repair underneath and on the sides of a 20 ft beam with substantial corrosion damage around the joint (Abdulhameed, 2018). A series of experiments conducted on beams repaired with FR-SCC concluded that FR-SCC provides better compressive strength with enhanced overall structural performance (up to 2.6 times higher) than the beam made with conventional vibrated concrete. Results showed that the fibers could replace 50% of reinforcement supposed to be provided for the tension repair zone without affecting the structural performance. In terms of chloride ion permeability and capillary porosity, the durability of FR-SCC was also shown to be better than conventional vibrated concrete (Kassemi, 2013).

In a research project by Abdulhameed (2018), ten full-scale beams were cast to study the flexural behavior of FR-SCC as a repair material. Two of the beams were built to the specified dimensions to obtain the baseline values for comparison (Figure 2.11(a)), while the remaining eight were built with exposed tension-steel as hatched in Figure 2.11(b). The beams were tested with third-point loading to observe the behavior of the repair under pure flexure. Despite a lower ultimate load for the repaired beams, the flexural cracking loads displayed significant improvement

compared to the control beams. Table 2.2 shows the cracking and ultimate loads for the tested beams.

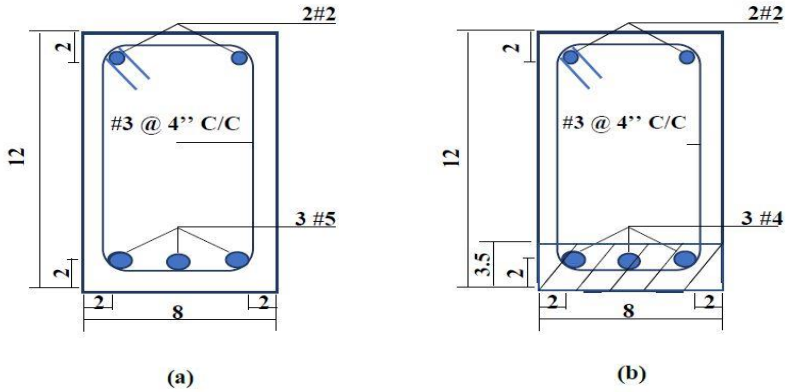

Figure 2.11: (a) Undamaged control beam and (b) damaged beam to be repaired with FR-SCC (all dimensions are in inches) (Abdulhameed, 2018)

Table 2.2: Cracking and Ultimate Loads for Beams Tested by Abdulhameed (2018)

Beam	Main reinforcement rebar size (#)	Cracking load (lb)	Increase in cracking load* (%)	Ultimate load (lb)
Control beam 1	5	4700	-	32000
Control beam 2	5	4600	-	30000
35SL25S	4	5500	18.3	24000
35SL15P	4	4900	5.4	22700
10SF25S	4	5500	18.3	26200
10SF10P	4	5500	18.3	23000
35SL50S	3	5700	22.6	16000
35SL20P	3	5100	9.7	15492
10SF50S	3	6000	29	19000
10SF15P	3	5700	22.6	15500

*Note: $Increase\ in\ cracking\ load = \frac{Composite\ flexural\ strength - substrate\ flexural\ strength}{substrate\ flexural\ strength}\ x\ 100$

The notation in Table 1.2 uses SL for slag, SF for silica fume, and P for polypropylene fibers with the preceding numbers indicating the percentage of each material. For example, 35SL25S means 35% slag + 0.25% steel fibers. It was further reported that while testing, the failure was at midspan, indicating a good bond between the substrate and repair. The bond strength was found to be directly proportional to the fiber content of the mix. Effects of repair thickness and compressive strength of the repair material on crack control were significant, while the area of tension steel and effective depth to the main steel were the controlling parameters for the ultimate load (Abdulhameed, 2018).

A recent study completed at the University of Oklahoma (Choate 2018) evaluated the ability of FR-SCC to repair a severely damaged, full scale, AASHTO Type II girder. The girder was removed from the I-244 bridge over the Arkansas River and transported to the Donald G. Fears Structural Engineering Laboratory in Norman, OK. Each end of the girder was then tested in shear to failure. Subsequent repairs to the girder involved extensive concrete removal, repairs to internal reinforcement, and placement of an FR-SCC mixture developed in an earlier research project at the University of Oklahoma (Wirkman 2016). This FR-SCC mixture incorporated macro polypropylene fibers and a shrinkage compensating cement. Subsequent testing revealed that the repairs restored 83% of the original tested capacity of the girder and 116% of the required factored load capacity for the bridge structure (Choate 2018). Wirkman (2016) conducted small-scale and large-scale flexural tests of composite beams cast using FR-SCC as a repair material. These tests showed similar performance of the repaired beams when compared to control monolithic beams cast with conventional concrete.

2.2.5 Magnesium-Alumino-Liquid Phosphate (MALP) Concrete

MALP concrete is a relatively new material for concrete structure repair, only available since 1990. It contains a pre-packed magnesium-alumino-aggregate dry powder with a mono-aluminum-liquid phosphate activator. This material can be used to repair horizontal, vertical, and overhead surfaces with a rapid strength gain that brings the structure back to service faster. Once the MALP concrete is cast, it expands and creates an excellent bond with the substrate and provides very low permeability for chloride ions. It also stops steel corrosion by converting iron oxide to metal phosphate, which coats the reinforcement and prevents further corrosion (Concrete repair products, 2020). MALP concrete gains compressive strength rapidly with up to 4000 psi within 1 hour, 4500 psi in 3 hours, and 6000 psi in 24 hours (TSP2, 2014). It does not exhibit shrinkage cracks, with a ±0.05% change in length after 28 days (Concrete repair products, 2020). For improving the mechanical characteristics of MALP concrete, fiber-reinforced polymer (FRP) microfibers can be added to the dry mix (TSP2, 2014). MALP concrete has been used to repair many bridges in New York, and these bridges are under examination to determine the long-and short-term behavior of the repair material.

2.3 End Region Failure Mechanisms

There are multiple possible ways for prestressed concrete beams to fail. The original and repaired beams can fail in shear, flexure, strand bond loss, or a hybrid mechanism. According to Naji et al. (2016), a prestressed girder's failure behavior at the end regions can be classified into four types. These failure types are bond-shear, bond-flexure, flexure-bond, and bond-shear/flexure failure. Based on the research, bond failure can occur at lower load levels than the

nominal shear or flexure capacities. Figure 2.12 shows the crack pattern and conceptual structural load vs. deflection behavior for each type of failure listed. Also, a brief of every failure type is explained in the following sections and is further elaborated with Figure 2.13 and a flowchart.

1. *Bond-shear failure:* The failure starts with inclined cracks in the web and the bottom flange at the end regions. When the bottom flange cracks intercept the strands, it causes bond loss between the concrete and the strands. This bond loss causes a premature shear failure of the member. The failure is most probable when the ratio of shear span to effective depth (a/d) is less than 3.
2. *Bond-flexure failure:* For bond flexure failure, the initial cracks may not cause strand slip; however, after the member loses its stiffness due to cracks, the load-deflection relation becomes non-linear. Bond loss occurs after cracks further increase and intersect the strands. The slip causes the cracks to open wider and increases the flexural strains. The final failure is by crushing the top flange or the deck. Bond-flexure failure typically occurs when the a/d ratio is greater than 2.5.
3. *Flexure-bond:* This failure is very similar to the conventional flexure failure, except that there is a slight strand slip close to the peak load. Flexure-bond failure happens when the a/d ratio is greater than 2.5.
4. *Bond-shear/flexure:* Bond-shear/flexure is a hybrid mode of failure in which bond loss is the primary failure and is followed by both flexure and shear failure. Bond-shear/flexure failure typically happens at an a/d of 2.5 or less.

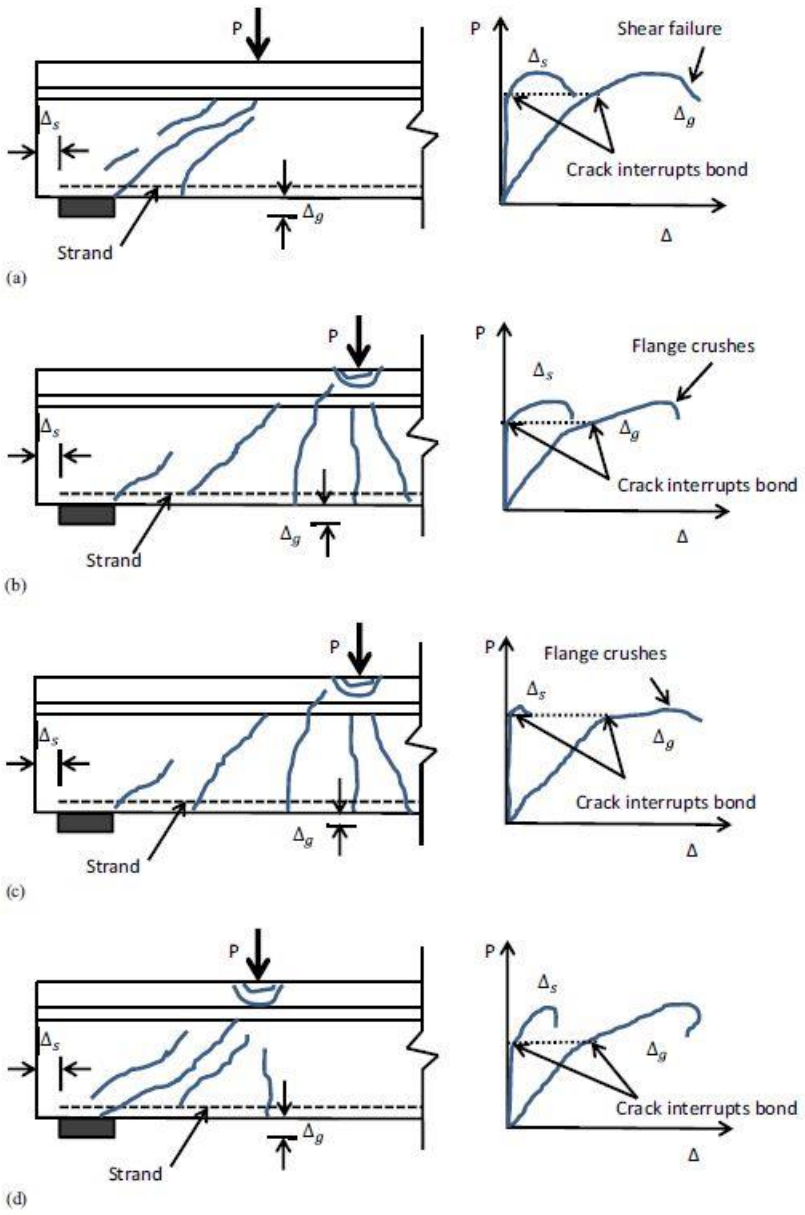

Figure 2.12: Typical crack pattern and structural behavior for: (a) bond shear; (b) bond-flexure; (c) flexure-bond; (d) bond-shear/flexure (Naji, 2016)

Figure 2.13 presents a flowchart developed by Naji (2016) for categorizing bond-loss failure in prestressed concrete beams. The chart was used in the research described in this thesis to identify the failure type for the original and repaired beams.

Failure mechanism analysis helps distinguish different types of failure for a prestressed girder loaded in flexure by relating the vertical deflection under the point load to the strand slip. This concept is necessary to ensure that an accurate capacity is calculated for situations where bond loss may reduce the strength of the girder. It also helps to comment on the effect of repair for changing the failure type of the girder. For instance, if a bond-shear behavior of an unrepaired member changes to a bond-flexure behavior after repair, then the repaired beam's behavior is similar to the unrepaired beam with the point load farther from the support than its initial test. In other words, understanding the failure mechanism can help in deciding about the repair dimensions to get the desired failure type.

2.4 Summary

In summary, the literature review discussed previous research regarding different repair materials like polymeric materials (FRC), steel, and different types of concrete (UHPC, FR-SCC, MALP) to repair the end regions of prestressed girders. The results indicate that they provide increased stiffness and strength for the repaired member. The major limitation of all the previous repairs was that they were primarily intended for minor and moderate damage, not for severe. The repairs examined in previous research were mainly designed to restore the design capacity. The research described in this thesis aimed to cover all three types of damage, including severe damage, and is expected to increase the stiffness and provide a much higher load-bearing

capacity than the design load. The repair also encapsulates the member and protects it from further deterioration by providing a solid and impermeable barrier around the repair zone.

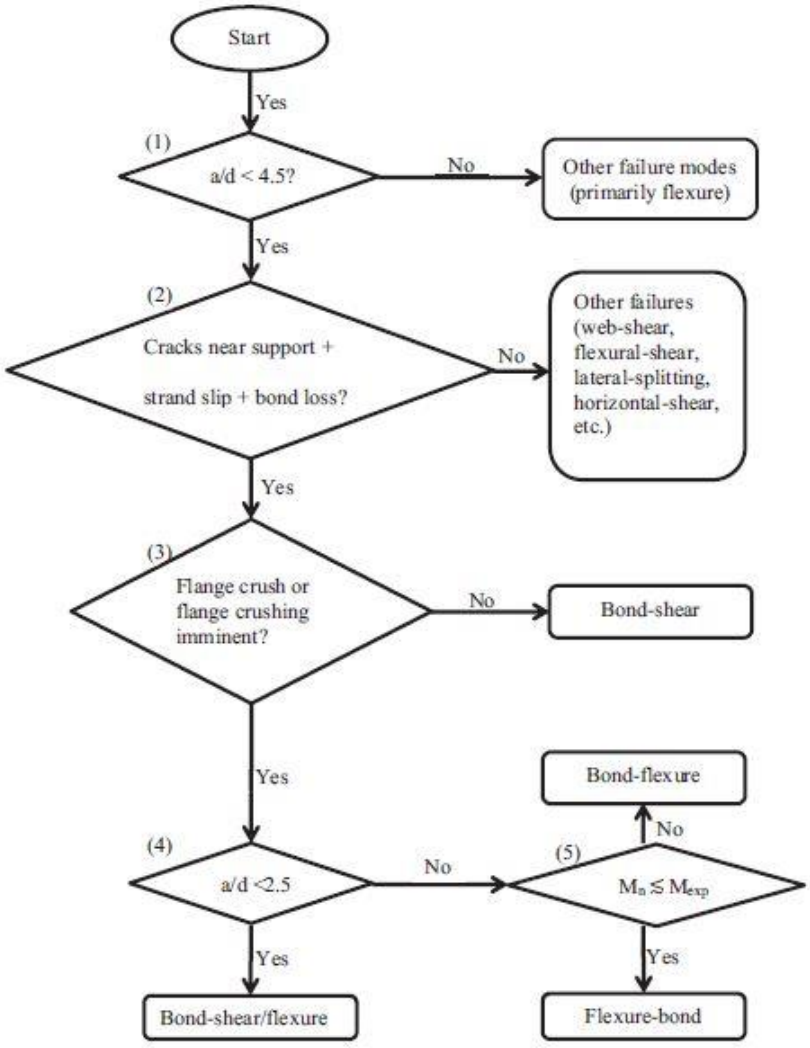

Figure 2.13: Flowchart for characterizing types of bond-loss failure (Naji, 2016)

Chapter 3: Methods and Approaches

In this chapter, the methods used for the construction of the beam specimens and procedures used for testing are discussed. For this work, six 18 ft long approximately half-scale AASHTO Type II girder specimens were constructed using self-consolidating concrete (SCC) for the girders and ordinary ODOT Class AA bridge deck concrete for the decks. The girders were initially loaded at 3.5 ft from the end on a simple span configuration to induce a shear failure. The damaged region was then encapsulated using UHPC, FR-SCC, and MALP concrete to restore the lost shear capacity. The thickness of the repair differed for the UHPC, but the same thickness was used for FR-SCC and MALP. Otherwise, the same dimensions were used for all repairs. After the repair materials gained strength, the beams were tested using the same loading arrangement as the first test, and the failure load was compared to the original girder. The results provide an assessment of the efficiency of the tested materials for shear repair purposes.

3.1 Prestressed Girder Design and Construction

3.1.1 Specimen Design

At this stage, the cross-sectional geometry, dimensions, strength, and material type were determined to provide the best representation of actual bridge girders. The SCC mix design was used from the work of a previous research student (Mayhorn, 2016), with the expectation to provide a minimum compressive strength of 4000 psi within the first 24 hours after casting for the prestress release and 8000 psi after 28 days. The mix proportion for the SCC is shown in Table 3.1.

Table 3.1: SCC Batch Quantities

Materials	Quantity
Portland cement (Type I/II) (lb/yd^3)	851
Water (lb/yd^3)	314.9
Fine Aggregate (lb/yd^3)	1459
Coarse Aggregate (lb/yd^3)	1372
High Range Water Reducer (Glenium 7920) (oz/cwt)	6

Note that in the above table, oz/cwt means fluid ounces per cement weight. This means that for each 100 pounds of the combined cementitious materials (e.g., cement, silica fume, Komponent, fly ash), one ounce of HRWR was used. Table 3.1 is based on the saturated surface dry condition of the sand and coarse aggregate. This mix was designed for 4000 psi after 24 hours and more than 8000 psi after 28 days.

Dimensions of the beam specimens, including the composite deck section, are shown in Figure 3.1. These dimensions are based on an approximately half-scale AASHTO Type II girder and a deck section that provides the same moment capacity as the full half-scale deck. Two Grade 270 low relaxation strands having 0.52 in. diameter (1/2 in. special) were placed centered 2 in. from the bottom of the bottom flange for applying prestressing force, as shown in Figure 3.2. During design, it was found that stress at the girder top at the midspan exceeded the tension limits given by ACI 318-19 section 24.5.3 at prestress release. To counter the tension force and satisfy the code requirements, two No. 5, Grade 60 reinforcing bars were provided in the top flange of the beam, which was designed to resist the entire tension force. For shear reinforcement, double No. 3 C-shaped stirrups were used along with four stirrup spacing intervals in the 18 ft length of the girder with extra projection at the top of the beam for deck placement, as shown in Figures 3.2 and 3.3.

The composite deck section had dimensions of 9 in. x 4.625 in. which was made of ordinary ODOT Class AA bridge deck concrete supplied by a local ready-mix company and was cast after the beam concrete reached a minimum of 28 days of age. Therefore, the elastic prestress losses were calculated based on non-composite section properties, while long-term losses were calculated for both before casting the deck and after the deck was cast to the testing day. Four No. 5, grade 60 reinforcing bars were placed in the deck to provide sufficient flexural strength and avoid shrinkage cracks.

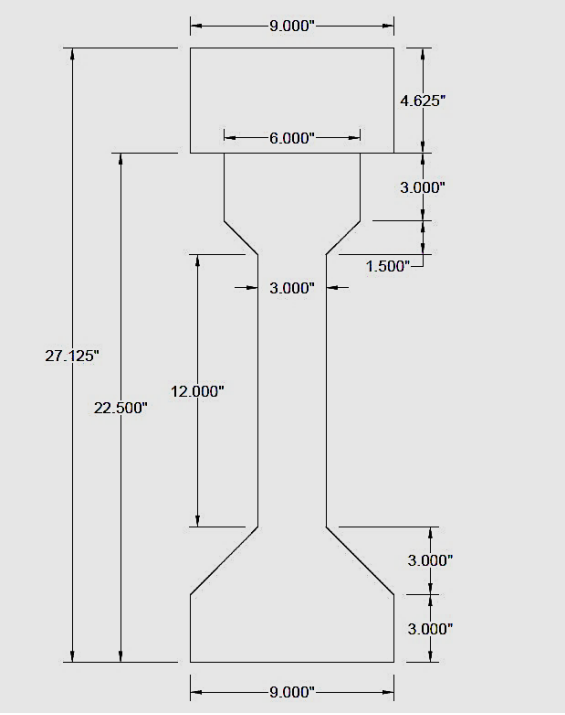

Figure 3.1: Beam cross-section

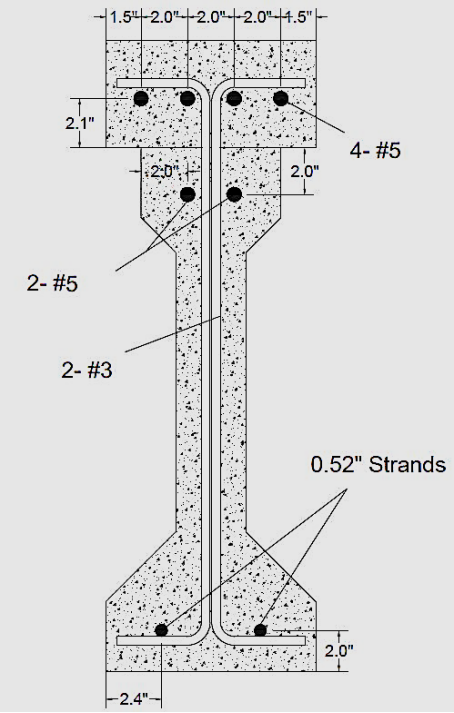

Figure 3.2: Reinforcement details

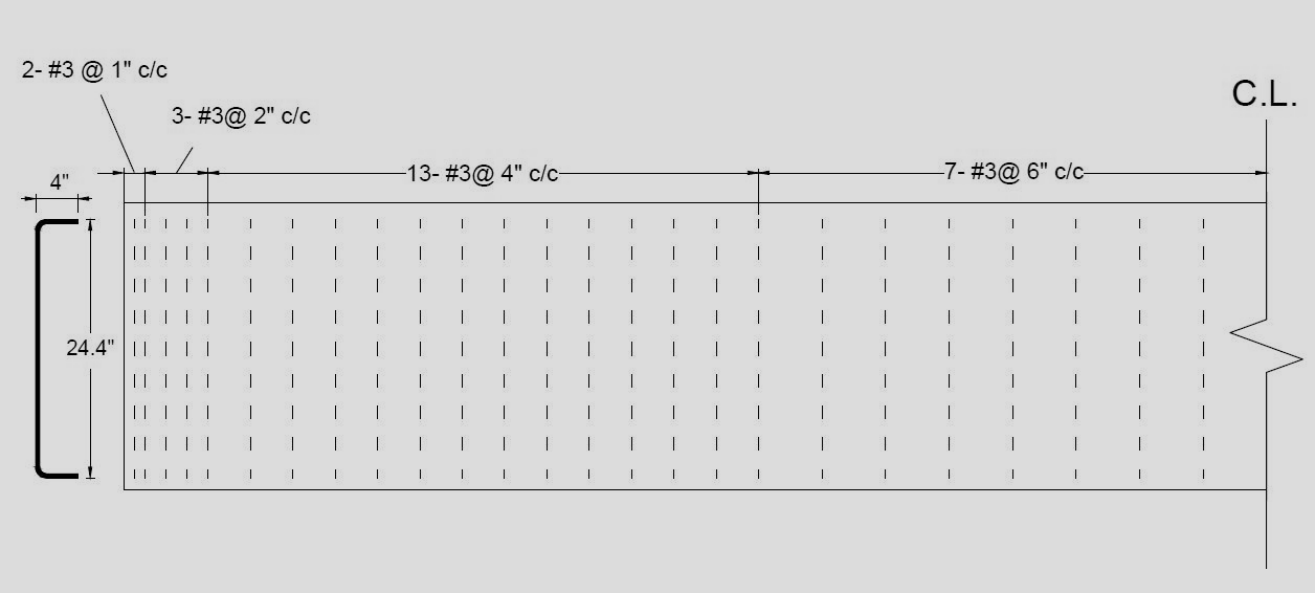

Figure 3.3: Stirrups distribution along the half-length of the girder

3.1.2 Beam Construction

All girders were cast at Fears Structural Engineering Lab using the available prestressing bed consisting of two steel abutments anchored to the strong floor. Due to space constraints from other testing in the lab, only one beam could be constructed at a time. Construction of the girders started with cutting and bending the shear stirrups. The stirrups were then tied to the top steel to create a reinforcement cage. After making the reinforcement cage, the prestressing bed was leveled and oiled to avoid concrete sticking to the bed while hardening. Then the cage was placed on the prestressing bed, and the steel beam form was fixed on one side. At this stage, the prestressing strands were put in the cage and were carefully placed to avoid contact with the oiled bed. Figure 3.4 shows the prestressing bed after placement of the reinforcement cage and prestressing strands. The live end is defined as where the strands were pulled for tensioning and the dead end as where strands are only anchored.

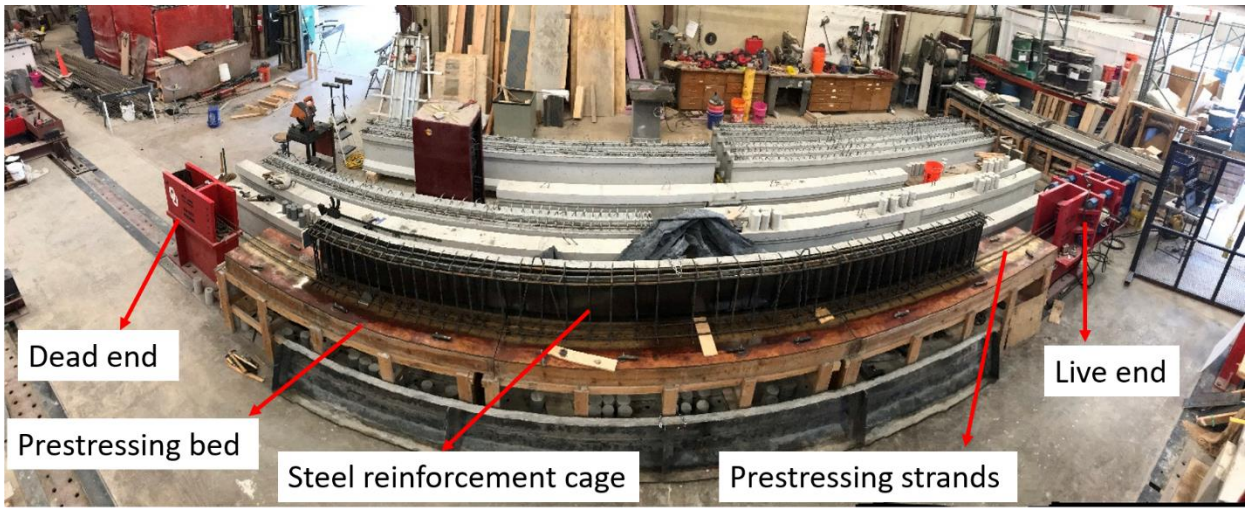

Figure 3.4: Panoramic picture of the prestressing setup

The strands were cut approximately 34 ft long to provide an extension beyond the prestressing bed at each end for the chucks to grip for proper application of pre-tensioning. Chucks were then placed on the strands at abutments to hold the strands in place for tensioning, and strands were marked to notice their slip in the chucks when they were tensioned. Measurements were taken between the mark and the back of the chuck before and after tensioning. A 50-kip capacity through hole load cell was attached to one of the strands between the chuck and abutment at the live end of the prestressing bed to show the instantaneous amount of applied load to the strands, as shown in Figure 3.5.

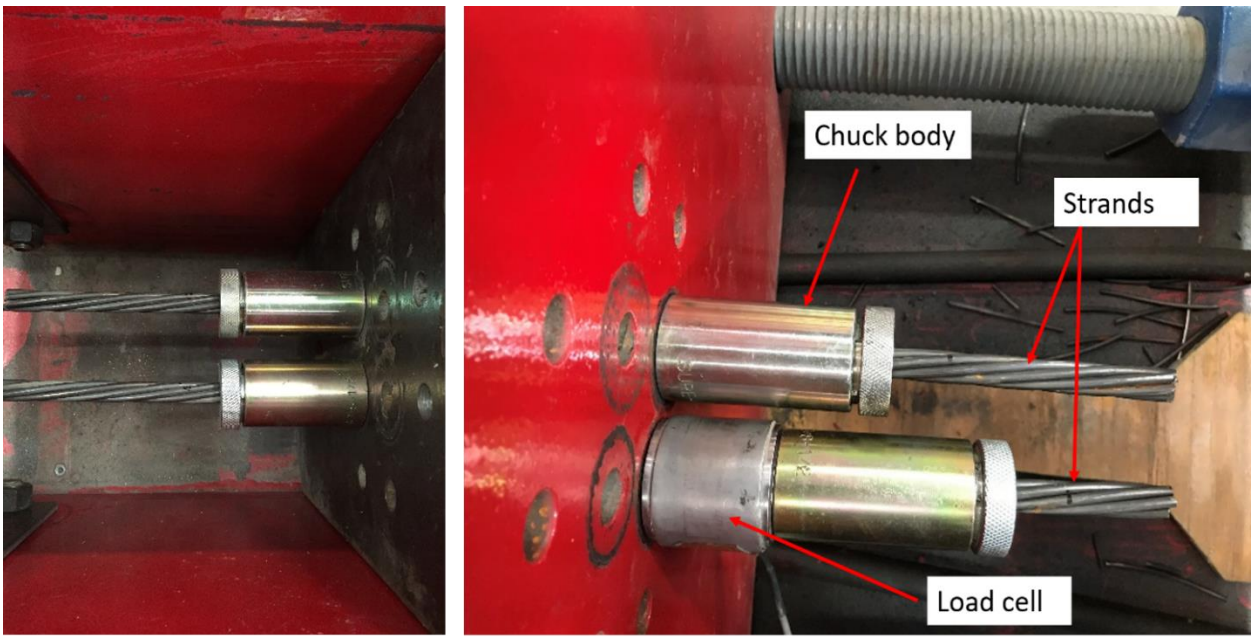

(a) (b)

Figure 3.5: Chuck assembly for anchoring the prestressing strands at the (a) dead-end, and (b) live end

The elongation of the strands was also noted using a ruler attached at the abutment with provision for chuck slip and strand sag to ensure the load cell was working properly and to avoid

overstressing the strands. Strands were stressed to 75% of their ultimate strength (f_{pu} =270 ksi) plus approximately 1.5% extra to count for minor anchor slip. The strain for applying the target stress (0.75 x f_{pu}) in the strand is 0.7%, producing 3.5-4 in. elongation over the prestressing bed length. The strands were tensioned by applying a steady load to the large plate on the live end until the desired load was reached. The plate was then held in place using large nuts. After prestressing, the reinforcement cage was checked to make sure it had not moved during the prestress application, and adjustments were made if required. Figure 3.6 shows the completed reinforcement cage after prestressing.

Figure 3.6: Reinforcement cage for a typical girder immediately after prestressing

Next, the other side of the steel form was put in place, and concrete was cast. Concrete was mixed using a large rotary mixer at Fears Lab and was transported to the beam using a concrete transfer bucket. The SCC mix used for the beams was prepared in the proportion specified in Table 3.1. The coarse aggregate used for the mix was a 3/8 in. limestone aggregate,

and the fine aggregate was a washed concrete sand. The order used for mixing the components is as follows:

- Before adding the materials to the mixer, add half of the High Range Water Reducer (HRWR) to the water prepared for the batch.
- Wet the mixer.
- Add all the aggregate and sand to the mixer.
- Add half of the water prepared for the batch and mix it for at least 1 minute.
- Add the cement and gradually pour the remaining water evenly over the mixture.
- Add the remaining half of the HRWR.
- Mix all the materials for 2-5 minutes.
- Add additional HRWR if necessary to achieve the desired flowability

For each beam, nine 4 in. x 8 in. concrete cylinder specimens were prepared for compressive strength testing. Three of them were tested after twenty-four hours to determine the concrete release strength, f'_{ci}, and to ensure that the strength was high enough for prestressing release. Three more were tested for the 28-day compressive strength, f'_c, and the final three were tested on the initial load test day. The slump flow values were also noted for each beam batch to ensure the mix had adequate workability for the compaction requirements of the girders.

After 24 hours, almost all compression tests indicated a higher f'_{ci} than 4000 psi, which was deemed satisfactory, and the prestress force was transferred to the beam by loosening the nuts and allowing the hydraulic pressure to release gradually. Just before releasing the prestressing strands, the value of applied stress was noted based on the load cell readout, which

was later used as the jacking force (f_j) in analysis calculations. The same work cycle described in the previous section was used for all six beams.

After 28 days, the formwork for deck placement was constructed, as shown in Figure 3.7. Based on the design, reinforcement was added to the deck, and the tops of the beams were wetted with water spray and the deck sections were cast using ordinary ODOT Class AA concrete obtained from Dolese Bros. with a different compressive strength than the girders. The concrete was cast for all six beams at the same time along with 18 cylinders of 4 in. x 8 in. dimensions for determining the compressive strength on the test day. The beam concrete was vibrated throughout the length to remove the air and consolidate the concrete. After casting, the deck concrete was covered with plastic, and burlaps placed on the top of the decks were regularly watered for 7-days to ensure proper curing. Eighteen 4 in. x 8 in. cylinders were cast from the overall deck concrete mix to determine the actual deck concrete strength for 28 days and test days for each of the beams.

(a) (b)

Figure 3.7: (a) Deck formwork and (b) deck concrete casting

3.2 Initial Testing of the Girders

Since the objective of this research was to repair shear cracks in the girders, each girder was initially loaded to failure to provide induced shear damage for repair. Each girder was tested on a simply supported span with a single point load applied using a load frame and hydraulic cylinder. The beam was supported on neoprene bearing pads at each end, as shown in Figures 3.8 and 3.9. While applying the point load, the pads undergo some amount of deflection; however, its value is neglected in the calculations.

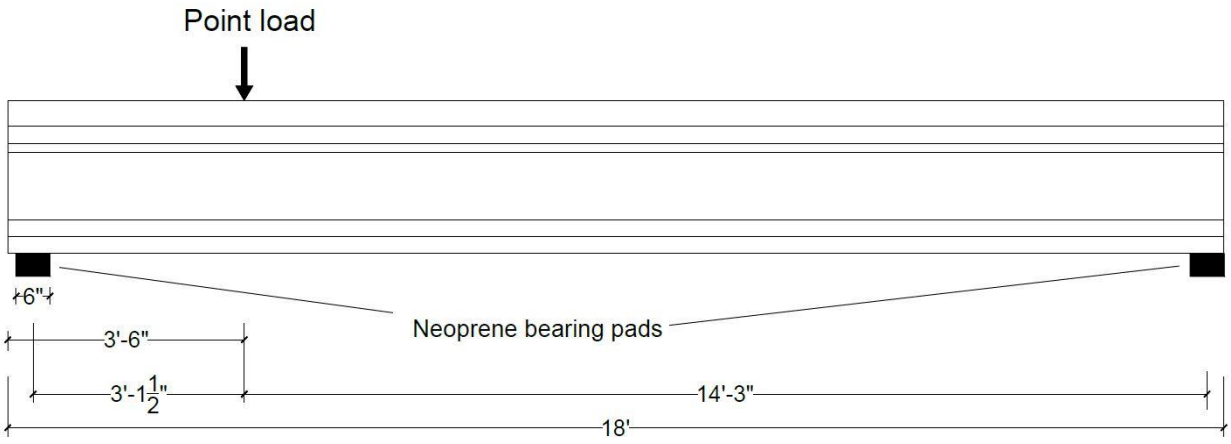

Figure 3.8: Initial test load setup

Before testing, the girders were analyzed to determine the location of the point load application that causes cracks in shear before flexural failure. A point 3.5 ft from the beam end was chosen for this loading. During each test, four linear voltage differential transformers (LVDTs) were attached to the exposed portion of each strand (two at each end) and used to measure the strand slip, which was used to determine if a bond failure contributed to the shear failure of each beam. Two-wire potentiometers (wire-pots) were used to measure the vertical deflection below the point load, and a load cell was used to record the applied loads.

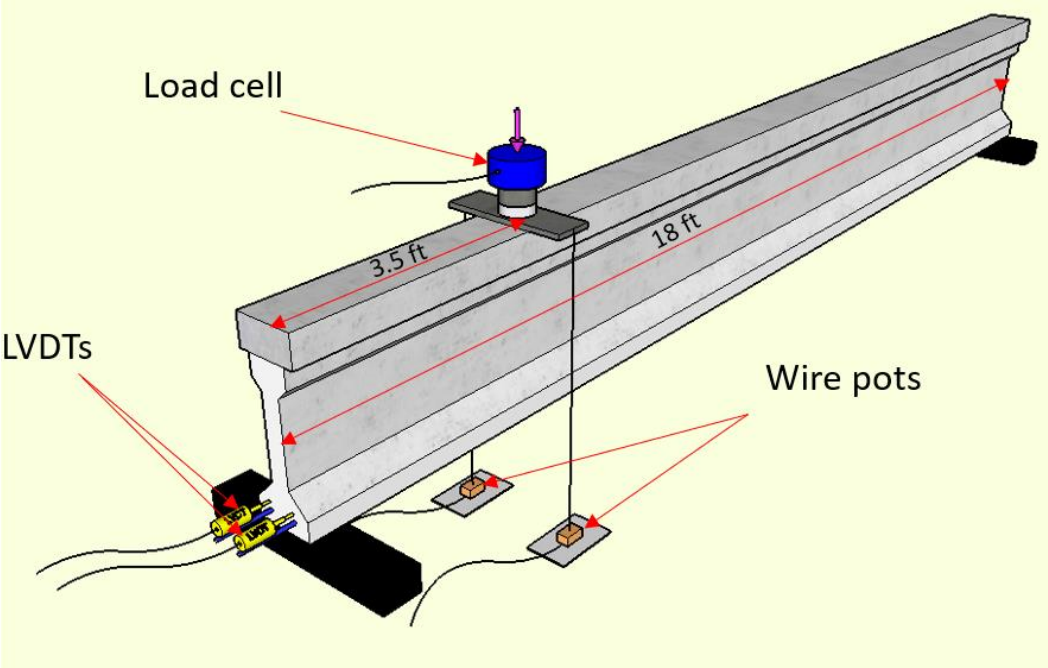

Figure 3.9: A Sketchup model of the initial load test setup

The load testing setup showing the sensors is presented in Figure 3.10. All sensors were connected to a single data acquisition system to collect the data. The beams were then loaded incrementally until the formation of shear cracks propagating from the bottom flange through the whole web and, in some cases, even to the top flange. Cracks were marked on the beam after each 5 kips load increment. With the formation of cracks, the strands' bond in the transfer zone was also reduced, causing the strands to slip and further increase the cracks' size. The loading was stopped after achieving a noticeable deflection, significant strand slip, or a halt/drop in load cell readings.

After removing the point load, tracing paper was used to document the cracks on both sides of each beam's damaged end (Figure 3.11), which were superimposed to the repaired beams once tested to failure. This comparison was intended to develop a relationship between the cracks of both the original member and repair material.

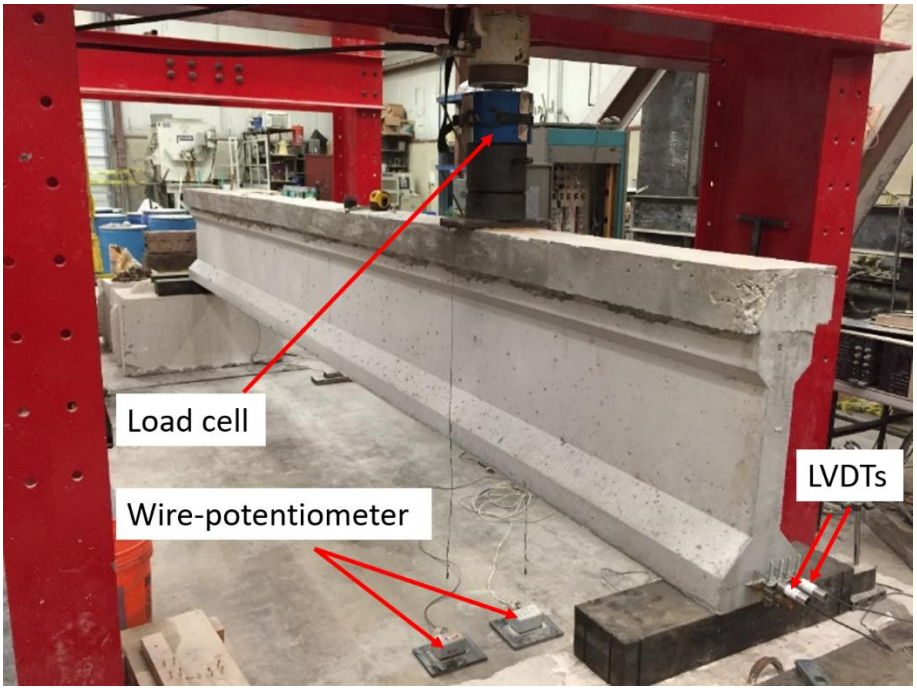

Figure 3.10: Uncracked girder with the test setup

Figure 3.11: Tracing paper on one side of the cracked girder to copy the cracks' location

3.3 Repair Procedure

After the girders were tested to induce damage, the end was repaired to restore the lost capacity using an encapsulation with UHPC, FR-SCC, or MALP concrete on the section between the beam end and the point load location (3.5 ft from the end). One of the main challenges for concrete repair materials is their bond with the parent structure. Two techniques were used to increase the bond between the girder and the repair material. First, the girder's surface throughout the 3.5 ft repair length was roughened using a grinding disk on an angle grinder. The roughened surface was then cleaned using compressed air to remove the dust from the surface.

Second, eighteen ¼ in. diameter and 3-1/4 in. length Tapcon® concrete screw anchors with 1.5 in. embedment in the web, as shown in Figure 3.12(a), were used throughout the repair region to increase further the interlocking between the original member and the repair. The total number of screws was distributed in an alternate pattern on both sides of the girder, as shown in Figure 3.12(b) and (c), and the required number was rounded up to provide additional redundancy. The holes were first drilled using a masonry drill bit and hammer drill. The screws were then tightened in those holes using a drill with a screwdriver bit, as shown in Figure 3.13. The number of screws and their spacing was determined using the interface shear transfer provisions of AASHTO LRFD (2017) Section 5.7.4.3 and considering concrete shear friction. The force demand was based on the shear force concentration in the 3.5 ft section of the girder end calculated using a strut and tie model, shown in Figure 3.14. The details of the strut and tie model calculations can be found in Chapter 7. The forms for the repair were put in place, creating a 3 in. projection from the vertical portion of the bottom flange on each side along the 3.5 ft repair length for the FR-SCC and MALP repairs and a 1.5 in. projection for the UHPC repair as shown in Figures 3.15 and 3.16. A 2 in. cover was also provided on the bottom of the

bottom flange to depict the strands' protection in the field against moisture ingress, assuming cracks propagate to the bottom of the girder. The mentioned repair dimensions were selected based on the research work of a student, Mike Mesigh, working on the same sponsored project.

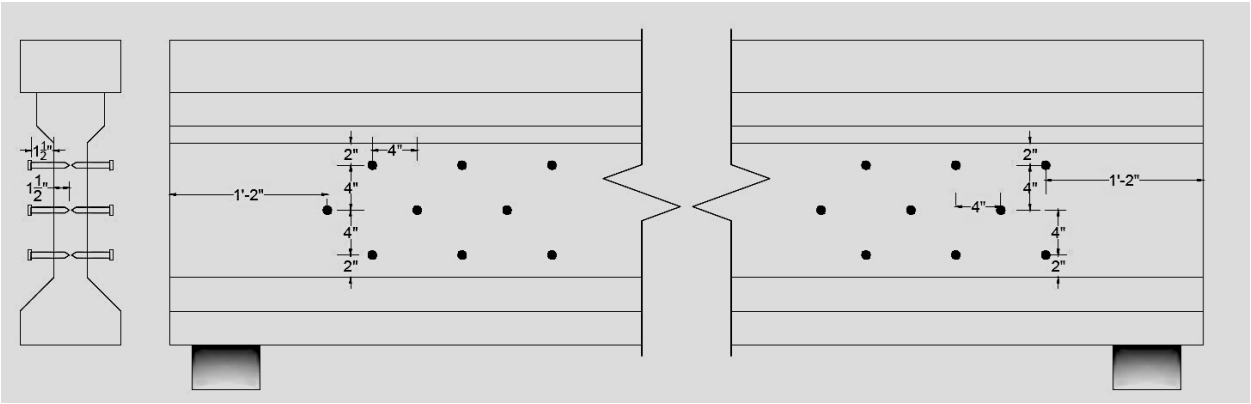

(a) (b) (c)

Figure 3.12: (a) Cross-sectional view of shear screws, (b) front face of shear screws distribution, and (c) back face of shear screws distribution

Figure 3.13: Screws used for shear studs in the web

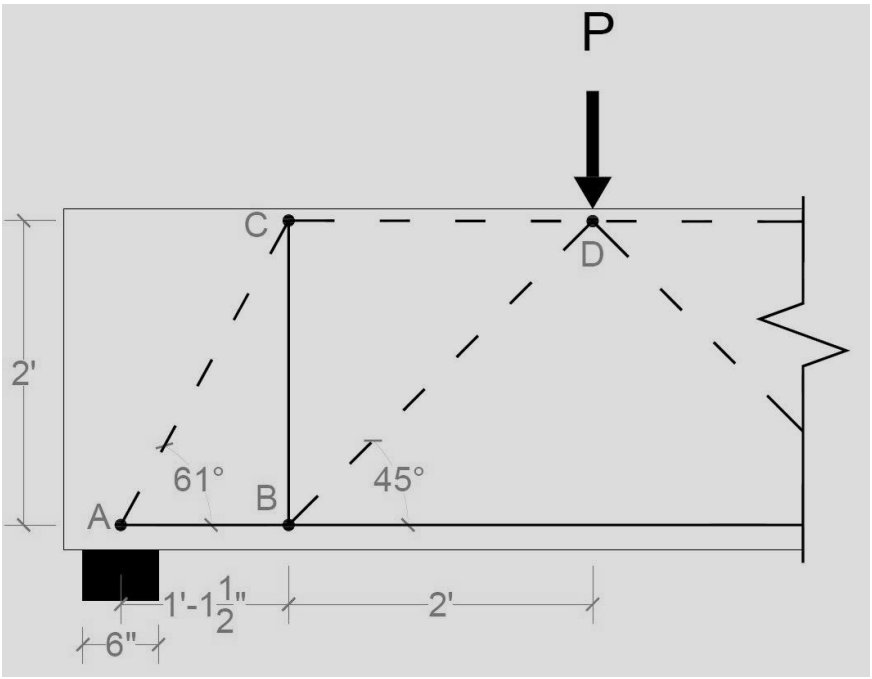

Figure 3.14: Strut and tie model of the end region

Figure 3.15: Repair formwork

After sealing the forms with silicone, the repair material was poured into the forms and was left to cure until gaining sufficient strength. After removing the formwork the FR-SCC was covered with wet burlap for 7 days, but no curing was applied for the UHPC and MALP. After 28 days, the repaired beams were tested with the same loading arrangement as the original girders. The results were compared with those from the undamaged beams, which is explained in the Chapter 4, Results.

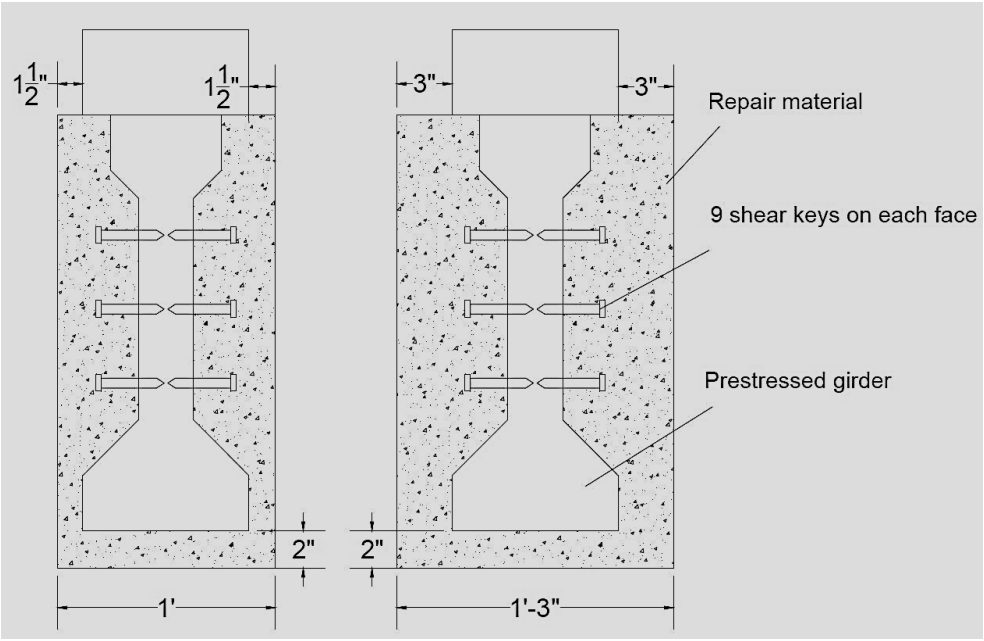

(a) (b)

Figure 3.16: (a) Repair dimension for UHPC and (b) repair dimensions for FR-SCC and MALP

3.4 Mix Preparation for the Repair Materials

3.4.1 FR-SCC Repair Mix

FR-SCC is very sensitive to water content; therefore, before the actual repair batch was mixed, a number of trial batches were performed based on the FR-SCC mix design used by Choate (2018) and Wirkman (2016), to determine the water content that gives the desired slump. The design compressive strength for the FR-SCC mix is 4000 psi with a slump of 28 ± 2 in. Table 3.2 shows the quantity of the materials in pounds per cubic yard of the mix after adjustment. Note that Table 3.2 is based on the saturated surface dry condition, which needs to be adjusted for the actual moisture content of the sand and coarse aggregate.

Table 3.2: FR-SCC Batch Quantities

Material	Quantity
Portland cement (Type I) (lb/yd^3)	412.5
Water (lb/yd^3)	229.8
Fine Aggregate (lb/yd^3)	1441
Coarse Aggregate (3/8 in. River Rock) (lb/yd^3)	1275.7
Air Entrainer (Master Builders AE-90) (lb/yd^3)	0.54
High Range Water Reducer (Glenium 7920) (lb/yd^3)	4.02
Type K Cement (Komponent) (lb/yd^3)	112.6
Citric Acid (lb/yd^3)	0.4
Fly Ash (lb/yd^3)	224.9
Polypropylene Fibers (lb/yd^3)	7.7

The key points for the mixing process of the FR-SCC repair are as follows:

- Add all the aggregates with half the water and mix for one minute.
- Add fly ash, cement, and Komponent.
- Add HRWR and then the remaining water to get the desired flow.
- Add one full dose of citric acid along with the polypropylene fibers.
- Mix all the materials for 3 minutes, then allow materials to rest for 3 minutes, followed by 2 minutes of mixing.
- Keep the mixer turning until the repair casting is finished, and add an additional full citric acid dose after every 15 minutes to retard the setting of cement. The dose can be reduced proportionally to the remaining concrete.

Water was sprayed on the damaged zone of each beam to ensure that the surface did not absorb water from the FR-SCC. After preparing the mix, the slump was measured to check the flowability of the FR-SCC while casting, as shown in Figure 3.17. The mix was transported from the mixer using a concrete transfer bucket and was poured inside the formwork only from one side to avoid entrapping air below the bottom flange. Once the material exceeded the formwork's half-depth, it was poured from the opposite side to keep the repair height equal for both faces. Once the material hardened, the formwork was removed, as shown in Figure 3.18. For the FR-SCC repair material, 8 cylinders with 6 in. x 12 in. dimensions were cast to determine the compressive strength in the specified intervals. The reason for increasing the size of the cylinders for FR-SCC is to provide enough space for the 2.1 in. long polypropylene fibers to flow into the cylindrical molds.

Figure 3.17: FR-SCC flow for the slump measurement

(a) (b)

Figure 3.18: (a) FR-SCC repair for beam M-2 and (b) FR-SCC repair for beam M-3

3.4.2 MALP Concrete Repair Mix

For preparing the MALP concrete, one bottle of the mono- aluminum- liquid phosphate activator was first added to a plastic bucket. Then one bag of the pre-packaged magnesium-alumino- aggregate dry powder was added, and the two were mixed for 45-60 seconds with a drill-mounted paddle provided by the MALP concrete manufacturer. The activators were kept in a cold place to slow down the chemical reaction after mixing and the setting time of the mixture. As soon as a batch was mixed, it was placed in the forms, and another batch was started immediately. After each pour, the MALP concrete was compacted with a steel rod to fill the gaps and avoid honeycombing. In the same way as the FR-SCC, the casting started from one side of the formwork to let the MALP flow below the bottom flange without trapping air. Upon reaching the half-height of the formwork, the mix was poured alternatively into the form openings on both sides to produce an equal height of the repair for both faces. This process was continued until the forms were filled. Eight 4 in. x 8 in. cylinders, four for each type of MALP, were prepared for compressive strength testing at different time intervals.

MALP concrete hardens in a few minutes after mixing, which generates a significant amount of heat and the material expands, as shown in Figure 3.19(a). This expansion further increases the interlocking between the repair material and the girder. Two different shipments of MALP concrete were used for the repair. For the beam M-1 newly acquired activator and dry powder were used, whereas for beam M-4 older (approximately 2 years old) MALP materials were used. The bags of dry material for the old MALP had lumps which could have been due to long-term compaction under other bags or due to chemical reactions. Lumps were broken up using a rubber hammer before pouring the bag into the bucket. The workability of the old MALP material was better compare to the new one and expanded slightly more than the new MALP

after casting. The set time of the old MALP was also longer compared to the newly acquired material. It was also noted that the color of the activator for the old and new MALP repair materials was different, which could be a reason for the difference in the physical and mechanical behavior of the mixture. The new MALP was more viscous and harder to mix. The completed MALP concrete repairs are shown in Figure 3.20. As shown in Figure 3.20, the repair's texture appears to be in separate layers, which is due to the hardening of the lower layer while pouring the top one.

After the forms were removed, it was noted that the repair cast with the old MALP had a better surface finish compared to the new material. Some construction defects were also noted, as shown in Figure 3.19(b) and Figure 3.20(b). These included lesser flow of the new MALP material to some portions of the bottom flange and slight honeycombing which was due to difficult mixing process and higher viscosity of the new MALP. However, the web of the girder, which is responsible for resisting the shear force, was fully covered with repair materials having a smooth surface finish.

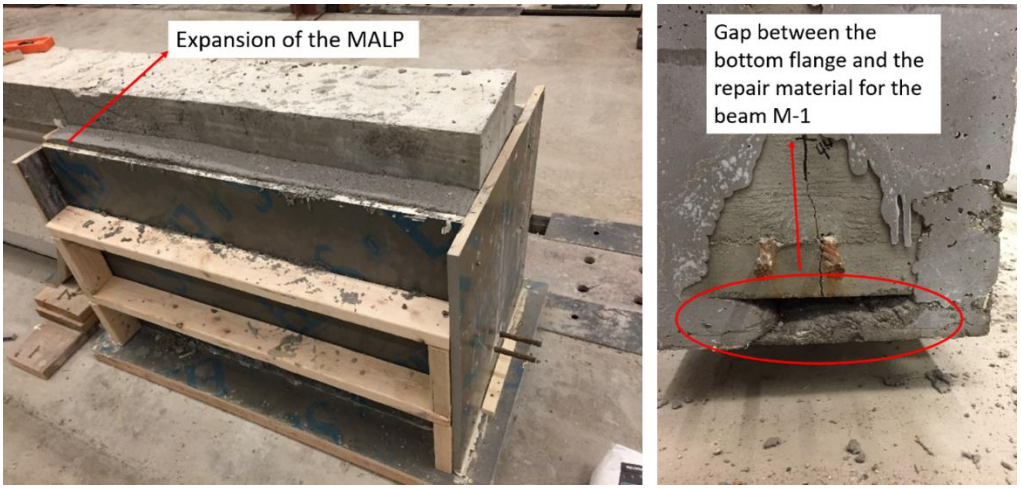

(a) (b)

Figure 3.19: (a) Expansion of the MALP above the formwork and (b) gap under the beam resulting from less flowability of the new MALP

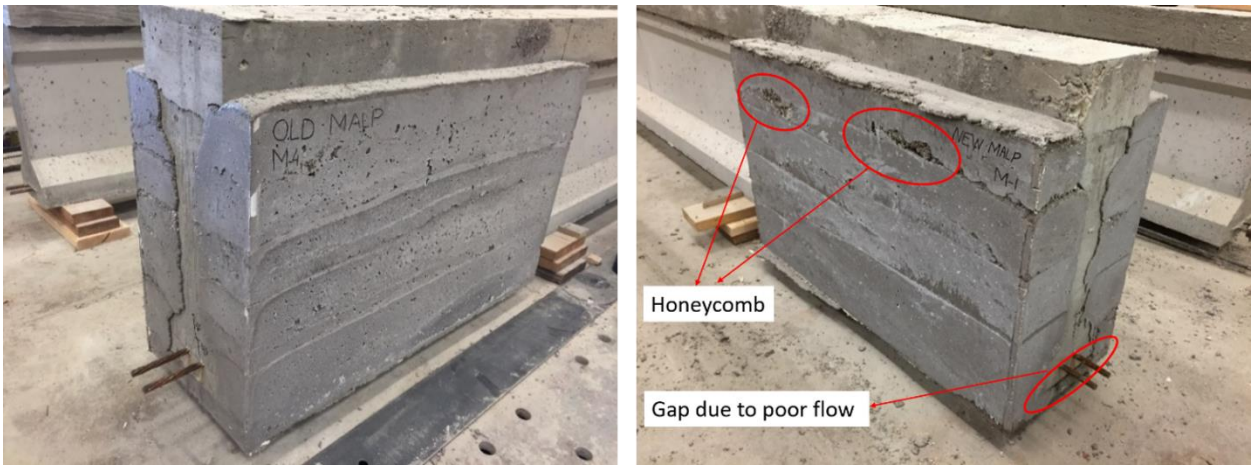

(a) (b)

Figure 3.20: (a) Old MALP repair for beam M-4 and (b) new MALP repair for beam M-1

3.4.3 J-3 UHPC Repair Mix

A non-proprietary UHPC mix design developed at the University of Oklahoma (Looney et al., 2019) was used for the repairs. The design strength for this UHPC is 18 ksi, and the mix proportion is presented in Table 3.3. For preparing the UHPC, oven-dry sand was first poured into the mixer. Subsequently, cementitious materials (e.g., cement, slag, and silica fume) were added over the sand, and all were mixed in a dry condition for 10 minutes. Water, combined with half of the HRWR, was added to the mix gradually over 2 minutes. All the materials were mixed for 1 minute, and the remaining HRWR was added over 1 minute; and again all the components were mixed for around 10-15 minutes, or until the mixture turned from a dry to a more fluid state. After a thorough mix of the materials, steel fibers were added, and the mixing process continued for a few more minutes to ensure uniform distribution of fibers in the mixture. Once the UHPC became ready, a flow test was performed according to ASTM C1856 to ensure its proper flow during casting. The surface of the repaired element was sprayed with water to avoid

absorbing the moisture of the UHPC. The mixture was carried from the mixer using buckets and was dumped into the forms. A total of 8 cylinders with 3 in. x 6 in. dimensions were cast for the UHPC repair material. Since the compressive strength of UHPC is significantly higher than traditional concrete, and since no coarse aggregate is included, it is preferred to keep the cylinders' dimensions smaller to not exceed limitations on testing equipment. It is also typical to test UHPC at least after the third day of casting since it typically has a longer set time. Figure 3.21 shows the repaired beams after removing the formwork.

Table 3.3: UHPC Batch Quantities

Material	**Quantity**
Type I Cement (lb/yd^3)	1179.6
Slag (lb/yd^3)	589.8
Silica Fume (lb/yd^3)	196.6
w/cm (lb/yd^3)	0.2
Water (lb/yd^3)	393.2
Fine Masonry Sand (lb/yd^3)	1966
Steel Fibers (lb/yd^3)	255.2
Steel Fibers (%)	2.0
Glenium 7920 (oz/cwt)	18.0
Glenium 7920 (lb/yd^3)	22.1

In the Table 3.3, w/cm ratio is the ratio of the weight of water to the total cementitious materials.

(a) (b)

Figure 3.21: UHPC repair for the beams (a) M-5 and (b) M-6

3.5 Post-Repair Test

Once the beams were repaired, the next step was to test them. The tests were intended to determine the contribution of the repair materials for the strength recovery of damaged beams. The loading arrangement is the same as that of the original beam test, as shown in Figures 3.22 and 3.23. Three instruments were used to record the response of the beam to the applied load. They include a load cell, wire-potentiometers (wire-pots), and LVDTs. The load cell was used to measure the applied load to the beam, the wire-pots to measure the deflection under the point load, and LVDTs mounted on the strands on both ends of the beam were used to measure the strand slip. All instruments were monitored continuously throughout each test. A 2 in. steel plate was provided below the neoprene pad at the far end of the beam to counter the 2 in. bottom concrete cover added to the beam due to the repair and keep the beam horizontal.

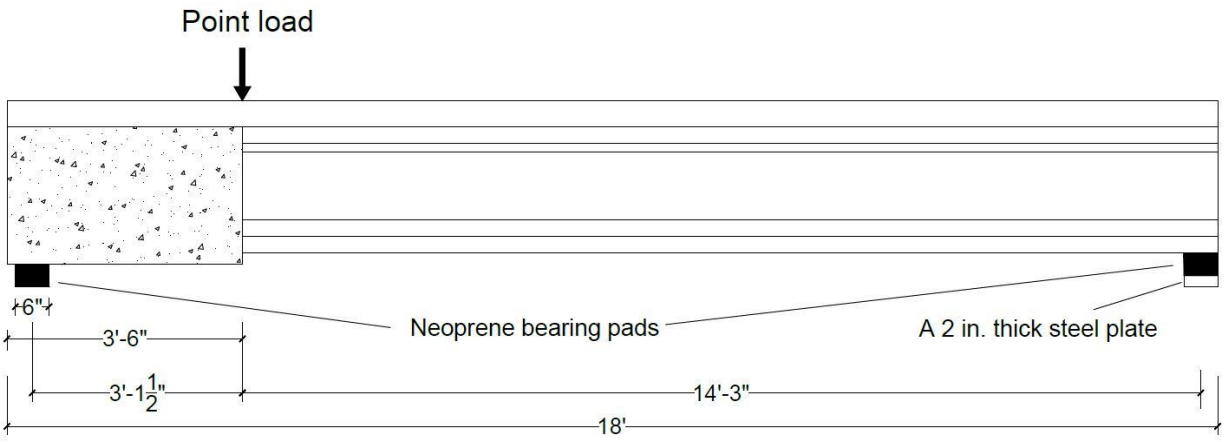

Figure 3.22: Longitudinal profile of the repaired beam

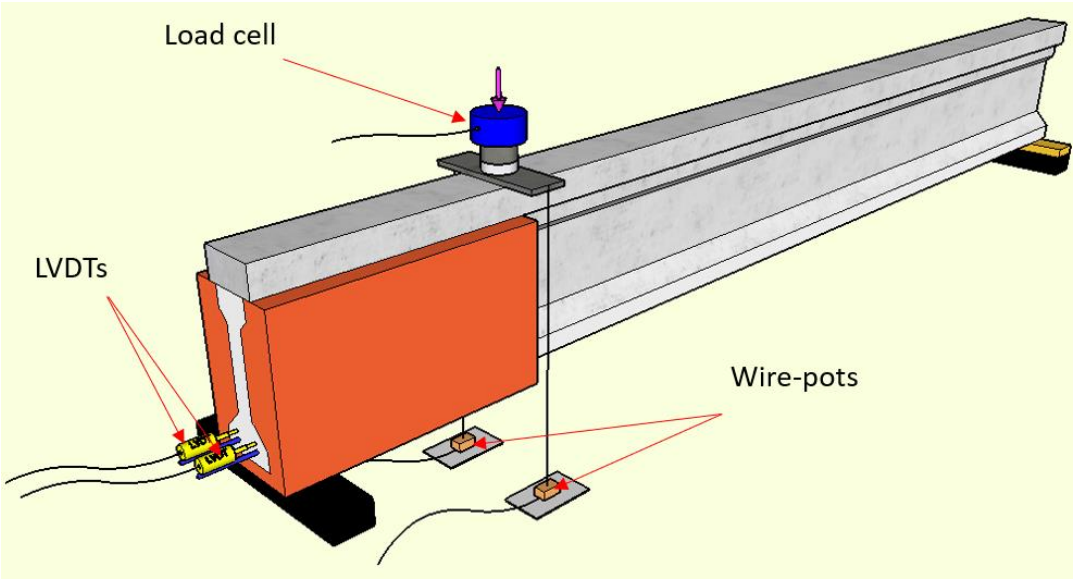

Figure 3.23: Test setup for the repaired beam

The load was applied in 5 kips intervals until the first crack was observed. For improving the precision of the data, the loading increment was decreased to 2 kips after the first crack and continued at that increment up to the final failure. After each load increment was applied, cracks were marked on the surface of the beam and later on the repair material. Each crack was traced with a permanent marker and labeled with the load increment, which helps to identify the load

corresponding to each crack and the failure mechanism of the beams. The test was stopped when the beam could no longer sustain load or the deck exhibited concrete crushing, and the beam exhibited at least 0.8 in. of deflection.

Chapter 4: Results

4.1 Compressive Strength of the Materials

Table 4.1 shows the slump flow values for both the member and the repair materials. Note that for the SCC and FR-SCC, slump flow was measured using ASTM C1611 and for the UHPC ASTM C1856. The slump value for FR-SCC is 24 in. which is less than the targeted 28 ± 2 in. The values in the Table 4.1 are based on the average of the largest and smalles diameter of the concrete flow. Compressive strength for the girder concrete is shown in Table 4.2. The numbers corresponding to SCC in Table 4.2 are based on the average of three cylinders for each testing age. The one-day strength for SCC is used to ensure that the member concrete gained sufficient strength to resist the strands' applied forces at prestress release.

Table 4.3 illustrates the compressive strength of the repair materials. For each repair material, a total of 8 cylinders were cast, and two cylinders were tested for each time interval. This testing pattern is slightly different for UHPC as there is no one-day strength test; instead, four cylinders were used for the test-day strength. The table also shows a significant difference between the compressive strength of the old and the new MALP. This difference was attributed to some unknown difference between the two shipments of the material or due to the age of the old MALP. Compressive strength results for the UHPC specimens shown in Table 4.3 were lower than anticipated at 28 days but were in the anticipated range (18 ksi) on testing day.

Table 4.1: Slump Flow of the Concrete Used for the Girders (SCC) And the Repair Materials

Member/Material	**M-1**	**M-2**	**M-3**	**M-4**	**M-5**	**M-6**	**FR-SCC (M-2, M-3)**	**UHPC (M-5, M-6)**
Slump Flow (in.)	19.5	22.25	19	21.5	27	25.5	24	10

Table 4.2: Compressive Strength of the Girder Concrete (SCC and Class AA)

Member	M-1	M-2	M-3	M-4	M-5	M-6
1-day strength (psi)	5645	6220	6730	5980	6600	5935
28-day strength (psi)	8050	9100	9450	8800	9170	8650
Test-day strength (psi)	8300	8970	5870	8770	8750	8910
Deck test-day strength (psi)	4403	4330	4510	4510	4160	4590

Table 4.3: Compressive Strength of the Repair Materials

Material	New-MALP (M-1)	Old-MALP (M-4)	FR-SCC (M-2)	FR-SCC (M-3)	UHPC (M-5, M-6)
1-day strength (psi)	8834	3770	2100	2100	-
7-day strength (psi)	8311	3480	5260	5260	12790
28-day strength (psi)	10595	3878	6400	6400	14400
Test-day strength (psi)	12490	3329	6680	6680	17320

For beam M-3, the test day compressive strength value is substantially lower than its one-day and 28-day strengths, which is not consistent with the other beams and is less than the targeted 8000 psi. On the other hand, no peculiar behavior was observed while testing the M3-U girder, which indicates sufficient concrete strength on the test day. The error could be due to the cylinders' having an uneven surface after grinding or any other problem with the cylinders loading setup; therefore, for this beam only, the 28-day compressive strength is used as the base value for assessment.

4.2 MALP Repair Beams

4.2.1 Beam M-1

In order to induce shear damage to beam M1-U (beam 1-undamaged), a point load was applied at 3.5 ft from the end of the girder, as described in Figures 3.8 and 3.9. The load was increased gradually, and corresponding deflection and strand end slip were noted. The induced damage leads to the exposure of the shear stirrups and large cracks throughout the web. Figure 4.1 shows the shear damage to M1-U and M1-R (beam 1-repaired) after the initial and final test.

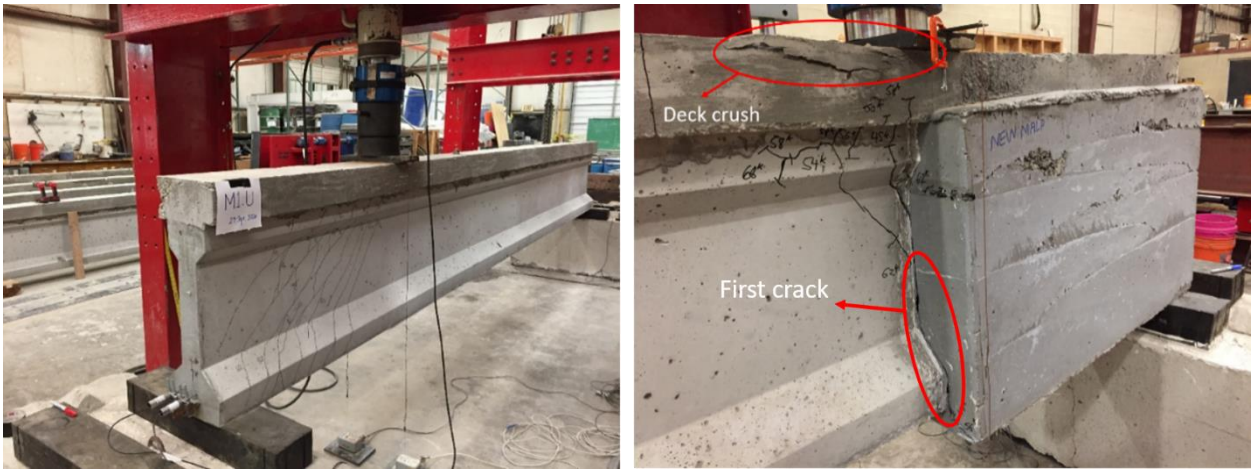

(a) (b)

Figure 4.1: Beam M-1 after (a) initial test and (b) final test

Beam M1-U was repaired with the new MALP, having a compressive strength of 12,490 psi on the test day. The loading arrangement used for the test of M1-R is shown in Figures 3.22 and 3.23. Figure 4.1(b) shows the failed beam M1-R after the test. It can be observed that no crack is visible in the repaired section, which indicates the repair was sufficiently designed to handle the load and caused the failure zone to successfully move away from the pre-damaged end region. The repair material maintained a good bond with the beam throughout the test, and

no delamination or differential movement was observed. Failure started with vertical cracks in the bottom flange at the junction of the beam with the repair material and dispersed diagonally to the corner of the repair material. The cracks also propagated upward and turned diagonally as they moved above the half-depth point in the web. They further divided into small branches around the girder's top flange. As the load was approaching the ultimate capacity, the deck started crushing and formed a hinge at the load application point. Once the deck began to crush, the loading was stopped. Figure 4.2 shows the longitudinal profile of the M1-R during the load test.

Figure 4.2: Beam M1-R during the load test

4.2.1.1 *Load vs. Deflection Behavior for Beam M-1*

The load and deflection readings were recorded using the load cell and wire-pots, respectively, described in Figure 3.22. For the deflection, the average reading of both wire-pots was used. Figure 4.3 shows the load vs. deflection curves for the M1-U and M1-R beam tests.

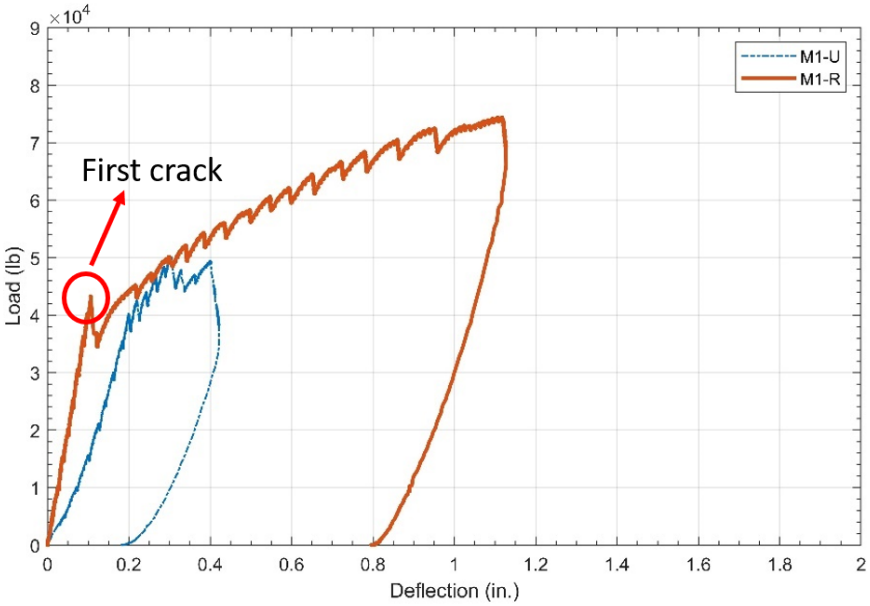

Figure 4.3: Load vs. deflection curves for beam M-1

After reaching 50 kips load for the original beam, the member failed in bond-shear and could not resist more loads; thus, the deflection increased for a constant load, and loading was stopped.

The repaired beam outperformed the original in both the elastic and inelastic ranges. The load vs. deflection curve's initial slope for M1-R is larger compared to M1-U, which indicates an increase in the member stiffness. In addition, after the first crack in the repaired beam (highlighted as the first sudden drop in load in Figure 4.3), the load still increased proportionally

with the deformation, providing a significant increase to the member's ultimate strength compared to the original M1-U.

4.2.1.2 Load vs. Slip Curves for Beam M-1

For M1-U, the calculated peak load based on failure analysis using AASHTO LRFD (AASHTO, 2017) was expected to be 65.5 kips, whereas, for all the original beams, the failure happened at a load around 50 kips, and significant strand slip was observed. Strand slip, which is the average value of both the LVDTs for the support close to the loading point, substantially decreased the shear capacity by increasing the transfer length and reducing the prestress near the end of the beam. Figure 4.4 shows that the first strand slip and initial crack for beam M1-U occurred with the same load. The first cracks occurred at 40 kips load for the web and 42 kips for the bottom flange close to the support. With cracks intercepting the strands, debonding starts, and slip occurs. For these tests the ratio of a/d = (37.5 in/25.125 in) = 1.49 is less than 2.5. Using the previously mentioned observations in Figure 2.13 (Naji, 2016), the failure of M1-U is classified as a bond-shear failure. This indicates that the capacity determined by AASHTO methods would not be accurate, and capacity should be determined taking the bond behavior into account.

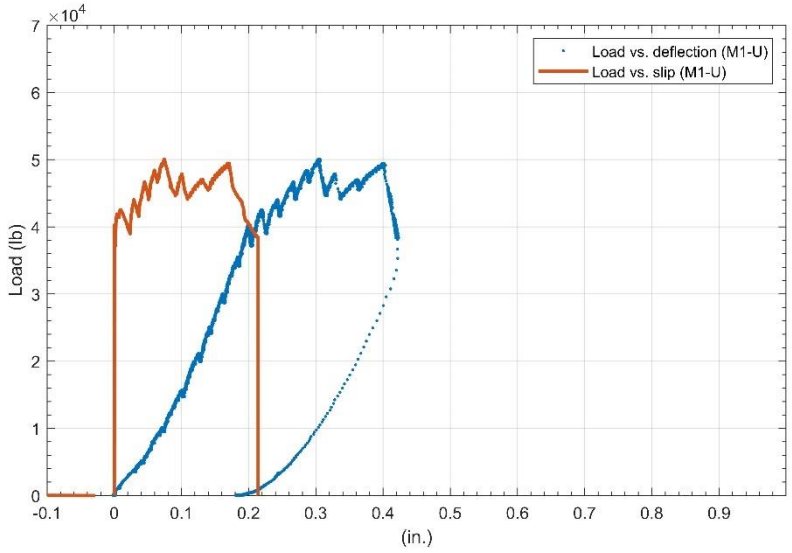

Figure 4.4: Load vs. deflection and load vs. strand slip curves for test M1-U

For M1-R (Figure 4.5), the first observed crack started in the bottom flange outside the repaired zone and moved vertically upward. The web cracks were very few; instead, they concentrated on the top-flange and moved to the deck close to the ultimate load. The repair material remained sound with no visible cracks. According to Figure 4.4, strand movement started with the first crack of the member and continued up to the failure load. Considering the previously mentioned behaviors and following the failure type flowchart in Figure 2.13, it can be concluded that the failure type for the repaired beam (M1-R) was a bond-flexure failure.

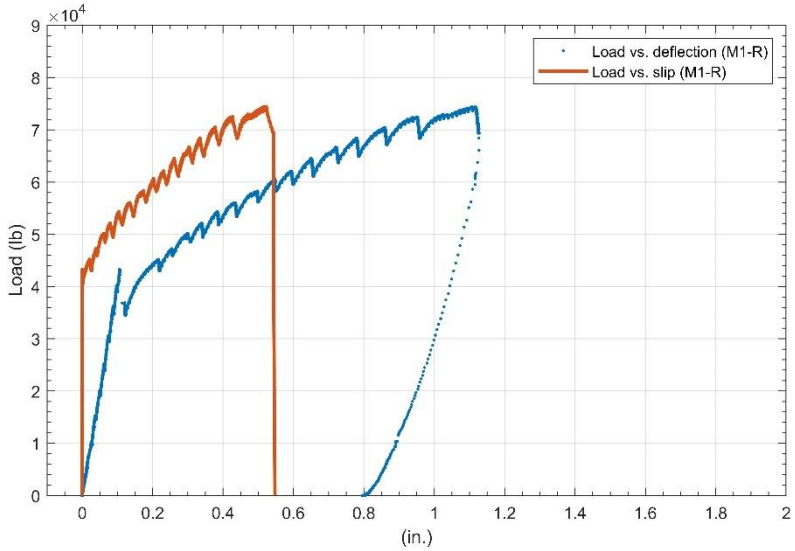

Figure 4.5: Load vs. deflection and load vs. strand slip curves for M1-R

4.2.2 Beam M-4

Figure 4.6 (a) shows beam M-4 after its initial test. The first cracks occurred in the web at a load of 40 kips and extended to the top and bottom flanges as the load increased, shown in Figure 4.6(b). Loading continued up to a maximum of 50 kips until severe shear damage was observed.

(a) (b)

Figure 4.6: Beam M-4 after (a) initial test and (b) final test

Beam M4-R was repaired with the old MALP. The compressive strength of the old MALP is the lowest out of all the repair materials reaching only 3329 psi on the test day. No vertical crack was observed at 3.5 ft from the end of the beam in the initial load test; however, a wide vertical crack was observed at the junction of the repair material and web in the repaired beam after the load test, followed by the deck crushing. Figure 4.7 shows beam M4-R during the load test.

Figure 4.7: Beam M4-R during the load test

4.2.2.1 Load vs. Deflection Curves for Beam M-4

The load-deflection curve for M4-U (Figure 4.8) shows that after the initial crack at 40 kips, the loading continued until a drop in the load value was observed at approximately 50 kips. It was further reloaded to 50 kips, but the load value did not show a noticeable increase. Beam MR-4 first cracked at 30 kips, and the curve remains below the reference values from M4-U up to 0.35 in. deflection. Unlike the new MALP, there is only a slight increase in the stiffness of the repaired beam. The ultimate load improves from 50 kips to 68 kips, but the deflection at peak load is 1.45 in. which is more than the 1.1 in. observed for the new MALP repair (beam M1-R). The difference in deflection can be related to the lower compressive strength of the old MALP.

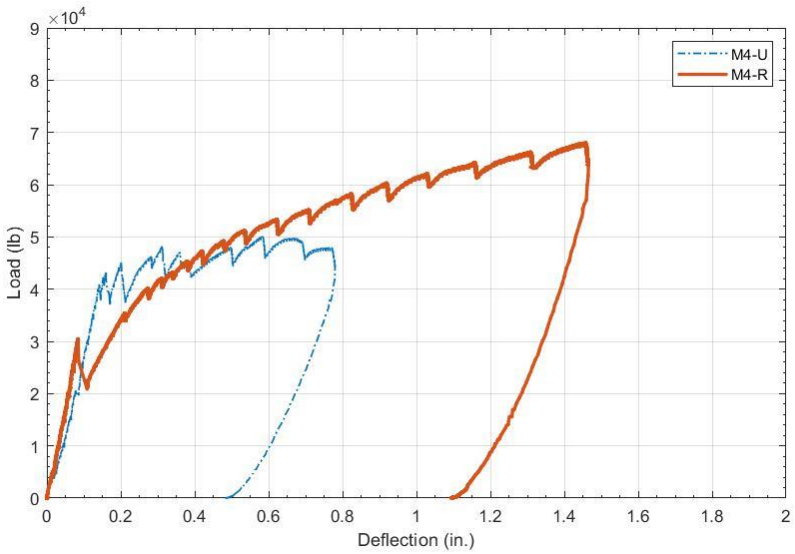

Figure 4.8: Load vs. deflection curves for beam M-4

4.2.2.2 Load vs. Slip Curves for Beam M-4

For the M4-U beam in Figure 4.9, web shear cracks along with strand slip started at 40 kips and extended to the bottom flange close to the support at 42 kips. The failure type for M4-U was a bond-shear failure, which is similar to beam M1-U. For beam M4-R, the first crack occurred before strands' debonding, which can be observed in Figure 4.10. Unlike M4-U, the load in Figure 4.10 is proportionally increasing with the strand slip, indicating that the repair offers higher resistance to the load despite the slip. The failure type for M4-R is a bond-flexure failure, similar to M1-R. For M4-U, 48 kips of load were required to produce 0.5 in. strand slip; however, 62 kips were required to produce the same amount of slip for M4-R, which shows a noticeable increase in resistance after the repair.

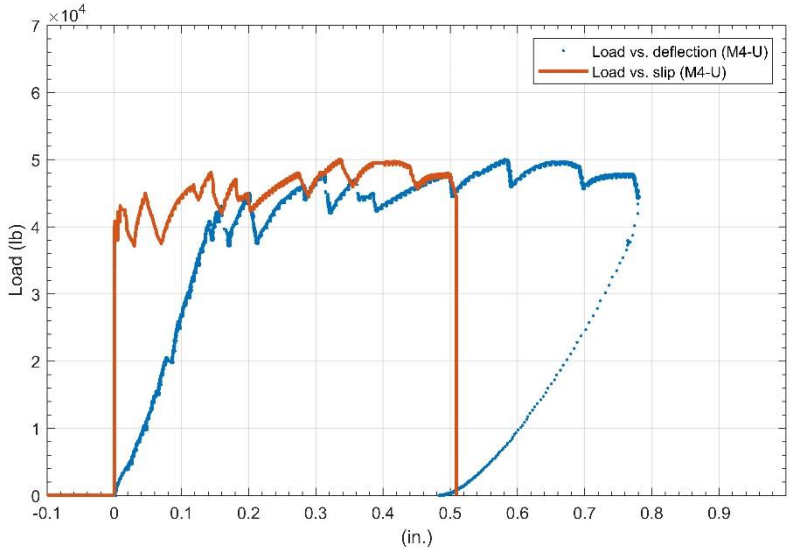

Figure 4.9: Load vs. deflection and load vs. strand slip curves for M4-U

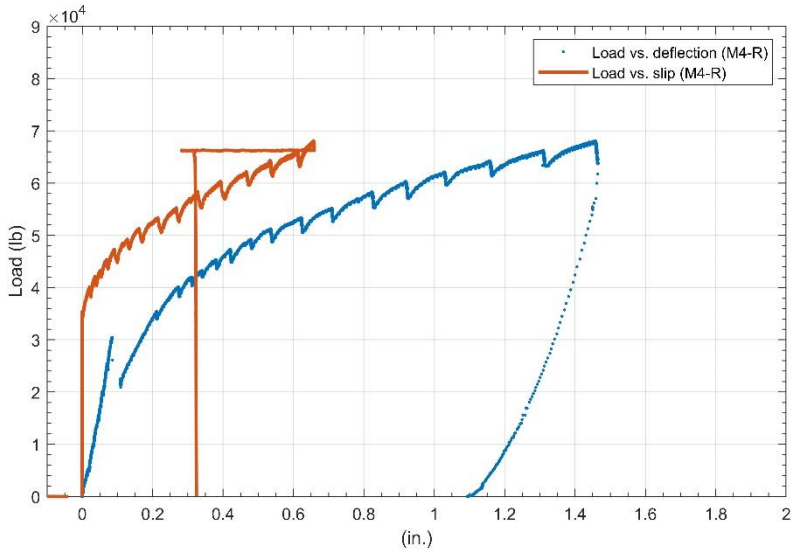

Figure 4.10: Load vs. deflection and load vs. strand slip curves for M4-R

4.3 FR-SCC Repairs

4.3.1 Beam M-2

Beam M2-U was tested using the same loading arrangement as shown in Figure 3.8. The first crack appeared at 43 kips on the web. The loading continued up to 54 kips, which is the beam's ultimate strength, resulting in severe damage to the web. This beam was repaired with FR-SCC, having a compressive strength of 6680 psi on the test day, which was lower than that of the beam at 8970 psi. Despite lower compressive strength than the member, the repair provided sufficient confinement to the damaged regions and significantly improved its shear behavior. During the test, no delamination was observed, indicating a strong bond between the repair and the member. As the load approached its ultimate value, the deck started crushing and formed a hinge at the load point. For this material, the cracks appeared at the repaired surface along the length of the beam with a bigger size than for the MALP and UHPC repairs. Figure 4.11 shows M2-U and M2-R after the tests, and Figure 4.12 shows the load test setup for M2-R.

(a) (b)

Figure 4.11: (a) Beam M2-U after the initial test and (b) beam M2-R after the final test

Figure 4.12: Beam M2-R during the load test

4.3.1.1 Load vs. Deflection Curves for Beam M-2

At a load of 29 kips, a wide crack appeared along the junction of the repair and the beam, which caused the first drop in the load vs. deflection curve, as shown in Figure 4.13. The repair beam cracked earlier compared to the original beam despite showing a higher ultimate strength. Figure 4.13 shows the load vs. deflection curve for the original and repaired beam M-2.

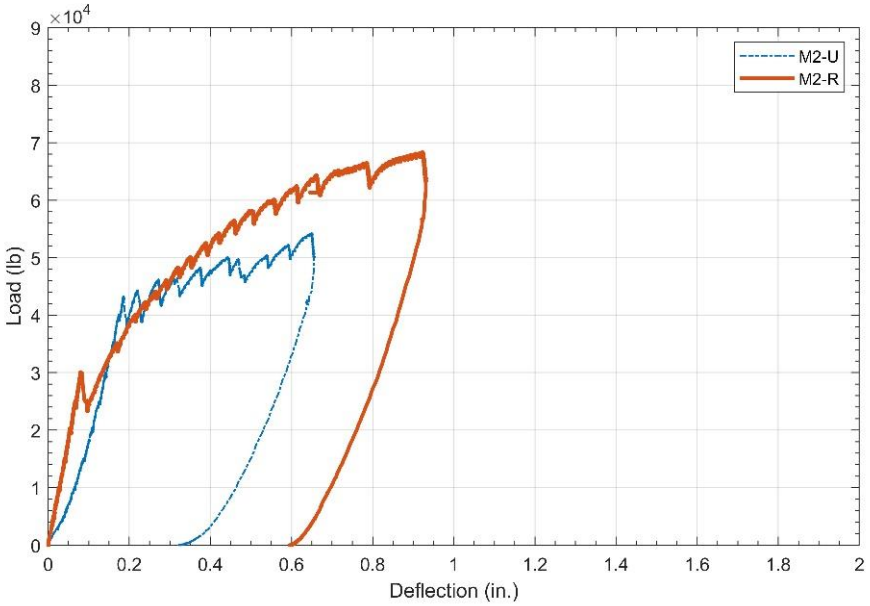

Figure 4.13: Load vs. deflection curves for beam M-2

4.3.1.2 Load vs. Slip Curves for Beam M-2

The load vs. slip curve for M2-U (Figure 4.14) indicates that the slip started at 43 kips load, which coincides with the first crack in the beam. The failure type was a bond-shear failure, similar to the other beams at their initial test. The first crack started at 29 kips for the repaired beam, whereas the strand slip started at 40 kips, as shown in Figure 4.15. The lag between the cracking load and slip for the repaired beam indicates the contribution of the FR-SCC repair for resisting the load. The cracks started earlier than the strand slip, yet significant strand slip and concrete crushing was observed before failure, resulting in a bond-flexure failure.

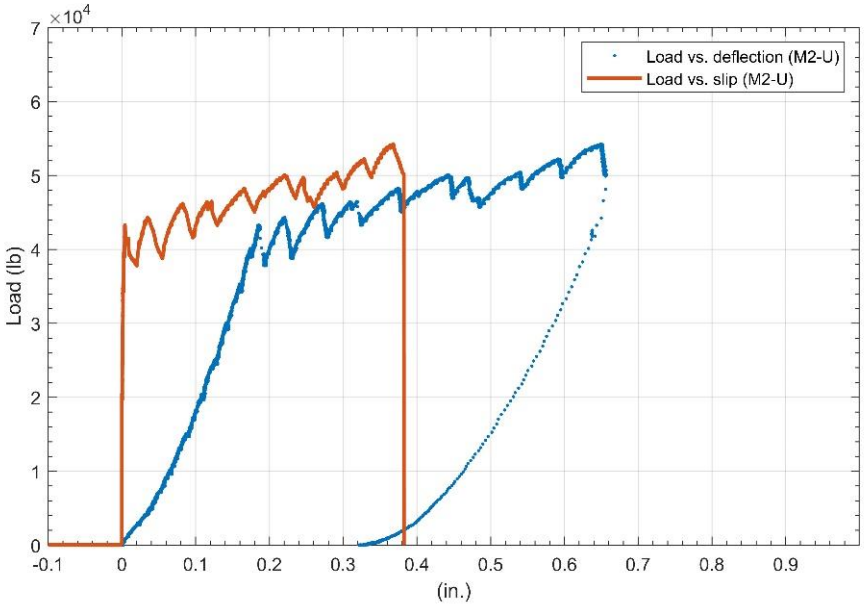

Figure 4.14: Load vs. deflection and load vs. strand slip curves for M2-U

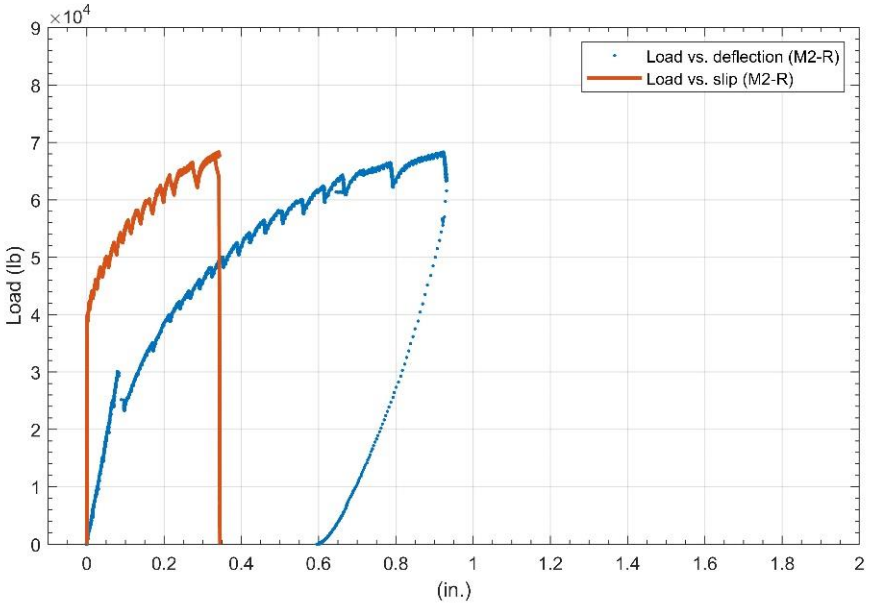

Figure 4.15: Load vs. deflection and load vs. strand slip curves for M2-R

By comparing the load vs. slip values for the M2-U and M2-R, the overall length of strand slip is almost the same for both cases; however, after repair, a load of 70 kips was required to produce the same amount of slip that occurred with 54 kips before repair.

4.3.2 Beam M-3

Beam M-3 is the second beam repaired with FR-SCC. Beam M3-U first cracked at 48 kips, and the loading continued up to 54 kips which induced wide cracks at the end regions. The loading configuration for the repaired beam is shown in Figures 3.22 and 3.23. M3-R is the only beam of all the six specimens that exhibited a wide crack throughout the repair face, indicating a strong bond that causes stress transfer between the member and FR-SCC repair. This crack appeared at 35 kips at the bottom of the repair surface and further extended upward with load addition. The beam started cracking at the junction with the repair, and the crack moved upward to the web. At higher loads, the cracks split and propagated to the web, the top flange, and extended beyond the load application point. There was no visible delamination or differential movement between the original girder and repair material during the test. Close to the ultimate load, cracks started appearing in the deck, similar to a common flexural failure. Figure 4.16 shows M3-U and M3-R after the load tests, and Figure 4.17 shows M3-R during the load test.

(a) (b)

Figure 4.16: (a) Beam M3-U after the initial test and (b) beam M3-R after the final test

Figure 4.17: Beam M3-R during the load test

4.3.2.1 Load vs. Deflection Curves for Beam M-3

Figure 4.18 shows the load-deflection relations for both the original and repaired beams. For M3-U, the first 45-degree shear crack appeared at a load of 46 kips, extending from the bottom flange to the top of the web. The loading continued up to 54 kips, beyond which the load only increased slightly with an increased deflection, as shown in Figure 4.18. The first crack that caused a drop in the load-deflection curve occurred at 44 kips for M3-R. As the load increased, the beam continued to resist load and reached an ultimate load of 72 kips at failure.

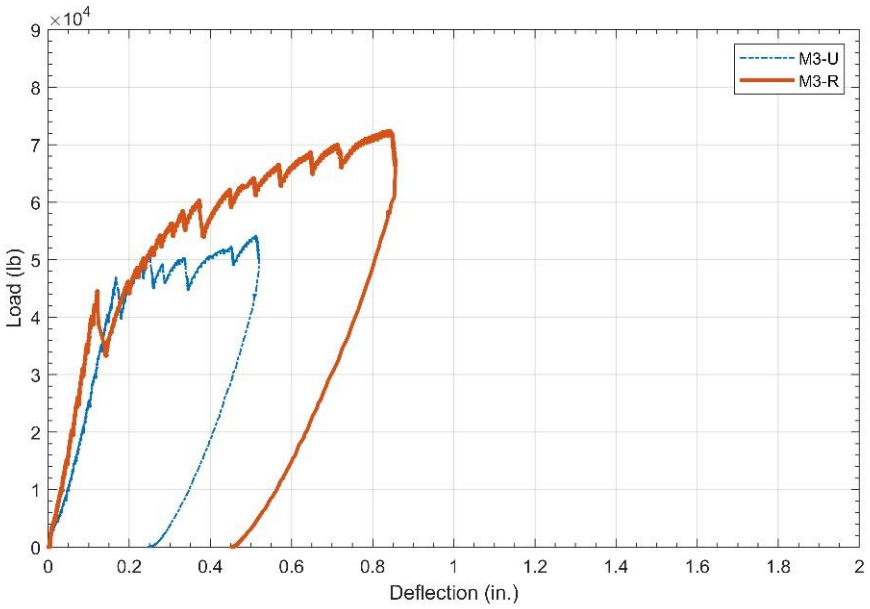

Figure 4.18: Load vs. deflection curves for beam M-3

4.3.2.2 Load vs. Slip Curves for Beam M-3

For beam M3-U, strand slip started at 46 kips with the first crack and continued throughout the test, as shown in Figure 4.19. There was no noticeable resistance to slip after the first crack, which caused an approximately constant load with increased strand slip. The failure type was a bond-shear failure for the original beam, similar to all the other original beams. For

the repaired beam M3-R (Figure 4.20), strand slip started just after the first crack, but load continued to increase even with higher slip values. For M3-U, the load corresponding to 0.28 in. strand slip is 54 kips; however, 72 kips were required to produce the same amount of slip for M3-R, indicating higher resistance after repair.

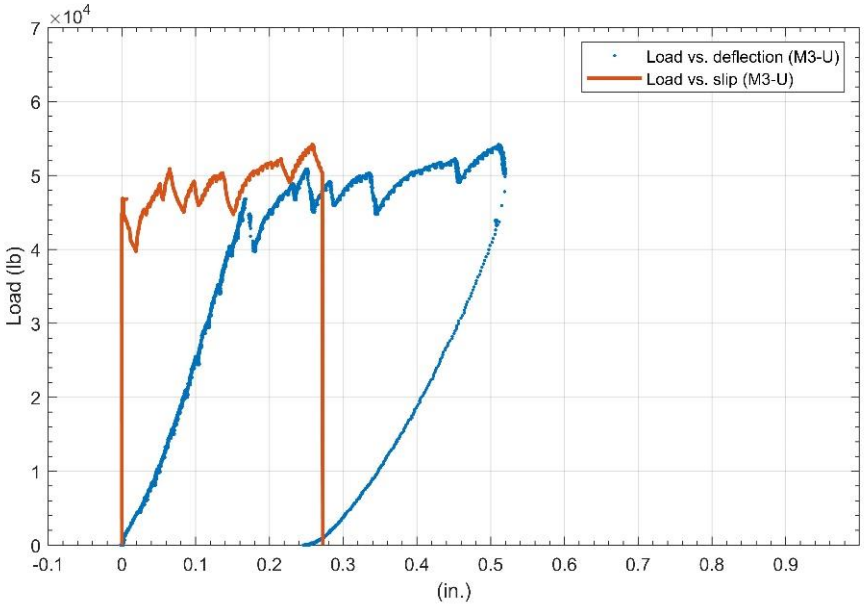

Figure 4.19: Load vs. deflection and load vs. strand slip curves for M3-U

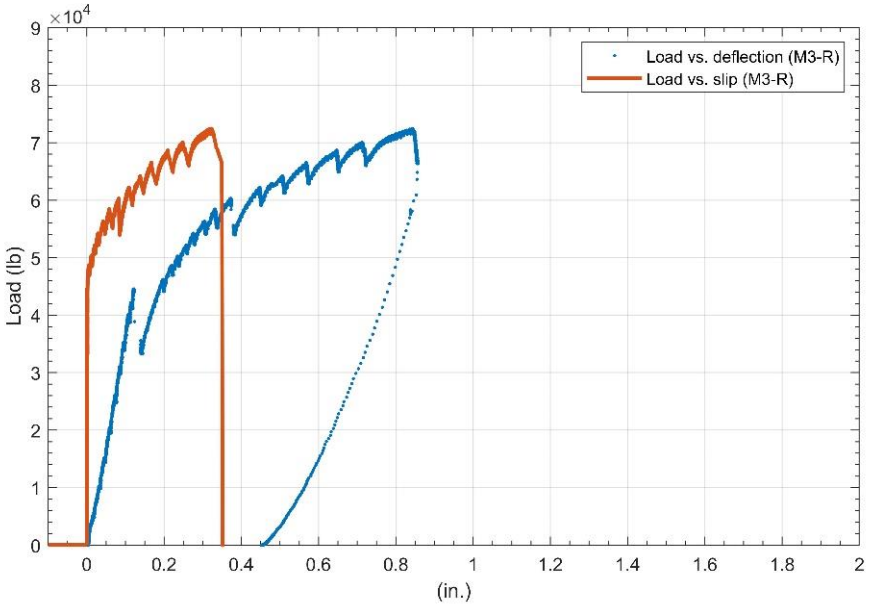

Figure 4.20: Load vs. deflection and load vs. strand slip curves for M3-R

4.4 UHPC Repairs

4.4.1 Beam M-5

Beam M5-U was tested using the same loading arrangement as shown in Figure 3.8. It was then repaired using UHPC with a minimum 1.5 in. thickness, which is less than the minimum 3 in. thickness of the MALP and FR-SCC repairs. On the test day, the compressive strength of the UHPC was 17,320 psi, which is significantly larger than the compressive strength of the MALP and FR-SCC and more than two times stronger than the beam. The repaired beam was tested using the same loading arrangement as that shown in Figures 3.22 and 3.23. Compared to the FR-SCC and MALP repair beams, the cracks shifted away from the end region damage and were vertical throughout most of the beam depth, which, combined with concrete crushing at the load point, indicates a flexural failure. Figure 4.21(a) shows M5-U after its initial

load test, Figure 4.21(b) is the repaired beam (M5-R) after the load test, and Figure 4.22 shows the longitudinal profile of M5-R during the load test.

(a) (b)

Figure 4.21: (a) Beam M5-U after the initial test and (b) beam M5-R after the final load test

Figure 4.22: Beam M5-R during the load test

4.4.1.1 Load vs. Deflection Curves for Beam M-5

For the beam M5-U, the initial cracks started at 45 kips with cracks in the web and bottom flange. The loading continued up to 53 kips, but the beam could not hold the additional load and exhibited a relatively constant load with increased deflection, resulting in severe shear damage. For the repaired beam (M5-R), small horizontal cracks started to appear on the bottom parts of the UHPC at 5 kips of load, but they did not result in any detrimental effect on beam performance. The slope of the curve's initial portion is greater when compared to the slope of the original beam curve, indicating a stiffer beam after the repair. The first crack was observed at 39 kips, but the load did not drop, which was unlike the other repairs. After a small constant load, the member continued resisting additional applied load up to the ultimate value of 82 kips, which resulted in the deck crushing. Figure 4.23 shows the load vs. deflection curves for both the original M5-U and repaired M5-R beams.

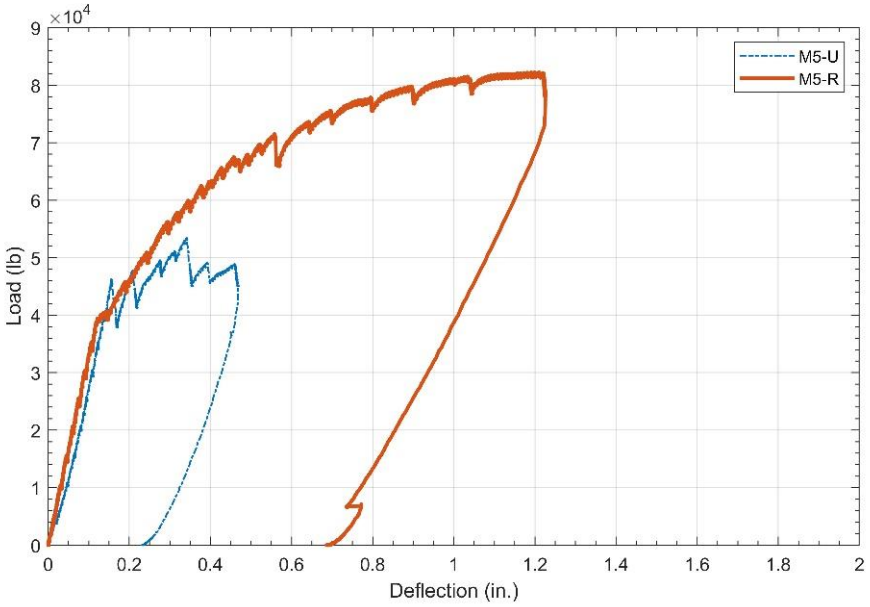

Figure 4.23: Load vs. deflection curves for beam M-5

4.4.1.2 Load vs. Slip Curves for Beam M-5

Figures 4.24 and 4.25 show the load vs. deflection and load vs. slip relationships for the M5-U and M5-R, respectively. For beam M5-U, load vs. deflection and load vs. strand slip curves are typical compared to the other undamaged beams in which bond loss coincides with the first crack. Moreover, the slip pattern is identical to the inelastic deflection, which indicates each slip increment started with the crack in the beam. For the repaired beam, strand slip started at 53 kips, higher than the initial slip load for all FR-SCC and MALP beams. The slip's delay indicates a failure type of bond-flexure including deck crushing, indicating a comparative higher efficiency of UHPC as a repair material despite having a smaller thickness than the FR-SCC and MALP repairs. M5-R had an ultimate load of 82 kips, higher than the other repair materials while having the least slip.

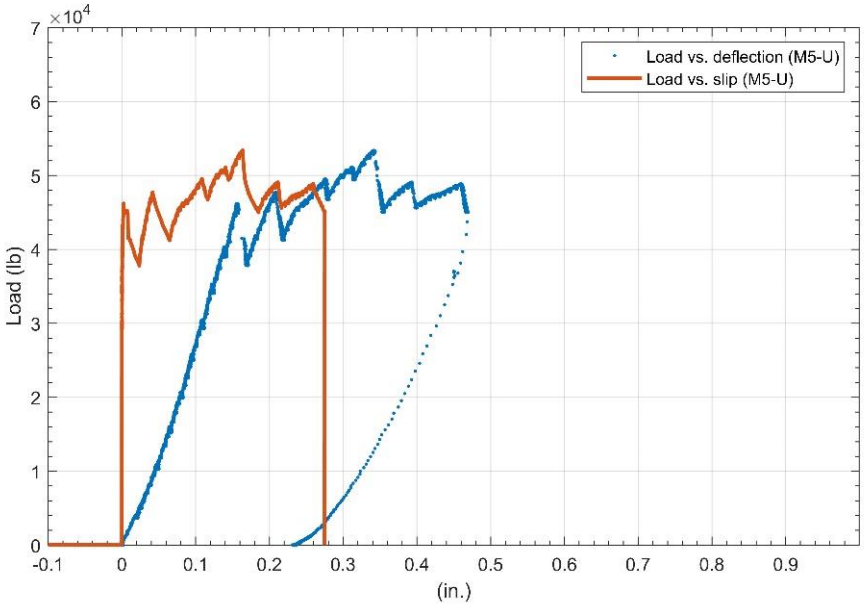

Figure 4.24: Load vs. deflection and load vs. strand slip curves for M5-U

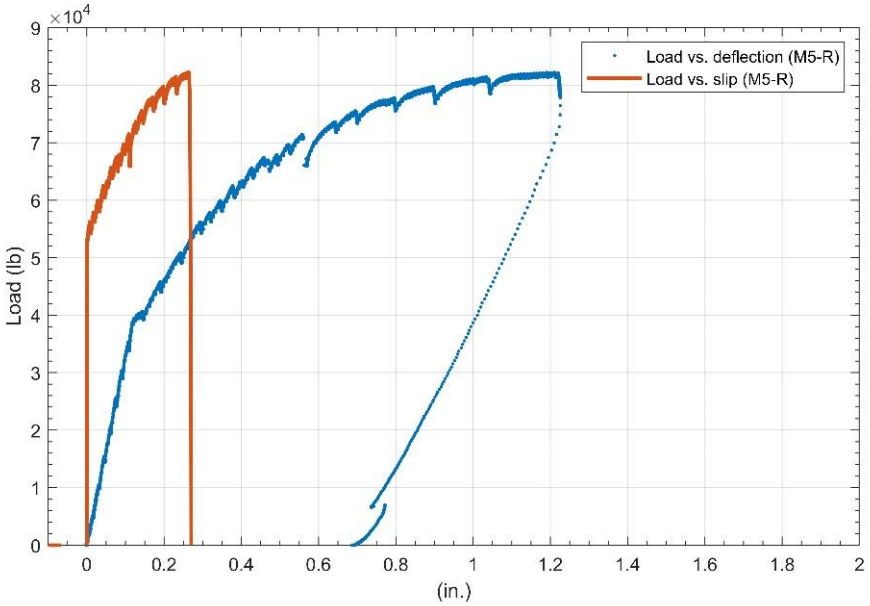

Figure 4.25: Load vs. deflection and load vs. strand slip curves for M5-R

4.4.2 Beam M-6

Beam M6-U was tested with a point load at 3.5 ft from its end, similar to all other tests. After inducing shear damage, it was encapsulated with a UHPC repair identical to the repair for beam M5-R. The compressive strength of the UHPC repair on the test day was 17,320 psi which is higher than the SCC used for the girder, FR-SCC, and MALP. For M6-U, the first crack started at 45 kips at the web and bottom flange interface close to the support. At higher loads, the cracks expanded to the web and continued to appear toward the point load, shown in Figure 4.26(a). For the repaired beam, small irregular cracks appeared on the repair surface at 10 kips and 25 kips, but they did not contribute to any strength loss. The repaired beam cracked at the top flange just outside of the repair and scattered to different branches, moving toward and crossing the load point. Some vertical cracks appeared at a distance from the load point on the

side opposite of the repair, indicating that the failure zone is shifted away from the damaged region. Figure 4.26(b) shows the repaired beam after the test.

(a) (b)

Figure 4.26: (a) Beam M6-U after the initial test and (b) beam M6-R after the final load test

The longitudinal profile of M6-R in Figure 4.27 shows a thinner repair than the MALP and FR-SCC, which means that the retrofit also maintains the beam's aesthetic besides providing additional strength.

Figure 4.27: Beam M6-R during the load test

4.4.2.1 Load vs. Deflection Curves for Beam M-6

The load vs. deflection relation for M6-U shows a drop in load with the first crack, and the drop in load with each additional crack continued up to the ultimate load of 49 kips, as shown in Figure 4.28. For the repaired beam M6-R, the curve's slope in the elastic zone is more than for M6-U, indicating a higher stiffness for the UHPC repaired beam. The first crack did not cause a drop in the load, and the beam continued to support higher loads with additional deflection. The curve becomes approximately horizontal at 80 kips, which is the ultimate capacity for beam M6-R.

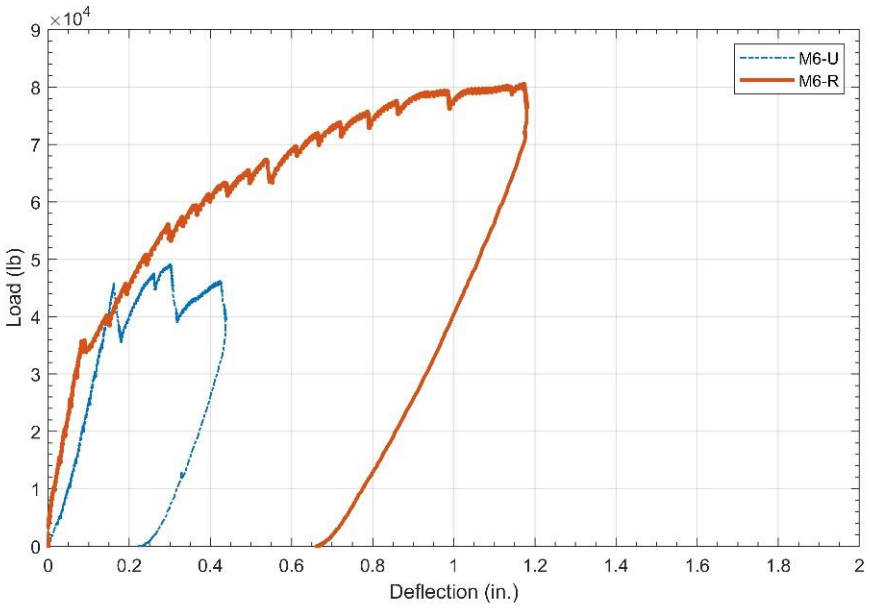

Figure 4.28: Load vs. deflection curves for beam M-6

4.4.2.2 Load vs. Slip Curves for Beam M-6

Figure 4.29 shows an identical pattern for both the load vs. deflection and the load vs. slip curves. The first crack and first slip occurred simultaneously at 45 kips; therefore, the failure type is a bond-shear failure. In the repaired beam M6-R (Figure 4.30), the slip starts at 51 kips, indicating that the repair has a significant contribution in preventing early debonding. This causes a change in the failure mechanism and a post-repair failure of bond-flexure, which also caused concrete crushing in the deck. The ultimate load slip for this beam is 0.35 in., which is less than the other repair materials, whereas the load corresponding to this slip is 80 kips, indicating a significant improvement in slip resistance after the repair.

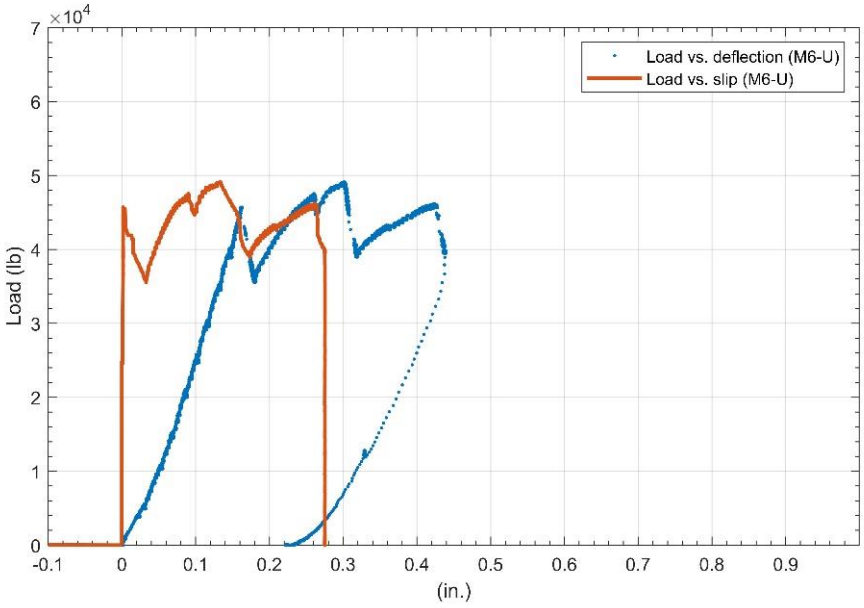

Figure 4.29: Load vs. deflection and load vs. strand slip curves for M6-U

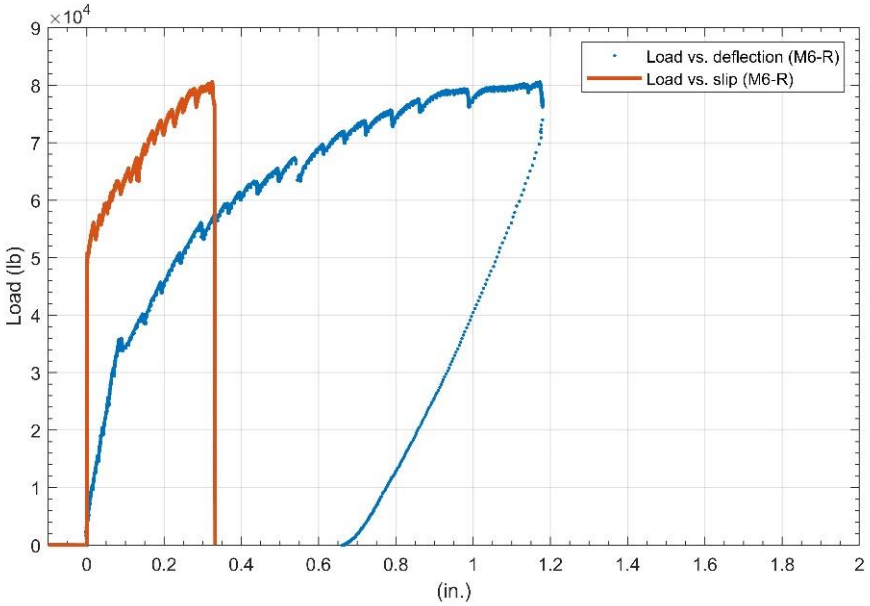

Figure 4.30: Load vs. deflection and load vs. strand slip curves for M6-R

4.5 Cost Estimation

Cost estimation is a crucial factor for determining the type of repair material appropriate for a given situation. Despite the cost of construction materials being highly dependent on the purchased quantity and location, this analysis can provide a relative comparison between different repair alternatives. Other factors, such as the speed of strength gain, allowing for traffic to be resumed more quickly, and the labor requirements would also need to be considered for a final estimate. The volume required for the FR-SCC and MALP repairs is 12.8 ft^3, and this value is 9.2 ft^3 for the UHPC due to the lesser thickness of repair. The mentioned volumes are for the two beams' repair material only, excluding the cylinders' volume and extra percentage for losses. Cost estimation is tabulated for all three repair materials in Tables 4.4, 4.5, and 4.6. The unit cost represents typical values for the construction materials in Oklahoma which was estimated based on previous purchases by the research team, discussions with manufacturers, and multiple online resources. The material quantity is based on the mix proportion described for each repair

material in the methods and approaches chapter. Multiplying the unit cost with the quantity results in the total cost for that material, and the sum of the total cost for each material yields the overall cost of repair. Table 4.4 expresses the cost estimation for the FR-SCC, which has the least cost of all the repairs. This can be attributed to the lower amount of cement and polypropylene fiber requirements. Table 4.5 describes the cost estimation for the UHPC. Despite having the least thickness of the repair, UHPC requires a large quantity of portland cement, which escalates the total cost. The second highest contributing factor for the UHPC cost is steel fibers, with the highest unit cost of all the materials at $2.00 per pound. MALP used for this research is a proprietary material which means it is a commercial product. To determine the quantity of the MALP in Table 4.6, the 12.8 ft^3 repair volume is divided by the volume of a kit (one bag of dry material and one jug of activator) which is 0.45 ft^3. MALP gives the highest repair cost, which is around 20 times higher than the FR-SCC and 5 times higher than the UHPC.

Table 4.4: Cost Estimation for FR-SCC

Material type	Unit	Unit cost (USD)	Cost Source	Quantity	Total cost (USD)
Portland Cement (Type I/II)	lb	0.057	Engineering News Record	195.56	11.15
Sand	lb	0.013	Purchase records	677.5	8.97
Coarse Aggregate	lb	0.025	Purchase records	600.1	15
Air Entrainer (Master Builders AE-90)	lb	0.78	Manufacturer	0.24	0.18
High Range Water Reducer (Glenium 7920)	lb	1.55	Manufacturer	1.775	2.75
Type K Cement (Komponent)	lb	0.23	Manufacturer	53.33	12.3
Citric Acid	lb	-		0.19	-
Fly Ash	lb	0.014	Internet research	106.7	1.49
Polypropylene Fibers	lb	2.0	Manufacturer	3.65	7.3
Total					59.14

The cost and amount of citric acid are negligible for the FR-SCC mix; therefore, it is ignored for the cost estimation.

Table 4.5: Cost Estimation for UHPC

Material type	Unit	Unit cost (USD)	Cost Source	Quantity	Total cost (USD)
Portland Cement (Type I/II)	lb	0.6	Engineering News Record	402	241.2
Slag	lb	0.02	Internet research	201	4.02
Silica Fume	lb	0.35	Internet research	600.1	67
Fine Masonry Sand	lb	0.01	Purchase records	670	6.7
Steel Fibers	lb	2.0	Purchase records	90.13	180.26
High Range Water Reducer (Glenium 7920)	lb	1.63	Manufacturer	12.2	19.88
Total					475.5

Table 4.6: Cost Estimation for MALP Concrete

Material type	Unit	Unit cost (USD)	Cost Source	Quantity	Total cost (USD)
Dry component+activator	1 bag+1 jug	85	Purchase records	28.4	2417.8
Total					2417.8

4.6 Results Summary

This section contains the outcome of all the experiments on both the original and the repaired beams. A summary of the results is included in Table 4.7. For a better comparison, calculations for the nominal flexural capacity were performed using strain compatibility and bond-shear failure method for shear capacity described by Ross (2013). The values in Table 4.7 are expressed in terms of the point load, which causes flexure or shear failure. The reaction of the support closest to the point load corresponding to the maximum applied load, and the self-weight of the girder is taken as the shear capacity, as mentioned in Table 4.7. The flexural capacity is determined by taking the support reaction multiplied by its distance from the point load and the moment generated by the self-weight about the load point subtracted from the result. In this way, the load can be converted to the shear and flexural capacities. The calculations are further illustrated in Chapter 6, and their result summary is included in Table 4.7. By observing the cracking load for the experimental results between the original (MU) and repaired (MR) beams in Table 4.7, it can be noticed that the cracking load is lower for the MR beams compare to the MU beams. The difference ranges from 0% to 32.5% because, for the repaired beams, the transfer length has further increased due to the induced end region damage, which indicates that there is little to no contribution from the prestressing for the repaired beams; however, the ultimate load values are much higher than the MU beams from 26% to 63.2%. The scattering percentage difference can also be attributed to the varying level of damage after the initial test or the variability of cracking strength.

Table 4.7: Summary of the Experimental and Analytical Results

Beam	Repair	Experimental						Analytical		
		Cracking Load (kips)			Ultimate load (kips)			Max. point load for nominal moment (kips)	Max. point load for nominal shear (kips)	
		MU	MR	% diff.	MU	MR	% diff.	Original/ repaired	MU	MR
M-1	New MALP	43	43	0	50	74	+48	58.4-75.4	43.2	118.9
M-2	FR-SCC	43	29	-32.5	54	68	+26	58.4-75.4	48	108.2
M-3	FR-SCC	46	44	-4.3	54	72	+33.3	58.4-75.4	48	108.2
M-4	OLD MALP	40	30	-25	50	68	+36	58.4-75.4	41.8	99.6
M-5	UHPC	46	39	-15.2	53	82	+54.7	58.4-75.4	38.54	102.5
M-6	UHPC	45	40	-11.1	49	80	+63.2	58.4-75.4	41.8	102.5

For the analytical results presented in Table 4.7, the maximum point load for nominal shear (estimated capacity) is closer to the MU experimental results, indicating the accuracy of the method offered by Ross et al. (2013) for predicting the failure load of the end regions including bond loss. The percentage difference uses the MU experimental values as a reference, and a positive sign means an improvement from the MU, whereas a negative sign indicates a lower value than the reference. The pre-and post-repair flexural capacity is the same and is calculated based on strain compatibility, as shown in Chapter 6. This value is higher than the shear capacity of the original beam; therefore, the failure of the beams in the first load test is due to shear and bond, but after the repair, the shear capacity exceeds the flexural capacity, which makes the final repaired beam failures primarily in flexure. For determining the flexural capacity of the repaired beam, the contribution of the repair materials is ignored. For the repaired beam, it is assumed that the flexural failure occurs in the unrepaired girder at the vicinity of repair, and this can be verified by observing the crack patterns of the load test for the repaired beams.

Figure 4.31 shows the experimental ultimate load comparison for the MU and MR beams. All the repaired girders show significant improvement in their ultimate strength; however, the difference between the ultimate load of each repaired beam is negligible. On the other hand, cost estimation shown in Figure 4.32 indicates a noticeable difference between each repair material which can help decide the type of repair material appropriate for a given situation.

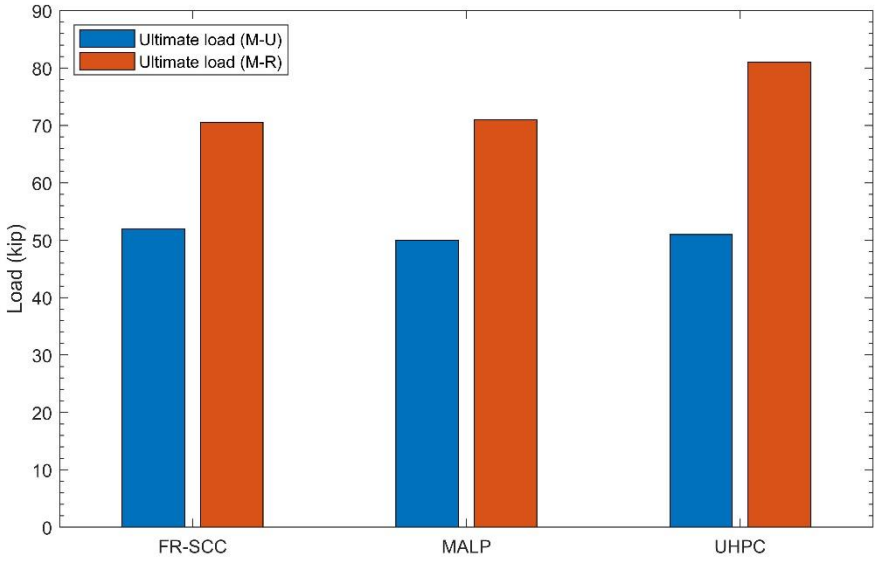

Figure 4.31: Experimental ultimate load comparison

Figure 4.33 shows the load vs. deflection curve comparison for all the repaired beams. It can be observed that the UHPC beams have the highest, and the old MALP has the lowest ultimate load value. Deflection for the old MALP is 1.45 in. which is more than all the other repaired beams, which can be related to the lower compressive strength of the material.

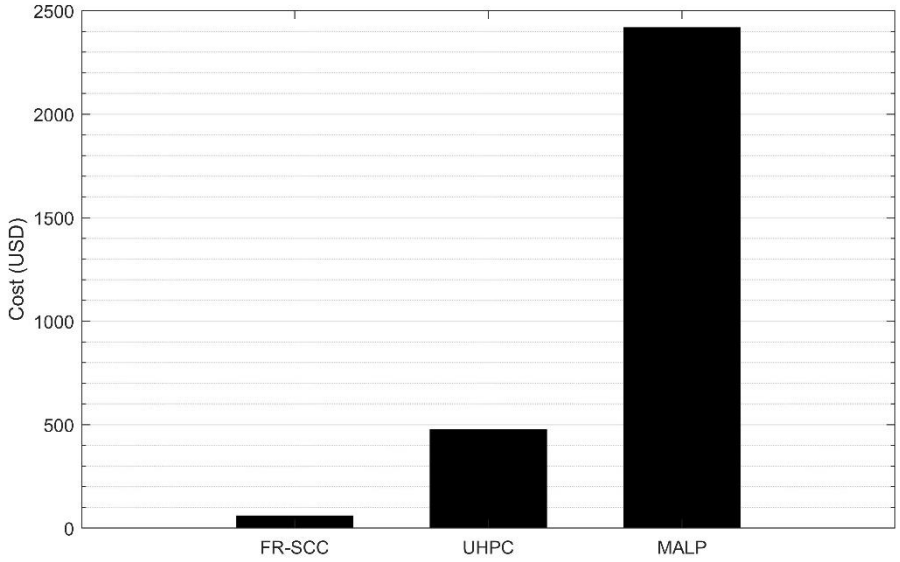

Figure 4.32: Cost estimation comparison

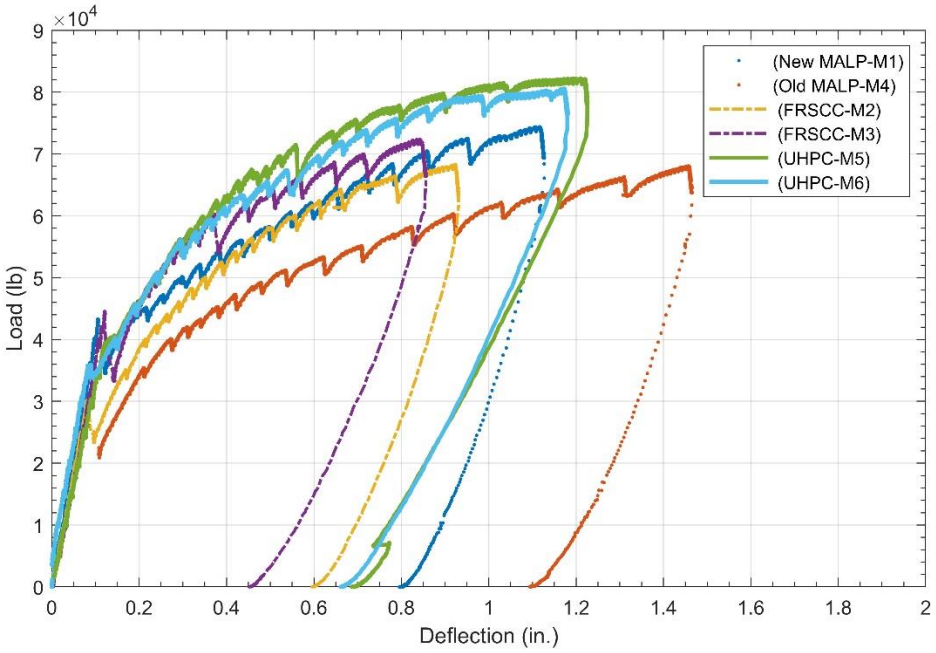

Figure 4.33: Repaired beams load vs. deflection curve comparison

Chapter 5: Conclusions and Recommendations

This research aimed to identify a functional and cost-effective repair technique to restore the lost shear capacity and protect the member from further deterioration. The goal was followed by constructing and testing the beam specimens, experimentally determining the strength of the repair materials, and comparing the beam test results with the analytical outcomes. Cost analysis and the ultimate strength comparison were performed to help decide the best repair type for a specific field application. Detailed calculations have been made in Chapter 7, which can help develop a relationship between parameters while revealing the accuracy of the different analytical approaches. A summary of the conclusions and recommendations is given below.

5.1 Conclusions

- Experimental results indicate a 26%-63% improvement for the repaired girders' ultimate strength with enhanced ductility.
- The repairs also changed the failure mechanism of the beams from a brittle bond-shear failure to a more ductile bond-flexure failure giving noticeable deflection with sustained capacity before the deck started crushing. This observation indicates that the repairs tested in this research can be used to change the beam failure mechanism.
- Beams repaired with UHPC outperformed the FR-SCC and MALP repairs in terms of both the cracking and ultimate loads despite having the smallest repair thickness, indicating a direct relationship between the repair material's efficiency and its compressive strength. Also, the high percentage of steel fibers gives UHPC a better post-crack performance than the other repair materials.

- No delamination or differential movement between repair and the member was observed at ultimate load which assures that the repaired beam can resist applied service loads without losing bond.
- For the MU beams, strand slip started with the first crack intersecting the strands, which is typical for all the initial tests. However, for the repaired beams, slip took place at a higher load than the first crack, which indicates the first crack is outside of the transfer length or does not contribute to the capacity loss. Contrary to the initial load test, slip proportionally increased with the load for the repaired beams.
- All the repair materials can be used for improving both the service and ultimate limit states.

5.2 Recommendations

- Despite significant improvement in the end regions after the repair, further research regarding the repair's long-term performance under cyclic load is recommended.
- Further research is required to optimize the thickness of the repair based on the type of damage.
- Epoxy can be used to fill the cracks before applying the repair. This provides a level of stability and increases the stiffness of the member.
- It may be better to provide a margin of extra repair length beyond the damaged section for the FR-SCC and MALP repairs to avoid cracks at the junction of repair and the beam. However, further research is required to proof this claim and to quantify the extension length since the applied load was placed at the end of the repair in this research.
- For determining the type of repair material, factors like the cost, the severity of the damage, mechanical properties of the repair materials, speed of construction, and

availability of raw materials should be considered. The workability of repair materials is another factor that should be considered before the field application. MALP quickly loses its workability due to the exothermic reaction, making it challenging to work with, especially in hot weather. FR-SCC is very sensitive to water content and quickly becomes unstable with a slight deviation from the optimal water content, requiring some trial batches before its application. The high level of repair materials' workability necessitates a leveled base for formwork, which should be sealed from all sides and corners to avoid leakage of the paste while casting.

Chapter 6: References

1. *AASHTO LRFD Bridge Design Specifications*. 2017. Washington, DC: American Association of State Highway and Transportation Officials.
2. Abdulhameed, H. A. (2018). "*Experimental and Analytical Study of Fiber- Reinforced Self-Consolidating Concrete as a Repair Material*." Dissertation, School of Graduate Studies Rutgers, The State University of New Jersey: ProQuest LLC (2018).
3. *ACI 318-19: Building code requirements for structural concrete: Commentary on building code requirements for structural concrete (ACI 318R-19)*. (2019). Farmington Hills, MI: American Concrete Institute.
4. Alkhrdaji, Tarek. 2021. "*Strengthening of Concrete Structures Using FRP Composites*." *STRUCTURE Magazine*. Accessed February 10. https://www.structuremag.org/?p=8643
5. Andrawes, Bassem, Ian Shaw, and Hang Zhao. 2018. "*Repair & Strengthening of Distressed/Damaged Ends of Prestressed Beams with FRP Composites.*" Research Report No. FHWA-ICT-18-001, doi:10.36501/0197-9191/18-001.
6. Ángel, C. M. (2012). *Compatibility of ultra-high performance concrete as repair material: Bond characterization with concrete under different loading scenarios* (Master's thesis, Department of Civil and Environmental Engineering, Michigan Technological University, 2012). ProQuest LLC.

7. ASTM International. C1856/C1856M-17 Standard Practice for Fabricating and Testing Specimens of Ultra-High Performance Concrete. West Conshohocken, PA; ASTM International, 2017. doi: https://doi-org.ezproxy.lib.ou.edu/10.1520/C1856_C1856M-17
8. ASTM International. C1611/C1611M-18 Standard Test Method for Slump Flow of Self-Consolidating Concrete. West Conshohocken, PA; ASTM International, 2018. doi: https://doi-org.ezproxy.lib.ou.edu/10.1520/C1611_C1611M-18
9. Choate, J. G. 2018. "*Implementing Fiber-Reinforced, Self-Consolidating Concrete as a Repair Material for AASHTO Prestressed Concrete Girders*." Thesis, Norman. University of Oklahoma-Norman.
10. "Concrete Repair Products - See Our Data Guides." 2020. Phoscrete Corporation. https://www.phoscrete.com/data-guides/
11. Department of Transportation/Federal Highway Administration. "*Ultra-High Performance Concrete*." 2011. U.S. Accessed November 30.
12. Foster, R. M.; Brindley. M.; Lees J. M.; Ibell T. J.; Morley C. T.; Darby A. P.; and Evernden M. C.. 2017. "*Experimental Investigation of Reinforced Concrete T-Beams Strengthened in Shear with Externally Bonded CFRP Sheets.*" Journal of Composites for Construction 21 (2): 04016086. doi:10.1061/(asce)cc.1943-5614.0000743.
13. Gangi, Michael E.; Justin E. Liesen; Jiaxing E. Zhou; Vanessa E. Pino; Thomas E. Cousins; Roberts E. Wollmann; Ioannis E. Koutromanos; and Antonio E. Nanni. 2018. Rep. "*Evaluation of Repair Techniques for Impact-Damaged Prestressed Beams*.". Report No: FHWA/VTRC 18-R8, Virginia Transportation Research Council.

14. Ghaffary, Azin; and Mohamed A. Moustafa. 2020. "*Synthesis of Repair Materials and Methods for Reinforced Concrete and Prestressed Bridge Girders*." Materials 13 (18): 4079. doi:10.3390/ma13184079.
15. Gunes, Oguz, Seda Yesilmen, Burcu Gunes, and Franz-Joseph Ulm. 2012. "*Use of UHPC in Bridge Structures: Material Modeling and Design.*" Advances in Materials Science and Engineering 2012: 1–12. doi:10.1155/2012/319285.
16. Harries, Kent A, Jarret A Kasan, and John A Aktas. 2009. Rep. *"Repair methods for prestressed concrete girders*." Report No: FHWA-PA-2009-008-PIT 006, Department of civil and environmental engineering, University of Pittsburgh, Pennsylvania.
17. Harries, Kent A; Jarret A Kasan; and Richard A Miller. 2012. Rep. "*Guide to recommended practice for the repair of impact-damaged prestressed concrete bridge girders."* Research Program (NCHRP) Project 20-07.
18. Jones, Mark Stevens. 2015. "*Repair of impact-damaged prestressed bridge girders with strand splices and fabric reinforced cementitious matrix systems."* Thesis, Virginia Polytechnic Institute, and State University, Blacksburg, VA.
19. Kassimi, Fodhil; Ahmed K. El-Sayed; and Kamal H. Khayat. 2014. "Performance of Fiber-Reinforced Self-Consolidating Concrete for Repair of Reinforced Concrete Beams." *ACI Structural Journal* 111 (6), Title No: 111-S108, doi:10.14359/51687031.
20. Kassimi, Fodhil. 2013. *"Development and Performance of Fiber-reinforced Self-Consolidating Concrete for Repair Applications.*" Thesis. Universite De Sherbrooke, Ottawa, Canada.

21. Khayat, Kamal H.; Fodhil Kassimi; and Parviz Ghoddousi. 2014. "Mixture Proportioning and Testing of Fiber-Reinforced Self-Consolidating Concrete." *ACI Materials Journal* 111 (2). doi:10.14359/51686722.

22. Looney, Trevor; Raina Coleman; Chandler Funderburg; Jeffery Volz; and Royce Floyd. 2021. "*Concrete Bond and Behavior of Nonproprietary Ultrahigh-Performance Concrete Bridge Slab Joints.*" Journal of Bridge Engineering 26 (2): 04020128. doi:10.1061/(ASCE)be.1943-5592.0001669.

23. Mayhorn, Darion Timothy. 2016. "*Investigation of the Effects of End Region Deterioration in Precast, Prestressed Concrete Bridge Girders.*" Thesis. University of Oklahoma.

24. Mosallam, Ayman; Hussein M. Elsanadedy;Tarek H. Almusallam; Yousef A. Al-Salloum; and Saleh H. Alsayed. 2015. "*Structural Evaluation of Reinforced Concrete Beams Strengthened with Innovative Bolted/Bonded Advanced FRP Composites Sandwich Panels.*" *Composite Structures* 124: 421–440. doi:10.1016/j.compstruct.2015.01.020.

25. Murthy, A. Ramachandra, B.l. Karihaloo, P. Vindhya Rani, and D. Shanmuga Priya. 2018. "*Fatigue Behaviour of Damaged RC Beams Strengthened with Ultra High-Performance Fibre Reinforced Concrete*." *International Journal of Fatigue* 116: 659–668. doi:10.1016/j.ijfatigue.2018.06.046.

26. Naji, Behnam, Brandon E. Ross, and Royce W. Floyd. 2017. "*Characterization of Bond-Loss Failures in Pretensioned Concrete Girders.*" Journal of Bridge Engineering 22 (4): 06016013. doi:10.1061/(asce)be.1943-5592.0001025.

27. Radlińska, Aleksandra, Leslie Myers Mccarthy, James Matzke, and Francis Nagel. 2014. "*Synthesis of DOT Use of Beam End Protection for Extending the Life of Bridges.*" International Journal of Concrete Structures and Materials 8 (3): 185–199. doi:10.1007/s40069-014-0077-0.

28. Ramseyer, Chris, and Thomas H.-K. Kang. 2012. "Post-Damage Repair of Prestressed Concrete Girders" *International Journal of Concrete Structures and Materials* 6 (3): 199–207. doi:10.1007/s40069-012-0019-7.

29. Rao, Gappa. 2001. "Generalization of Abrams Law for Cement Mortars." *Cement and Concrete Research* 31 (3): 495–502. doi:10.1016/s0008-8846(00)00473-7.

30. Ross, Brandon E., and Behnam Naji. 2014. "*Model for Nominal Bond-Shear Capacity of Pretensioned Concrete Girders.*" Transportation Research Record: Journal of the Transportation Research Board 2406 (1): 79–86. doi:10.3141/2406-09.

31. Seo Junwon; Eduardo Torres; William Schaffer; and Nadim Wehbe. 2017. Rep. *Self-Consolidating Concrete for Prestressed Bridge Girders*. Brookings, South Dakota.

32. Shafei, Behrous, Brent Phares, and Weizhuo Shi. 2020. *Beam End Repair for Prestressed Concrete Beams*. Report No: IHRB Project TR-715, IOWA State University, Ames, IA.

33. Shanafelt, George O., and Willis B. Horn. 1980. NCHRP Rep 226. *Damage evaluation and repair methods for prestressed concrete bridge members.* Washington, D.C: National Cooperative Highway Research Program.

34. Sobieck, Tyler. 2014. *"Predicting fatigue life extension of steel reinforcement in R.C. beams repaired with externally bonded CFRP."* Thesis, ProQuest LLC . Colorado State University, Fort Collins, CO.

35. Valerio, Pierfrancesco.; Timothy. J. Ibell, and Antony. P. Darby. 2009. "Deep Embedment of FRP for Concrete Shear Strengthening." *Proceedings of the Institution of Civil Engineers - Structures and Buildings* 162 (5): 311–321. doi:10.1680/stbu.2009.162.5.311.

36. Wirkman, Corey Michael. 2016. "*Performance of Fiber-Reinforced Self-Consolidating Concrete for Repair of Bridge Sub-Structures*." Thesis, Norman. University of Oklahoma.

37. Yuan, Jiqiu, and Benjamin Graybeal. 2016. "*Evaluation of Bond of Reinforcing Steel in UHPC: Design Parameters and Material Property Characterization.*" Proceedings of the First International Interactive Symposium on UHPC. doi:10.21838/uhpc.2016.102.

38. Zmetra, Kevin M., Kevin F. Mcmullen, Arash E. Zaghi, and Kay Wille. 2017. "*Experimental Study of UHPC Repair for Corrosion-Damaged Steel Girder Ends*." *Journal of Bridge Engineering* 22 (8): 04017037. doi:10.1061/(ASCE)be.1943-5592.0001067.

Chapter 7: Calculations

7.1 Shear Capacity Calculations Based on AASHTO LRFD Methods

This calculation aims to find out the load P and its location on the beam that causes shear failure before flexure. For this purpose, a spreadsheet was developed using the modified compression field theory method outlined in AASHTO LRFD (2017), which helped to find the load and the location causing shear failure of the end regions before the girder fails in flexure. After many iterations, this load came out to be P=65.5 kips acting at 3.5 ft from the end of the beam. To show how the spreadsheet worked and to verify that at P=65.5 k acting at 3.5 ft from the end, the beam fails in shear before flexure, the following calculation is performed:

Input data:

$A_{ps} = 0.334\ in^2$

$d_p = 25.375\ in.$

$A_s = 0.62\ in^2$

$f_s = 60\ ksi;\ (after\ verifying\ that\ tension\ steel\ yields\ using\ strain\ compatibility)$

$d_s = 3.875\ in.;\ (\ using\ strain\ compatibility)$

$f_{pu} = 270\ ksi$

$f_{py} = 0.9\ f_{pu} = 243\ kips$

$\alpha = 0.85\ (for\ f'_c \leq 10\ ksi);\quad \beta_1 = 0.65\ (\ for\ f'_c = 8\ ksi)$

$A'_s = 1.24\ in^2$; (area of compression steel)

$b = 9\ in$; (width on the section in compression)

$E_s = 29{,}000\ ksi$; (modulus of elasticity of mild steel)

$f_{pu} = 270\ ksi$; (ultimate strength of the prestressing strands)

$f'_c = 8\ ksi$; (28- days compressive strength of concrete)

$w_u = 0.15\frac{k}{ft}$; (self-weight of the girder)

$f'_s = 10.6\ ksi$; (stress in compression steel)

$h = 27.125\ in.$; (height of the composite section)

$L = 17.5\ ft$; (span length)

$x = 3.5\ ft$; (location of load application from the end of the girder)

$P = 65.5\ kips$; (point load)

$A_V = 0.22\ in^2$; (area of double-leg shear stirrups)

$A_{ct} = 69.43\ in^2$; (area of the concrete on the flexural tension side of the member

$\alpha_2 = 90°$; (for vertical stirrups)

λ= 1.0; (concrete density modification factor)

$b_v = 3\ in.$; (width of the web)

$h_f = 4.625\ in.$; (height of the flange)

$b_f = 6\ in.$; (width of the flange)

Required:

To prove that if P=65.5 kips is applied at 3.5 ft from the end of the beam, it is expected to fail in shear before flexure.

Solution:

$$k = 2 \cdot \left(1.04 - \frac{f_{py}}{f_{pu}}\right) = 2 \cdot \left(1.04 - \frac{(0.9)(270\ ksi)}{270\ ksi}\right) = 0.28 \quad (1)$$

$$c = 2.85\ in.;\ (from\ strain\ compatibility\ equation\ explained\ in\ section\ 7.4)$$

$$a = \beta \cdot c = 0.65 \cdot 2.85\ in = 1.85\ in. \quad (2)$$

$f_{ps} = 268$ ksi; (from strain compatibility section 7.4)

$$d_e = \frac{A_{ps} \cdot f_{ps} \cdot d_p + A_s \cdot f_y \cdot d_s}{A_{ps} \cdot f_{ps} + A_s \cdot f_y} =$$

$$\frac{(0.334\ in^2)(268\ ksi)(25.375\ in) + (0.62\ in^2)(60\ ksi)(3.875\ in)}{(0.334\ in^2)(268\ ksi) + (0.62\ in^2)(60\ ksi)} = 19.06\ in. \quad (3)$$

$$d_{v1} = 0.9 \cdot d_e = 0.9 \cdot 19.06\ in. = 17.156\ in. \quad (4)$$

$$d_{v2} = 0.72 \cdot h = 0.9 \cdot 27.125\ in. = 19.53\ in. \quad (5)$$

The final d_v is the maximum of d_{v1} and d_{v2}, therefore, $d_v = 19.53\ in.$

$V_u\ at\ the\ support = Reaction\ due\ to\ selfweight + reaction\ due\ to\ point\ load$

$$V_u = \frac{(0.15\ k/ft)(17.5\ ft)}{2} + \frac{65.5\ k\ (17.5\ ft - 3.5\ ft)}{17.5\ ft} = 53.7\ kip$$

$M_u\ at\ the\ support = 0$

Note that during the calculation, the value of the effective distance between the load point and the support was not available; therefore, 3.5 ft was used for V_u calculation.

$$V_u \, at \, 3.5 \, ft = V_u \, \, at \, support - (x)(w_u)$$

$$V_u \, = 53.7 \, k - 3.5 \, ft \left(0.15 \frac{k}{ft}\right) = 53.2 \, k$$

$$M_u \, at \, 3.5 \, ft = \frac{1}{2} (\, V_u \, \, at \, support + V_u \, \, at \, 3.5 \, ft)(3.5 \, ft) = 0.5 \cdot (53.7 \, k + 53.2 \, k) \cdot 3.5 ft$$

$$M_u \, at \, 3.5 \, ft = 187.1 \, k - ft$$

$$\varepsilon_s = \frac{\frac{|M_u|}{d_v} + 0.5 \cdot N_u + |V_u - V_P| - A_{ps} \cdot f_{po}}{E_s \cdot A_s + E_P \cdot A_{PS}} \tag{6}$$

Where:

$$N_u \, = Factored \, axial \, force$$

$$V_p = Component \, of \, the \, prestressing \, force \, in \, the \, direction \, of \, shear \, force$$

$$\varepsilon_s = \frac{\frac{|(187.1)(12) k - in.|}{19.53 \, in.} + 0 + |53.2 \, k - 0| - 0.334 \, in^2 \cdot (0.7 \cdot 270 \, ksi)}{29{,}000 \, ksi \cdot 0.62 \, in^2 + 28500 \, ksi \cdot 0.334 \, in^2} = 0.00382$$

$$\varepsilon_s > 0, so \, \varepsilon_s = 0.00382$$

$$\beta = \frac{4.8}{1 + 750(\varepsilon_s)} = \frac{4.8}{1 + 750 \cdot (0.00382)} = 1.24 \tag{7}$$

$$V_C = 0.0316 \cdot \beta \cdot \sqrt{f'_c} \cdot \lambda \cdot b_v \cdot d_v \tag{8}$$

$$V_C = 0.0316 \cdot 1.24 \cdot \sqrt{8 \, ksi} \cdot 1 \cdot 3 \, in \cdot 19.53 \, in = \, 6.5 \, kips$$

$$\emptyset \cdot V_C = 0.85 \cdot 6.5\ k = 5.52\ k$$

$$\frac{\emptyset \cdot V_C}{2} = \frac{5.52\ k}{2} = 2.76\ k$$

Spacing of stirrups under point load is s=6 in. Therefore:

$$V_s = \frac{(A_v)\cdot(f_{yr})\cdot(d_v)\cdot(cot\theta + cot\alpha)\cdot sin(\alpha)}{s} \quad (9)$$

Where:

$$\alpha = 90°, for\ vertical\ shear\ reinforcement$$

$$\theta = 29 + 3500 \cdot \varepsilon_s \quad (10)$$

$$\theta = 29 + 3500 \cdot (0.00382) = 42.37°$$

$$V_s = \frac{(0.22\ in^2)\cdot(60\ ksi)\cdot(19.5\ in.)\cdot(cot42.37°)}{6\ in.} = 47.1 \text{ kips}$$

To find the total shear capacity, the values of V_s and V_c are added and compared with a minimum value written in b.

$$a = V_s + V_c \quad (11)$$

$$a = 53.6\ kips$$

$$b = 0.125 \cdot f'_c \cdot d_v \cdot b_v \quad (12)$$

$$b = 0.125 \cdot 8\ ksi \cdot 19.53\ in \cdot 3\ in = 58.6\ k$$

Shear capacity is the minimum of a and b.

$$\boldsymbol{V_n(capacity) = 53.6\ kips}$$

$$\boldsymbol{V\ (based\ on\ the\ P = 65.5\ k\ at\ 3.5\ ft) = 53.18\ kips}$$

From the above V values, it can be concluded that that at P=65.5 k, the reaction that generates Mu=187 k-ft is V=53.18 k. However, the moment capacity for the beam in section 7.4 is Mu=196.54 k-ft. This indicates that the support reaction should be greater than the 53.18 k to cause flexural failure. On the other hand, the support reaction which causes shear failure is 53.6 k, and a slight increase in the applied load exceeds the shear capacity and causes shear failure before flexure. It should be noted that for calculating both the flexural and shear capacities, the effect of transfer length was ignored.

7.2 Strut and Tie Model

To determine the number of shear keys for the damaged zones, a strut and tie model of the beam end regions was developed (Figure 3.14) and analyzed to determine the total compressive force of the end regions, which causes compression field action and is responsible for shear failure. To determine the compressive force in the struts AC and BD in Figure 3.14, the model has been analyzed as follows:

Max applied point load (P), which causes shear failure, based on AASHTO shear capacity calculation is P=65.5 kips. The reaction of this force for the closest support to the load is V_A=53.71 kips. Using the method of joints for the strut and tie model truss, the following analysis can be performed:

Joint A:

$$\sum Fy = 0$$

$$53.71\ kips + F_{AC} \cdot \sin(61°) = 0$$

$$F_{AC} = -61.4\ kips$$

$$\sum Fx = 0$$

$$F_{AB} + F_{AC} \cdot cos(61°) = 0$$

$$F_{AB} = 29.8\ kips$$

Joint B:

$$\sum Fy = 0$$

$$F_{BC} + F_{BD} \cdot \sin(45°) = 0$$

$$F_{BC} = -0.707F_{BD}$$

$$\sum Fx = 0$$

$$-F_{AB} + F_{BE} + F_{BD}cos(45°) = 0$$

$$-29.8\ kips + F_{BE} + F_{BD}cos(45°) = 0$$

$$F_{BE} + 0.707F_{BD} = 29.8\ kips$$

$$F_{BE} + 0.707F_{BD} = 29.8\ kips$$

Joint C:

$$\sum Fx = 0$$

$$-F_{AC}cos(61°) + F_{CD} = 0$$

$$F_{CD} = -61.4\ kips \cdot cos(61°)$$

$$F_{CD} = 29.8\ kips$$

Joint D:

$$\sum Fy = 0$$

$$-65.5\ kips - F_{DB} \cdot cos(45°) - F_{DE} \cdot cos(45°) = 0$$

$$\therefore F_{DB} = F_{DE}$$

$$-F_{DB} \cdot cos(45°) - F_{DB} \cdot cos(45°) = 65.5\ kips$$

$$F_{DB} = -46.31\ kips$$

The summation of compressive force in the members AC and BD is equal to 107.7 kips. Based on AASHTO (2017), section 5.7.4.3, the nominal shear resistance of the interface plane shall be taken as:

$$V_{ni} = c \cdot A_{CV} + \mu(A_{vf} \cdot f_y + P_c) \quad (13)$$

Where:

V_{ni} = nominal interface shear resistance (kip)

c = cohesion factor specified in AASHTO (2017), Article 5.7.4.4 (ksi)

A_{CV} = interface area. $A_{CV} = b_{vi} \cdot l_{vi}$;

Where: $b_{vi} = interface\ width$ and, $l_{vi} = interface\ length$

μ = friction factor specified in AASHTO (2017), Article 5.7.4.4

A_{vf}= interface shear reinforcement. In this case, this value is zero.

f_y= yield strength of interface reinforcement

P_c = permanent net compressive force normal to the shear plane, if force is tensile P_c=0

V_{ni} should not exceed:

$$V_{ni} \leq k1 \cdot f'c \cdot A_{CV} \quad (14)$$

$$V_{ni} \leq k2 \cdot A_{CV} \quad (15)$$

Where:

$k1$ = friction of concrete strength available to resist interface shear, as specified in AASHTO (2017), Article 5.7.4.4

$k2$ = limiting interface shear resistance specified in AASHTO (2017), Article 5.7.4.4 (ksi)

$f'c =$ design concrete compressive strength of the weaker concrete on either side of the interface (ksi)

Based on AASHTO (2017), section 5.7.4.4, for a clean concrete surface, not intentionally roughened, the values are:

c = 0.075 ksi

μ = 0.6

$k1$ = 0.2

$k2$ = 0.8 ksi

Note that the actual surface is a roughened surface, however, to be more conservative, the surface roughness is ignored. For calculating the interface area (A_{cv}), the value of b_{vi}= 16.5 in. and l_{vi}= 3.5 ft=42 in. Therefore:

A_{CV}= (16.5 in) (42 in) = 693 in^2

$$V_{ni} = c \cdot A_{CV} + 0 = (0.075\ ksi) \cdot (693\ ksi) + 0 \cong 52\ kips$$

As repair concrete is provided for both faces of the damaged zone, therefore, total $V_{ni} = 2 \cdot 52\ kips = 104\ kips$. The force which needs to be taken by the shear keys is:

Force to be taken by shear keys= $107.7\ kips - 104\ kips = 3.7\ kips$

Number of Tapcon® screws for f'c=4000 psi; screw diameter=1/4 in.; minimum embedment length=1.5 in.; and shear strength of one screw v=1380 lb is as follows:

$$Number\ of\ shear\ keys = \frac{3.7\ kips}{1.38\ kips} = 2.68, say\ 3$$

$$Number\ of\ shear\ keys\ for\ one\ face = \frac{3\ screws}{2} = 1.5 \text{ say } 2$$

This means that the total number of screws required for each face of the end region is 2. However, to avoid stress concentration in a smaller area and to count for redundancy, 9 shear keys were used on each face, as shown in Figures 3.12 and 3.13.

7.3 Shear Capacity for the Original Beams Using a Model for Nominal Bond-Shear Capacity of Prestressed Concrete Girders (Ross, 2014)

7.3.1 M1-U

$$V_{nBV} = \frac{T}{\cot\theta_c} + \frac{V_s \cdot X_s}{d \cdot \cot\theta_c} + \frac{V_n \cdot d_h}{d} + \frac{H_h \cdot d_h}{\mathrm{d} \cdot \cot\theta_c} \quad (16)$$

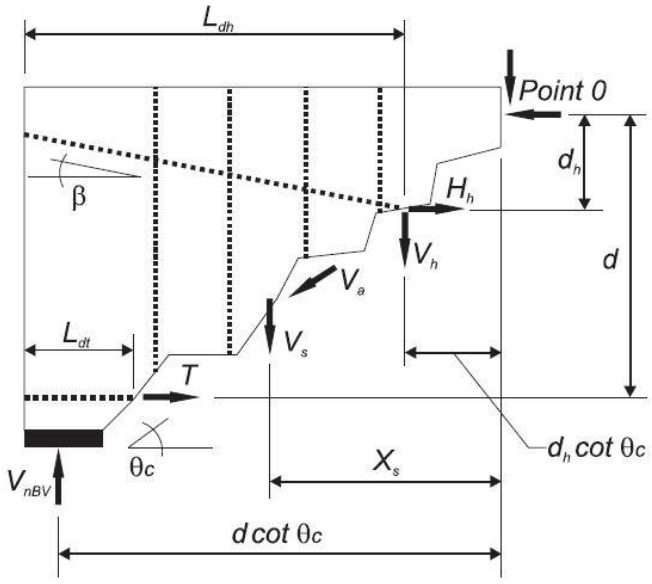

Where:

d = Flexural depth of tension tie
d_h = Depth of harped strands at crack interface
H_h = Horizontal force in harped strands
L_{dh} = Available embedment length of harped strands
L_{dt} = Available embedment length of tension tie
V_h = Vertical force in harped strands
V_{nBV} = Nominal bond-shear capacity
X_s = Horizontal distance to vertical steel centriod
β = Inclination angle of harped strands
θ_c = Inclination angle of crack

Figure 6.1. Free body diagram of end region for a bond-shear model (Ross, 2014)

$$T = As \cdot f_{sBV} + Aps \cdot f_{PBV} \quad (17)$$

$$f_{sBV} = f_y \cdot \left(\frac{L_{dt}}{l_{db}}\right) < f_y$$

$$f_{PBV} = f_{pe} \cdot \left(\frac{L_{dt}}{l_t}\right) < f_{pe}$$

$$T = 0 + 2 \cdot 0.167\ in^2 \cdot f_{PBV}$$

Where:

f_{sBV} =stress in reinforcement bars accounting for available development length

f_{PBV} =stress in prestressing strands accounting for available development length

l_{db}= required development length of reinforcement bars

f_{pe}= effective prestress in strands

l_t= required transfer length for prestressing strand

For finding effective prestress (f_{pe}), losses were calculated based on AASHTO detailed, AASHTO approximate, and Zia et al. methods. Here, the value is selected based on AASHTO approximate and Zia et al., which is 170 ksi.

$$f_{pe} = 170\ ksi$$

$$L_t = 60 \cdot (d_b) = 60 \cdot 0.52\ in = 31.2\ \text{in} = 2.6\ ft \quad (18)$$

$$L_{dt} = X_{0h} + X_{brg} + X_t \quad (19)$$

$$L_{dt} = 1.75\ \text{in} + 6\ \text{in} + 2\ \text{in} = 9.75\ \text{in}$$

Note: The variables of L_{dt} are explained in Figure 6.2.

$$f_{pBV} = 170\ ksi \cdot \left(\frac{9.75\ in}{31.2\ in}\right) = 53.125\ ksi < fpe \quad \dots ok \tag{20}$$

$$T = 2 \cdot 0.167\ in^2 \cdot 42.227\ ksi = 14.1\ ksi$$

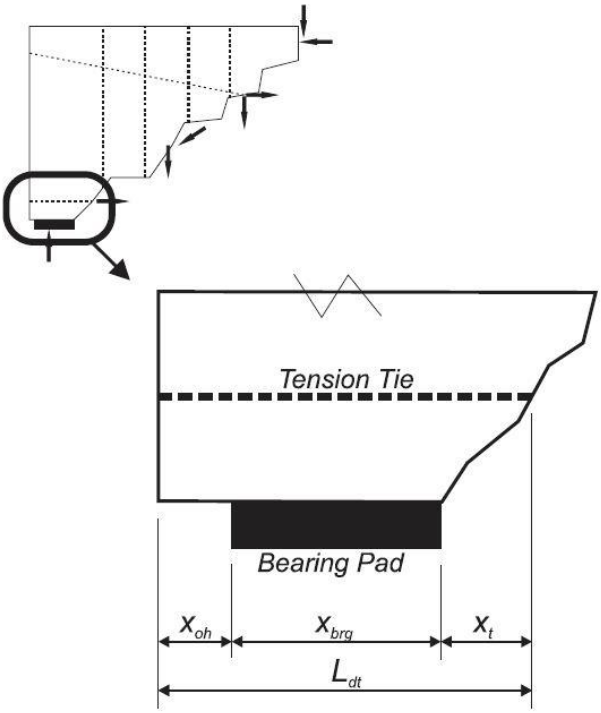

Figure 6.2. Parameters for available development length (Ross, 2014)

The number of stirrups intersecting the main crack is 5. If the number of stirrups intersecting the crack is required before the test, we can divide the member's depth, which is approximately equal to the horizontal length of the crack, by the centerline spacing between the stirrups (d/s).

$$Vs = Number\ of\ stirrups \cdot A_v \cdot f_{sv} \tag{21}$$

$$Vs = 5 \cdot 2 \cdot (0.11\ in)^2 \cdot 60\ ksi = 66\ kips$$

Where:

V_s= shear capacity provided by the stirrups

A_v= area of shear stirrups

f_{sv}= shear strength of stirrups

$Xs = 8\ in$

$\theta_c = 41°$

The value of θ_c was selected based on the actual crack of the girder after the test. If this value is required before the test, then $\cot\theta_c$ can be put equal to (a/d), and the value of θ_c can be obtained by taking the inverse of the cotangent. This rule only can be applied if the ratio of (a/d) is less than 2.5 (Ross, 2014).

$d = 18.8\ in$ (This value can be used instead of final dv in section 7.1)

$$V_{nBV} = \frac{14.1\ kips}{\cot 41°} + \frac{66\ kips \cdot 8\ in}{18.8\ in \cdot \cot 41°} + 0 + 0 \cong 36.7 kips$$

$$V_{nBV} = \frac{P \cdot b}{L}$$

Where:

d= distance between resultant compression and resultant tension

P= point load

b= distance between p and center line of far end support

L= effective span

$$P = (V_{nBV} - \frac{w \cdot L}{2}) \cdot \frac{L}{b} = (36.7\ kips - \frac{(0.15)\frac{k}{ft} \cdot (17.35)\ ft}{2}) \cdot \frac{17.35\ ft}{(17.35 - 3.125)\ ft} = 43.17\ kips$$

Where:

w= self-weight of the girder in kip/ft.

7.3.2 M2-U

For MU2, the procedure to find the shear capacity is the same except that the crack angle is slightly different from the other beam. This leads to a difference in the nominal shear capacity of the member.

$\theta_c = 44°$

$$V_{nBV} = \frac{14.1\ kips}{\cot 44°} + \frac{66\ kips \cdot 8\ in}{18.8\ in \cdot \cot 44°} + 0 + 0 \cong 40.7\ kips$$

$P = 48.05\ kips$

7.3.3 M3-U

$\theta_c = 44°$

$$V_{nBV} = \frac{14.1\ kips}{\cot 44°} + \frac{66\ kips \cdot 8\ in}{18.8\ in \cdot \cot 44°} + 0 + 0 \cong 40.07\ kips$$

$P = 48.05\ kips$

7.3.4 M4-U

$\theta_c = 40°$

$$V_{nBV} = \frac{14.1 kips}{\cot 40°} + \frac{66\ kips \cdot 8\ in}{18.8\ in \cdot \cot 40°} + 0 + 0 \cong 35.6\ kips$$

$$P = 41.8\ kips$$

7.3.5 M5-U

$\theta_c = 38°$

$$V_{nBV} = \frac{14.1\ kips}{\cot 38°} + \frac{66\ kips \cdot 8\ in}{18.8\ in \cdot \cot 38°} + 0 + 0 \cong 32.9\ kips$$

$$P = 38.54\ kips$$

7.3.6 M6-U

$\theta_c = 40°$

$$V_{nBV} = \frac{14.1\ kips}{\cot 40°} + \frac{66\ kips \cdot 8\ in}{18.8\ in \cdot \cot 40°} + 0 + 0 \cong 45.6\ kips$$

$$P = 41.8\ kips$$

7.4 Flexural Capacity of Both the MU and MR Beams- Strain Compatibility

Input data:

$f'_{ci} = 5.5\ ksi$	(compressive strength of the beam at prestressing release)
$f'_c = 8\ ksi$	(28-day compressive strength of the beam)
$b = 9\ in$	(width of the compression stress block
$f_{pu} = 270\ ksi$	(ultimate strength of the prestressing strands)
$A_{ps} = 0.334\ in^2$	(area of prestressing strands)
$f_{se} = 170\ ksi$	(effective prestressing stress)
$L = 18\ ft$	(span length)
$d_p = 25.125\ in$	(depth of prestressing strands)

Required:

Nominal moment capacity (Mn).

Solution:

$A_s = 0.62\ in^2;\ \ A'_s = 1.24\ in^2;\ \ d = 6.625\ in.;\ \ d' = 2.5\ in.$

Where:

A_s= area of mild steel in tension

A'$_s$= area of mild steel in compression

d= depth of tension mild steel from the top

d'= depth of compression mild steel from the top

$Assume\ c = 2.85\ in.;\ \ a = \beta \cdot c = 0.65 \cdot 2.85 = 1.8525\ in.$

$e = y_{tr} - concrete\ cover = 14.133\ in. - 2\ in. = 12.133\ in.$

$$A_{tr} = Ag + (n-1) \cdot Aps \tag{22}$$

$$\therefore n = \frac{E_{ps}}{E_{ci}} = \frac{28600\ ksi}{\frac{57000 \cdot \sqrt{5500\ psi}}{1000}} = 6.76$$

$$A_{tr} = 147.375\ in^2 + (6.76 - 1) \cdot 0.334\ in^2 = 149.29$$

$$y_{tr} = \frac{A_g \cdot y_g + A_{ps,tr} \cdot y_{ps}}{A_g + A_{ps,tr}} \tag{23}$$

$$y_{tr} = \frac{147.375\ in^2 \cdot 14.161\ in. + 0.334\ in^2 (6.76-1) \cdot 2\ in.}{147.375\ in^2 + 1.92\ in^2} = 14\ in$$

$$I_{tr} = I_g + A_g \cdot {d_g}^2 + A_{ps,tr} \cdot {d_{ps}}^2 \tag{24}$$

$$I_{tr} = 12529.68\ in^2 + 147.375\ in^2 \cdot (14.133\ \text{in.} - 14.16\ \text{in})^2 + 1.92\ in^2 \cdot$$

$$(14.133\ in. - 2\ in.)^2 = 12553.1\ in^2$$

Where:

c= depth of compressive stress (location of neutral axis)

a=Whitney's equivalent depth of stress block

e= strand eccentricity

y_{tr}= transformed section centroidal location taken from the bottom

A_{tr}= transformed section area

I_{tr}= transformed section moment of inertia

I_g= gross section moment of inertia

$$C_c = 0.85 \cdot f_c' \cdot b \cdot a \tag{25}$$

$$C_c = 0.85 \cdot 8\ ksi \cdot 9\ in. \cdot 1.8525\ in. = 113.373\ kips$$

$$\varepsilon_1 = \varepsilon_{se} = \frac{f_{se}}{E_{ps}} \tag{26}$$

$$\varepsilon_1 = \frac{170\ ksi}{28600\ ksi} = 0.00594$$

$$P_e = A_{ps} \cdot f_{se} \tag{27}$$

$$P_e = 0.334\ in^2 \cdot 170\ ksi = 56.78\ kips$$

$$\therefore Ec = \frac{57000 \cdot \sqrt{8000\ psi}}{1000} = 4227.23\ ksi$$

$$\varepsilon_2 = \left(\frac{P_e}{A} + \left(P_e \cdot \frac{e^2}{I}\right)\right) . \frac{1}{Ec} \tag{28}$$

$$\varepsilon_2 = \left(\frac{56.78\ kips}{149.29\ in^2} + \frac{56.78\ kips \cdot (12.133\ in)^2}{12553.1\ in^4}\right) \cdot \frac{1}{4227.23\ ksi}$$

$$\varepsilon_2 = 0.000103$$

$$\varepsilon_3 = \left(\frac{0.003}{c}\right) \cdot (d_p - c) \tag{29}$$

$$\varepsilon_3 = \left(\frac{0.003}{2.85\ in.}\right) \cdot (25.125\ in. - 2.85\ in.) = 0.0234$$

$$\varepsilon_{ps} = \varepsilon_1 + \varepsilon_2 + \varepsilon_3 \tag{30}$$

$$\varepsilon_{ps} = 0.00594 + 0.000103 + 0.0234 = 0.0294 > 0.0085$$

$$f_{ps} = 270 - \frac{0.04}{\varepsilon_{ps} - 0.007} \tag{31}$$

$$f_{ps} = 270 - \frac{0.04}{0.0294 - 0.007} = 268.21\ ksi$$

$$\frac{\varepsilon_{ms}}{6.625\ in. - 2.85\ in.} = \frac{0.003}{2.85} \quad \rightarrow \ \varepsilon_{ms} = 0.00397$$

$$\frac{0.003}{2.85\ in.} = \frac{\varepsilon_{s'}}{2.85\ in. - 2.5\ in.} \quad \rightarrow \ \varepsilon_{s'} = 0.000368$$

$$\varepsilon_y = \frac{60\ ksi}{29000\ ksi} = 0.002$$

Where:

C_c= compressive force of concrete

ε_1= strain at strand due to effective prestress

P_e= effective prestress force

ε_2=strain corresponding to zero compression stress at the level of the prestressing steel (decompression strain)

ε_3= strain resulting from bending between decompression and ultimate

ε_{ps}= strain in the prestressing strand at ultimate

f_{ps}= stress in the prestressing strand at ultimate

ε_{ms}= strain in the mild steel in tension

$\varepsilon_{s'}$= strain in the compression steel

ε_y= yield strain of mild steel

$$f_s' = (E_s) \cdot (\varepsilon_s') \quad (32)$$

$$f_s' = 29000\ ksi \cdot 0.000368 = 10.672\ ksi$$

$$C_s = A_s' \cdot f_s' \quad (33)$$

$$C_s = 1.24\ in^2 \cdot 10.68\ ksi = 13.24\ kips$$

$$C_c = 0.85 \cdot f_c' b \cdot a \quad (34)$$

$$C_c = 0.85 \cdot 8\ ksi \cdot 9\ in. \cdot 1.8525\ in. = 113.373\ kips$$

$$T_{ps} = A_{ps} \cdot f_{ps} \tag{35}$$

$$T_{ps} = 0.334\ in^2 \cdot 268.23\ ksi = 89.58\ kips$$

$$T_{ms} = A_s \cdot f_s \tag{36}$$

$$T_{ms} = 0.62\ in^2 \cdot 60\ ksi = 37.2\ kips$$

$$Total\ tensile\ force = T_{ps} + T_{ms} = 89.58\ kips + 37.2\ kips = 126.78\ kips$$

$$Total\ compressive\ force = C_s + C_c = 126.613\ kip$$

As total tension is equal to the total compression, therefore, the assumed c value is correct.

Where:

f'_s= stress in mild steel in tension

C_s= compression force in compression steel

T_{ps}= Tensile force of prestressing strand

T_{ms}= Tensile force of mild steel in tension

Moment capacity about the neutral axis is:

$$M_n = T_{ps} \cdot \left(d_p - c\right) + T_{ms} \cdot (d - c) + C_c \cdot \left(c - \frac{a}{2}\right) + C_s \cdot (c - d') \tag{37}$$

$$M_n = 89.58\ kips \cdot (25.125\ in. - 2.85\ in.) + 37.2\ kips \cdot (6.625\ in. - 2.85\ in.) +$$

$$+ 113.373\ kips \cdot \left(2.85\ in. - \frac{1.8525\ in.}{2}\right) + 13.24\ kips \cdot (2.85\ in. - 2.5\ in.) = 196.54\ \text{k} - \text{ft}$$

$$M_n = 196.54\ k - ft$$

The effective span between the point load and the near support is $l = 3.125\ in.$, as shown in Figure 3.8.

$$M = R \cdot l - \left(w \cdot \frac{l^2}{2}\right) \rightarrow \quad R = \frac{M + \frac{w \cdot l^2}{2}}{l} = \frac{196.54\ k-ft + \frac{0.15\frac{k}{ft} \cdot (3.125\ ft)^2}{2}}{3.125\ ft} = 63.127\ kips$$

$$R = P \cdot \frac{L-l}{L} + \left(w \cdot \frac{L}{2}\right) \rightarrow \quad P = \left(R - \frac{w \cdot L}{2}\right) . \frac{L}{L-l} = \left(63.127\ kip - 0.15\frac{k}{ft} \cdot \frac{17.35\ ft}{2}\right) \cdot$$

$$\cdot \left(\frac{(17.35\ ft)}{17.35\ ft - 3.125\ ft}\right) = 75.4\ kips$$

Based on the strain compatibility procedure, the point load that causes moment failure is 75.4 kips. This value is based on the assumption that the f_{ps} at the loading location fully develops during the test. However, considering the effect of development length calculated using the equation

$$l_d = \left(\frac{f_{se}}{3000}\right) \cdot d_b + \frac{f_{ps} - f_{se}}{1000} \cdot d_b \qquad (38)$$

in Section 25.4.8.1 of ACI 318R-14 gives a different value for P. The first term of the equation is transfer length which is the distance from the girder's end required to develop the effective prestress in prestressing steel, f_{se}. The second term is the length required to develop the nominal strength of the prestressing strand, f_{ps}. The available length from the end of the girder to the

maximum moment (point of load application) is 3.5 ft, which is 42 in. The required development length is:

$$l_d = \left(170\frac{ksi}{3000}\right) \cdot 0.52in + \frac{268.23\ ksi - 170\ ksi}{1000} \cdot 0.52\ in = 29.46\ in + 51.08\ in = 80.546\ in$$

In the above equation, the first term (29.46 in.) is the transfer length which is less than the available development length (42 in.); however, the second term does not fully fit in the available transfer length, which indicates the full f_{ps} does not develop; instead, it is based on the ratio of $\frac{Available\ length\ for\ f_{ps}}{Required\ length\ for\ f_{ps}} \leq 1$, which is equal to $\frac{42\ in - 29.46\ in}{51.08\ in} = 0.245$ This yields a modified value of $f_{ps} = (0.245) \cdot (268.23\ ksi - 170) + 170 = 194.1\ ksi$

If we repeat the whole calculations from the beginning based on the new f_{ps}, it gives the depth of compression zone $c = 2.54\ in.$ and $Mn = 149.12\ k - ft$. The value of the reaction for the near end support is as $R = \left(\frac{Moment\ capacity + moment\ due\ to\ self-weight}{Moment\ arm}\right) =$

$\frac{149.12\ k-ft + 0.15\frac{k}{ft}\cdot\frac{(3.125\ ft^2)}{2}}{3.125\ ft} = 47.9\ k$. For R=47.9 k, the value point load value is $P = 58.4\ kips$. This indicates that the actual value of P, which is the load for nominal moment capacity, can be between 58.4 kips and the previous value of 75.4 kips. The difference can be due to the strand slip which changes the development length and decreases the ability of the member to transfer the force.

All the original beams failed in bond-shear; however, the numerical values for shear capacity after the repair are higher than the moment, making flexure a controlling failure type.

7.5 Shear Capacity for the Repaired Beams

7.5.1 UHPC

For the repaired beams shear resistance is offered only by the shear stirrups (V_s) and the repair concrete (V_c). The member's concrete is cracked and prestress is lost due to slip from the previous test, therefore its contribution is ignored.

$$V_s = Number\ of\ stirrups\ crossing\ a\ crack \cdot A_v \cdot f_y \quad (39)$$

$$V_s = 5 \cdot 2 \cdot 0.11\ in^2 \cdot 60\ ksi = 66\ kips$$

$$V_c = 2 \cdot \sqrt{f_c'} \cdot b \cdot d$$

Where:

V_s= shear capacity of stirrups

A_v= area of shear stirrups

f_y= yield strength of stirrups

f'_c= compressive strength of the repair material

d= depth of the repair material

b= smallest repair thickness present throughout the section (conservative)

$$d = 22.5\ in. + 2\ in. = 24.5\ in.$$

$b = 1.5\ in.$

$V_c = \frac{2 \cdot \sqrt{17320\ psi} \cdot 2 \cdot 1.5\ in. \cdot 24.5\ in.}{1000} = 19.35\ kips$

$V = V_s + V_c$

$V = 66\ kips + 19.32\ kips = 85.32\ kips$

$$P = \left(V - \frac{wl}{2}\right) \cdot \frac{L}{L-l} \quad (40)$$

$P = (85.32\ kip - 0.15 \frac{k}{ft} \cdot \frac{17.35\ ft}{2}) \cdot \frac{17.35\ ft}{17.35\ ft - 3.125\ ft} = 102.5\ kips$

7.5.2 NEW MALP

For the repaired beam, shear resistance is offered only by the shear stirrups (V_s) and the repair concrete (V_c). The member's concrete is cracked and prestress is lost due to slip from the previous test, therefore its contribution is ignored.

$V_s = Number\ of\ stirrups\ in\ a\ crack \cdot A_v \cdot f_y = 5 \cdot 2 \cdot 0.11\ in^2 \cdot 60\ ksi = 66\ kips$

$V_c = 2 \cdot \sqrt{f_c'} \cdot b \cdot d$

$d = 22.5\ in + 2\ in = 24.5\ in$

$b = 1.5\ in$

$V_c = \frac{2 \cdot \sqrt{12490\ psi} \cdot 2 \cdot 3\ in. \cdot 24.5\ in.}{1000} = 32.85\ kips$

$V = V_s + V_c = 66\ kips + 32.85\ kips = 98.85\ kips$

$$P = \left(V - \frac{wl}{2}\right) \cdot \frac{L}{L-l} = (98.85\ kip - 0.15\frac{k}{ft} \cdot \frac{17.35\ ft}{2}) \cdot \frac{17.35\ ft}{17.35\ ft - 3.125\ ft} = 118.9\ kips$$

7.5.3 OLD MALP

For the repaired beam, shear resistance is offered only by the shear stirrups (V_s) and the repair concrete (V_c). The member's concrete is cracked and prestress is lost due to slip from the previous test, therefore its contribution is ignored.

$$V_s = Number\ of\ stirrups\ in\ a\ crack \cdot A_v \cdot f_y = 5 \cdot 2 \cdot 0.11\ in^2 \cdot 60\ kis = 66\ kips$$

$$V_c = 2 \cdot \sqrt{fc'} \cdot b \cdot d$$

$$d = 22.5\ in + 2\ in = 24.5\ in$$

$$b = 1.5\ in$$

$$V_c = \frac{2 \cdot \sqrt{3329\ psi} \cdot 2 \cdot 3\ in \cdot 24.5\ in}{1000} = 16.96\ ksi$$

$$V = V_s + V_c = 66\ kips + 16.96\ kips = 82.96\ kips$$

$$P = \left(V - \frac{wl}{2}\right) \cdot \frac{L}{L-l} = (82.96\ kip - 0.15\frac{k}{ft} \cdot \frac{17.35\ ft}{2}) \cdot \frac{17.35\ ft}{17.35\ ft - 3.125\ ft} = 99.6\ kips$$

7.5.4 FR-SCC

For the repaired beam, shear resistance is offered only by the shear stirrups (V_s) and the repair concrete (V_c). As the member's concrete is cracked therefore its contribution is ignored.

$$V_s = Number\ of\ stirrups\ in\ a\ crack \cdot A_v \cdot f_y = 5 \cdot 2 \cdot 0.11\ in^2 \cdot 60\ ksi = 66\ kips$$

$$V_c = 2 \cdot \sqrt{f_c'} \cdot b \cdot d$$

$$d = 22.5\ in. + 2\ in. = 24.5\ in.$$

$$b = 1.5\ in.$$

$$V_c = \frac{2 \cdot \sqrt{6680\ psi} \cdot 2 \cdot 3\ in. \cdot 24.5\ in.}{1000} \cong 24\ kips$$

$$V = V_s + V_c = 66\ kips + 24\ kips = 90\ kips$$

$$P = \left(V - \frac{wl}{2}\right) \cdot \frac{L}{L-l} = (90\ kips - 0.15 \frac{k}{ft} \cdot \frac{17.35\ ft}{2}) \cdot \frac{17.35\ ft}{17.35\ ft - 3.125\ ft} = 108.18\ kips$$